

**THE DEVELOPMENT OF A VEHICLE AND ROAD LOAD
SIMULATION FOR AN ENGINE DYNAMOMETER INTENDED
FOR EMISSIONS TESTING AND POWERTRAIN DEVELOPMENT**

Daniel Kunniger

A Dissertation submitted to the Faculty of Engineering and the Built Environment,
University of the Witwatersrand, in fulfillment of the requirements for the degree
of Master of Science in Engineering.

Johannesburg, 2012

DECLARATION

I declare that this dissertation is my own unaided work. It is being submitted to the Degree of Masters of Science to the University of Witwatersrand, Johannesburg. It has not been submitted before for any degree or examination to any other University.

.....
(Signature of Candidate)

.....day of.....year.....
day month year

ABSTRACT

This dissertation documents the development and evaluation of a vehicle and road load simulation program for an engine dynamometer intended for emissions testing and power-train development. The document summarizes the reviewed vehicle emissions testing, engine testing and test equipment documentation, as part of the conducted literature study. It continues to describe the existing dynamic test cell at Cape Advanced Engineering used for the development and evaluation of the described system as well as the changes that were implemented to the test cell to enable full transient vehicle simulation. The development of an offline simulation model, a preprocessing simulation model and real time hardware in the loop simulation model are discussed. The progression made from one developed model to the next as well as the reasons for the progression are stated and discussed. The evaluation process of the hardware in the loop model as well as the conducted evaluation by the simulation of the European Communities Transient Test Cycle is discussed and the derived simulation accuracy of 7% based on fuel consumption over the duration of the test cycle is documented. Improvements made to the simulation model during the evaluation and the vehicle and power-train effective rotational inertia that was used in the model are reviewed and their effects discussed. Fields of application as well as future recommendations to the derived system are provided.

In appreciation of all those who gave so much to allow me to keep my feet on the ground and reach for the stars.

ACKNOWLEDGEMENTS

I would like to thank:

Prof. D Cipolat for all his assistance, guidance and willingness to allow me to do what so many others would not.

Dr. A Taylor, Mr. C van Vuuren and Mr. W Bester of Cape Advanced Engineering for all their assistance and use of their equipment.

National Instruments South Africa for their sponsorship of development software which without, none of this would have been possible.

Mr. N Bhana, Mr. R Allsopp and Mr. W Duncan of Volkswagen South Africa for the use of their test engines and related test equipment as well as their support of this project.

Lastly, to my family and friends without whom none of this would have be possible.

CONTENTS

DECLARATION	2
ABSTRACT	3
ACKNOWLEDGEMENTS	5
CONTENTS	6
LIST OF FIGURES	8
LIST OF TABLES	10
LIST OF SYMBOLS	11
NOMENCLATURE	12
1 PROBLEM STATEMENT	13
2 PROPOSED SOLUTION	15
3 LITERATURE STUDY	16
3.1 Emissions Testing	16
3.1.1 Light duty vehicle emissions testing	18
3.1.2 Heavy duty vehicle emissions testing	24
3.1.3 Emissions test equipment	30
3.2 Road Load and Vehicle Simulation	33
3.2.1 Aerodynamic drag force	34
3.2.2 Rolling resistance	35
3.2.3 Vehicle and rotating component Inertia's	37
3.3 Real-Time Computing	39
4 DEVELOPMENT OF THE ROAD LOAD SIMULATION PROGRAM	42
4.1 Existing CAE Test Stand and Infrastructure	42
4.2 System Operating Principles	45
4.2.1 Software and hardware selection	47
4.2.2 LabVIEW RT operating principles	50
4.2.3 System integration and hardware interfaces	50
4.3 Data Acquisition	54
4.3.1 Engine torque measurement	55
4.3.2 Engine speed measurement	58
4.3.3 Throttle demand signal	60
4.4 Engine Characterization	61

4.5	First Simulation Program	62
4.5.1	The terrain VI	64
4.5.2	Driver VI	65
4.5.3	Vehicle VI	66
4.6	Second Simulation Program	67
4.6.1	Simulated vehicle braking VI	71
4.6.2	Simulated clutch locked-up VI	72
4.6.3	Simulated clutch-slip VI	75
4.7	Third Simulation Program	80
5	SIMULATION PROGRAM TESTING AND EVALUATION	83
5.1	First Simulation	84
5.2	Second Simulation Program	87
5.3	Third Simulation Program	88
5.3.1	Simulation accuracy	91
5.3.2	Ability to follow a provided cycle	103
5.3.3	Repeatability and reproducibility of results	104
6	CONCLUSION	107
7	RECOMMENDATIONS	110
8	REFERENCES	111
Appendix A		113
Appendix B		116
Appendix C		117
Appendix D		119
Appendix E		122
Appendix F		123

LIST OF FIGURES

Figure 3. 1: Worldwide testing procedures and standards for light duty vehicles (Delphi, 2009)	19
Figure 3. 2: US test cycles for passenger cars and light commercial vehicles Bosch (2007)	20
Figure 3. 3: ECE European test cycle (European Communities 2009)	21
Figure 3. 4: Japanese JC08 test cycle (Delphi 2009: 46)	22
Figure 3. 5: Light duty vehicle emissions test set-up (Bosch 2007)	23
Figure 3. 6: Thirteen mode diesel emissions steady state test cycle (Merrion 2003)	24
Figure 3. 7: FTP transient driving schedule for diesel and gasoline heavy duty engines (Delphi 2008)	25
Figure 3. 8: European Communities 13-stage steady state heavy duty emissions test cycle (Delphi, 2008)	26
Figure 3. 9: Load response heavy duty emissions test cycle (Delphi, 2008)	27
Figure 3. 10: European Transient diesel and gasoline heavy duty emission test cycle (European communities, 1999)	28
Figure 3. 11: (Delphi, 2008) Japanese JC05 transient emissions cycle for diesel and gasoline vehicles	29
Figure 3. 12: Exhaust gas dilution tunnel (Plint, 1999)	32
Figure 3. 13: Coefficients of aerodynamic drag and associated power requirements for various body configurations	34
Figure 3. 14: Rolling resistance of radial car tyres on a road surface (Bosch, 2007)	36
Figure 3. 15: Determination of f_0 and f_1 (Taborek 2005)	37
Figure 3. 16: Sequential and concurrent threads (Hailperin, 2007)	39
Figure 4. 1: Existing CAE Hybrid dynamometer test stand	42
Figure 4.2: Target PC integration with the existing test stand equipment	51
Figure 4. 3: The C.V adapter flanges with 60-tooth disks and the torque flange.	52
Figure 4. 4: Dynamometer and drive motor mounting and support	55
Figure 4. 5: HBM torque flange components (HBM 2007)	57
Figure 4. 6: Torque-flange side engine speed magnetic pickup and 60-tooth disk	59
Figure 4. 7: Engine side engine speed magnetic pickup, 60-tooth disk and sensor mounting bracket relative to the engine.	59
Figure 4. 8: Steady-state engine characterization of a Volkswagen EA113, 1.6l engine.	61
Figure 4. 9: Simulation program 1 process overview block diagram	63
Figure 4. 10: Rolling resistance and aerodynamic drag VI block diagrams.	64
Figure 4. 11: Powertrain (left) and vehicle (right) inertia VI block diagrams.	66
Figure 4. 12: Simulation program 2 process overview block diagram	69
Figure 4. 13: Host PC user interface screen shot showing the five tabs	80
Figure 5. 1: Engine speed versus time for Simulation program 1, test 7. Recorded engine speed following a step, ramp and steady state input.	85
Figure 5. 2: Engine speed versus time for Simulation program1, test1. Measured engine speed while simulating two ECE urban cycles.	86

Figure 5. 3: Torque versus time for Simulation program1, test 1. Measured torque flange torque while simulating two ECE urban cycles.	87
Figure 5. 4: Simulation program 2 trouble shooting user interface.	88
Figure 5. 5: Load at tyre surface versus vehicle speed.	92
Figure 5. 6: Simulated vehicle speed versus time for gears 1 through 5.	94
Figure 5. 7: Inertia derived vehicle mass versus time for first gear.	95
Figure 5. 8: Inertia derived vehicle mass versus simulated vehicle speed for gears 1 through 5.	96
Figure 5. 9: Representative Powertrain system as used by Conradie (2001), Gillespie(1992) and Hong(1996)	98
Figure 5. 10: Powertrain system analogue as plotted by Hong (1996) and referenced by Conradie(2001)	98
Figure 5. 11: Equivalent Powertrain system analogue as was plotted by Gillespie(1992)	99
Figure 5. 12: Engine speed versus time for simulation program 3 while simulating an ECE cycle	100
Figure 5. 13: Simulated transient operating conditions including gear change simulation. Hong (1995)	101
Figure 5. 14: Torque versus time for simulation program 3 while simulating an ECE cycle	102
Figure 5. 15: Throttle demand versus time for simulation program 3 while simulation an ECE cycle	103
Figure 5. 16: Simulated vehicle speed versus time for simulation program 3 while simulating an ECE cycle	104
Figure 5. 17: Engine speed versus time for runs 16, 17 and 18	105
Figure 5. 18: Engine torque versus time for runs 16, 17 and 18	106

LIST OF TABLES

Table 3. 1: Vehicle categories (Ecopoint Incorporated, 2008)	18
Table 3. 2: Light duty emissions evaluation tests (Delphi, 2008)	18
Table 3. 3: Techniques of emissions analysis (Plint, 1999)	32
Table 4. 1: Froude EC 38 TA Specification	43
Table 4. 2: Siemens servo motor specification	43
Table 4. 3: Allen-Bradley drive specification	43
Table 4.4: Kepner-Tregoe Method applied to the determination of a software compiler	48
Table 4.5: Advantages and disadvantages of Real-time operating systems and FPGA's with respect to their implementation of this dissertation	49
Table 4. 6: Target PC data acquisition interface channels	51
Table 4. 7: HBM Torque flange specification	56
Table 4. 8: Digital magnetic pickup specification	58
Table 4. 9: Throttle demand driving current required from DAQ card.	60
Table 5. 1: Test vehicle technical specification.	83
Table 5. 2: Summarized ECE run configurations and fuel consumption results	90
Table D. 1: Procured hardware	119

LIST OF SYMBOLS

a	Acceleration	$[m/s^2]$
A_v	Vehicle frontal area	$[m^2]$
C_D	Co-efficient of drag	
f_0	Speed independent rolling resistance co-efficient	
f_1	Speed dependant rolling resistance co-efficient	
f_r	Co-efficient of rolling resistance	
F	Force	$[N]$
F_A	Aerodynamic drag force	$[N]$
F_I	Road incline resistance force	$[N]$
F_R	Rolling resistance force	$[N]$
G_f	Final drive gear ratio	
G_{ft}	Overall gear ratio	
G_t	Transmission gear ratio	
I	Inertia	$[Kg.m^2]$
J_D	Dynamometers moment of inertia	$[Kg.m^2]$
J_E	Engines moment of inertia	$[Kg.m^2]$
M_v	Mass	$[N]$
P	Momentum	$[Kg.m/s^2]$
P_r	Road load power	$[Kw]$
R	Tyre radius	$[m]$
T	Torque	$[N.m]$
T_C	Torque at the clutch	$[N.m]$
T_D	Dynamometer load torque	$[N.m]$
T_E	Engine torque	$[N.m]$
T_T	Total torque	$[N.m]$
U	Vehicle speed	$[Km/h]$
V	Vehicle velocity	$[m/s]$
W	Vehicle weight	$[Kg]$
α	Angular acceleration	$[rad/s^2]$
α_D	Dynamometer angular acceleration	$[rad/s^2]$
α_E	Engine angular acceleration	$[rad/s^2]$
α_E	Engine angular acceleration	$[rad/s^2]$
α_V	Vehicles relative angular acceleration	$[rad/s^2]$
ρ	Density	$[Kg/m^3]$

NOMENCLATURE

AC	Alternating Current
ASCI	Application-Specific Integrated Circuit
CAE	Cape Advanced Engineering
CARB	California Air Research Board
CI	Compression Ignition
CLB	Configurable Logic Block
DC	Direct Current
ECE	Economic Commission for Europe
EPA	Environmental Protections Agency
ETA	Engine Test Automation (CAE test automation software)
ETC	European transient Cycle
EU	European Union
EURO	European
FPGA	Field Point Gate Array
FTP	Federal Test Procedure
NEDC	New European Driving Cycle
IOB	Input Output Block
OBD	On-Board Diagnostics
OS	Operating System
PLD	Programmable Logic Device
PM	Particulate Matter
RTOS	Run Time Operating System
SABS	South African Bureau for Standards
SANS	South African National Standard
SFTP	Supplementary Federal Test Procedure
SI	Spark Ignition
U.S	United States of America
VI	Virtual Instrument
VWSA	Volkswagen South Africa
WS	Weighted Score

1 PROBLEM STATEMENT

South Africa is currently a major manufacturer of automobiles for the local and export markets. Unfortunately financial restraints and other determining factors have limited automotive development and design in South Africa.

Ever increasing awareness and understanding of the adverse effects of greenhouse gases as well as particulate matter have forced automotive emissions standards and regulations to become more stringent world-wide. Legislation is clamping down on the maximum permissible greenhouse gases and ozone depleting gases that vehicle are allowed to emit. These reductions have forced automobile manufacturers to introduce innovative methods of improving the efficiency of current designs to produce cleaner burning, more fuel efficient and cost effective automobiles.

A major contribution to the improved efficiency of the modern engine is provided by the continuously improving Engine Control Unit (ECU). The efficiency provided by the ability to accurately measure and control an engine's performance has come at the cost of development and calibration of the ECU. As the ECU grows in complexity to achieve even better engine efficiency, the calibration complexity also grows. Most of this calibration has traditionally been undertaken by engineers with the use of engine test stands. This calibration not only ensures optimal engine performance but also compliance with international standards such as the ECE emissions standard.

Current automotive emissions testing is performed on a rolling road dynamometer with a trained test driver attempting to follow predetermined driving cycles and gear selection (depending on cycle) for light duty vehicles. Heavy duty engine testing is done using an engine dynamometer and a vehicle simulation program applying predetermined, specified loads and engine speeds. The emissions test driving cycles are set out in national standards and are intended to be representative of those nations driving habits. Emissions test cycles are set by the respective countries emissions regulators and are subject to international pressures.

The inclusion of human drivers during emissions testing and ECU calibration (e.g. Drivability calibration/testing) has shown to be subject to the following factors:

1. Accuracy. Drivers tend to over and undershoot target set-points (e.g. a set vehicle velocity) throughout a test. This is often due to the human driver inability to act in fine enough increments and for less experienced test drivers, the tendency is to over compensate for an error once the error has propagated sufficiently to provide a visual error on the displays (relative to ECU calibration, the vehicle instrumentation increments are large). In the case of a vehicle being tested on a rolling road dynamometer, the problem is usually exaggerated as the driver's perception of speed is lost due to the vehicles stationary orientation.

2. Repeatability. This is a result of the driver's input. Human driver responses constantly vary thereby affecting the consistency between multiple test drivers and tests, making it difficult if not impossible to accurately compare the results of numerous tests.

Vehicle simulation engine test systems that allow testing to be done on an engine test stand using an engine dynamometer have been developed. This has resolved the issue of inaccuracy and repeatability by removing the direct influence of the human test driver by automating tests with a deterministic system. It has also removed the need for the use of a complete vehicle in order to test or evaluate internal combustion engine developments under real world driving conditions. The ability to simulate a vehicle on a test stand has also allowed for better transient ECU calibration, providing better performance, drivability and lower fuel consumption, collectively reducing emissions.

These types of vehicle simulation test systems, having been developed in Europe (AVL, Siemens, and Lotus Software), The United States of America (Raptor) and East Asia (Horiba) are unaffordable for local companies wanting to use such a development tools. This can be confirmed by the fact that CSIR, Volkswagen South Africa, Cape Advanced Engineering, University of the Witwatersrand, University of Johannesburg, University of Cape Town and Stellenbosch University; to mention but a few companies and institutions that could benefit from such a system but do not have such a system. The only South African company that currently has such a system is Sasol who hold a license but would greatly benefit from a more cost effective solution. The costs of basic models are out of reach for most South Africa institutions wanting to engage in this field of testing or research. For those that can afford it, it is still problematic as supporting test equipment, control systems and software from the same company is often required.

2 PROPOSED SOLUTION

It was proposed that a vehicle and road load simulation program that would allow South African companies and learning institutions to conduct transient power-train and emission testing be developed.

To make the simulation applicable to as many fields of development, research and testing as possible, the system needs to be as diverse as possible. This would require that the vehicle simulation model be capable of simulating various types of vehicle with various power-plant and power-train configurations. The simulation model will have to, at least, account for the following vehicle parameters:

1. Aerodynamic resistance
2. Vehicle rolling resistance
3. Dynamometer inertia
4. Engine inertia
5. Transmission/drive-train inertia
6. Various transmission and final drive ratios

The proposed simulation program will have to output the values required by the dynamometer controller to allow transient change in engine speed and load simultaneously. The model must be developed using commercially available products, must be able to function with variety of different dynamometer configurations and must require as few vehicle parameters as physically possible to obtain an acceptable result.

3 LITERATURE STUDY

A literature study was conducted to obtain a knowledge base of fields relevant to this research. This chapter is a compilation of information from the literature study found to be relevant to the implementation of the scope of work. The information provided includes details on various aspects relating to emissions testing, transient testing and real-time computing.

3.1 Emissions Testing

"Environmental concern, dating back to the 1960s, has led to an ever-increasing flood of legislation which is now perhaps the main driving force in the continuing development of the internal combustion engine" (Plint, 1995). In additions Plint (1995) states the majority of both engine development and of routine testing is concerned with the impact of environmental legislation. The main topics, with which this legislation is concerned with, are:

1. The harmful effects of airborne lead on health.
2. Carcinogenic properties of diesel engine emissions.
3. Acid rain.
4. Photochemical smog.
5. Global warming (the greenhouse effect).
6. Stratospheric ozone depletion.

The Bosch Automotive Handbook suggests that all industrialized countries have introduced emissions-control laws which define limits for gasoline and diesel engines, as well as test procedures employed to confirm compliance. It further indicates that the primary emissions-control legislation includes:

1. CARB legislation (California Air Resources Board).
2. EPA legislation (Environmental Protection Agency), USA.
3. EU legislation (European Union) and the corresponding ECE regulations (UN Economic Commission for Europe).
4. Japanese legislation.

The Bosch Automotive Handbook states: "Japan and the European Union have followed the lead of the United States by defining test procedures for certifying compliance with emissions limits. These procedures have been adopted in modified or unrevised form by other countries".

The Air Quality Act of 2004 replaced the Atmospheric Pollution Preventions Act of 1965 as the Act enforcing vehicle emissions legislation within South Africa. This legislation enforces all new light duty vehicles (classes M, M₁, N and N₁) to comply with the SABS standard titled, *Uniform provisions concerning the approval of vehicles with regard to the emission of pollutants according to engine fuel requirements*. Legislation further ensures that heavy duty vehicles (classes M₂, M₃, N₂ and N₃) comply to the SABS standard titled, *Uniform provisions concerning the approval of compression-ignition (C.I.) and natural gas (NG) as well as positive-ignition (P.L)*

engines fueled with liquefied petroleum gas (LPG) and vehicles equipped with C.I. and NG engines fuel with LPG, with regard to the emissions of pollutants by the engine to the level of ECE R49.02B.

Plint (1995) suggested that the outstanding characteristic of all emissions test procedures was that they involve transient operation of the engine.

Bosch (2007) states that countries with legal limits on motor-vehicle emissions divide vehicles into various classes as follows:

1. Passenger cars: Emissions testing is conducted on a chassis dynamometer.
2. Light commercial vehicles: Depending on national legislation, the top limit for gross weight rating is 3.5 to 6.35t. Testing is performed on a vehicle chassis dynamometer as for passenger cars.
3. Heavy commercial vehicles: Gross weight rating over 3.5 to 6.35t (depending on national legislation). The testing is conducted on an engine test bench. No provision is made for vehicle testing.
4. Off-highway (e.g. construction, agricultural, and forestry vehicles): Tested on an engine test bench, as for heavy commercial vehicles.

Light duty vehicle with CI and SI engines share a common standard although emissions limits are based on engine capacity and type. The test procedure for all designations of light duty vehicles is the same with the exception of CI engines requiring additional emission measurements. There are significant differences in test methodology between light duty and heavy duty vehicles and these will be discussed in the following sub sections.

Table 3. 1: Vehicle categories (Ecopoint Incorporated, 2008)

Category	Description
M	Motor vehicles with at least four wheels designed and constructed for the carriage of passengers.
M ₁	Vehicles designed and constructed for the carriage of passengers and comprising no more than eight seats in addition to the driver's seat
M ₂	Vehicles designed and constructed for the carriage of passengers, comprising more than eight seats in addition to the driver's seat, and having a maximum mass ("technically permissible maximum laden mass") not exceeding 5 tons
M ₃	Vehicles designed and constructed for the carriage of passengers, comprising more than eight seats in addition to the driver's seat, and having a maximum mass exceeding 5 tons
N	Motor vehicles with at least four wheels designed and constructed for the carriage of goods.
N ₁	Vehicles designed and constructed for the carriage of goods and having a maximum mass not exceeding 3.5 tons
N ₂	Vehicles designed and constructed for the carriage of goods and having a maximum mass exceeding 3.5 tons but not exceeding 12 tons
N ₃	Vehicles designed and constructed for the carriage of goods and having a maximum mass exceeding 12 tons
O	Trailers (including semi-trailers)
G*	Off-Road Vehicles
* - Symbol G shall be combined with either symbol M or N. For example, a vehicle of category N ₁ which is suited for off-road use shall be designated as N ₁ G.	

3.1.1 Light duty vehicle emissions testing

According to Delphi (2009) light duty emissions testing for the EU type approval consists of six tests as well as an evaluation of the OBD system installed in the test vehicle.

Table 3. 2: Light duty emissions evaluation tests (Delphi, 2008)

<u>Test</u>	<u>Description</u>
Type I	Tail pipe emissions after a cold engine start (part Transient testing).
Type II	CO emissions test at idling engine speed.
Type III	Emission of crankcase gases.
Type IV	Evaporative emissions.
Type V	Durability of anti-pollution devices
Type VI	Low temperature test
	OBD evaluation

"ECE regulations are similar to EU directives. A base regulation is updated with a consecutive series of amendments. Dates of implementation differ from country to country, depending on the approval status of the respective amendment in that country" (Delphi, 2009).

Figure 3. 1 shows the relation between the commonly referred to EURO standards in relation to their respective EU directive amendments as well as the equivalent USA and Japanese standards.

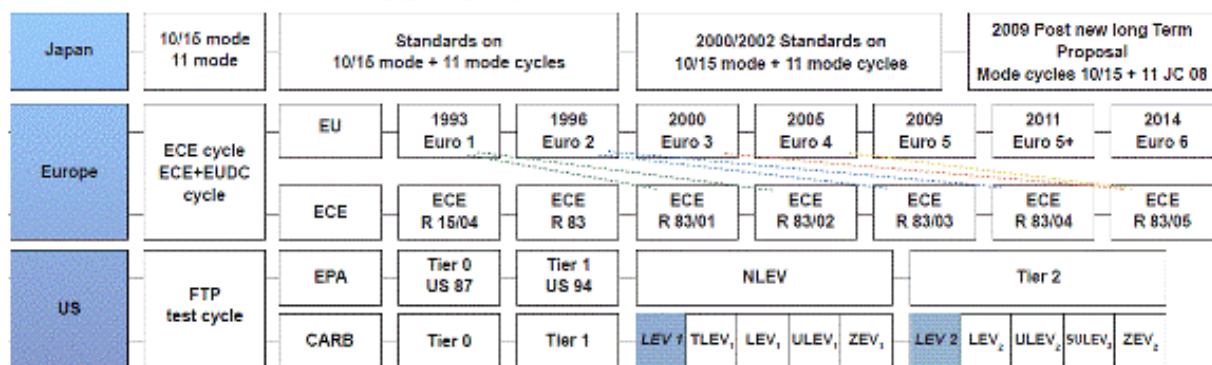


Figure 3. 1: Worldwide testing procedures and standards for light duty vehicles (Delphi, 2009)

For the purpose of this dissertation, the Type I test (Table 3. 1) was of interest. “The object of the test procedure is to establish the mass of each nominated exhaust component emitted during the test. The mass is computed from the measured concentrations of each pollutant in the known exhaust gas volume. Exhaust species are generated when the vehicle is operated on a chassis dynamometer according to the specified driving cycle” (Plint, 2009).

A brief overview of three common test cycles followed by a description of their applications is given below:

3.1.1.1 FTP test cycle

Bosch (2007) states that CARB and EPA Legislation prescribe the FTP 75 (Federal Test Procedure) for light duty vehicle emissions measurement. It continues to state “The FTP 75 test cycle consists of speed cycles that were actually recorded in commuter traffic in Los Angeles”. Delphi (2009) states as of 2004 the SFTP (Supplementary Federal Test Procedure) schedules came into full effect and consists of two driving cycles:

1. SC03
2. US06

Bosch (2007) stated that the extended tests were intended to examine the following additional driving conditions:

1. Aggressive driving.
2. Radical changes in vehicle speed.
3. Engine start and acceleration from a standing start.
4. Operation with frequent minor variations in speed.
5. Periods with vehicle parked.
6. Operation with air conditioner on.

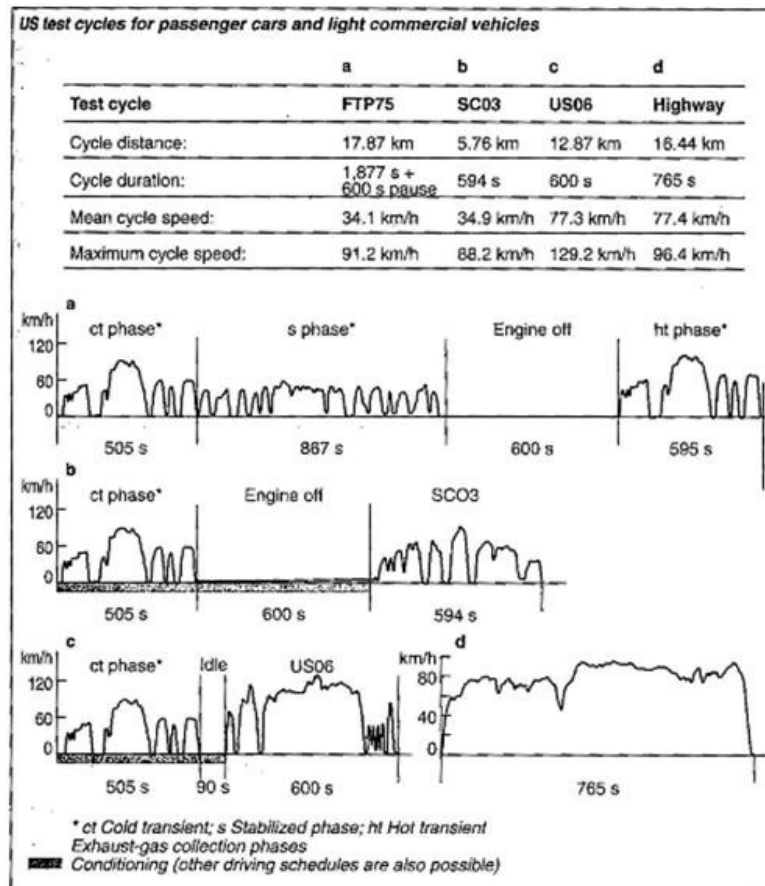


Figure 3. 2: US test cycles for passenger cars and light commercial vehicles Bosch (2007)

Figure 3. 2 depicts the US test cycles for light duty vehicles. Bosch (2007) states that the overall test results are based on a percentage ratio of the results of the various cycles but in addition “The SFTP and the FTP 75 test cycles must be successfully completed on an individual basis”.

3.1.1.2 ECE test cycle

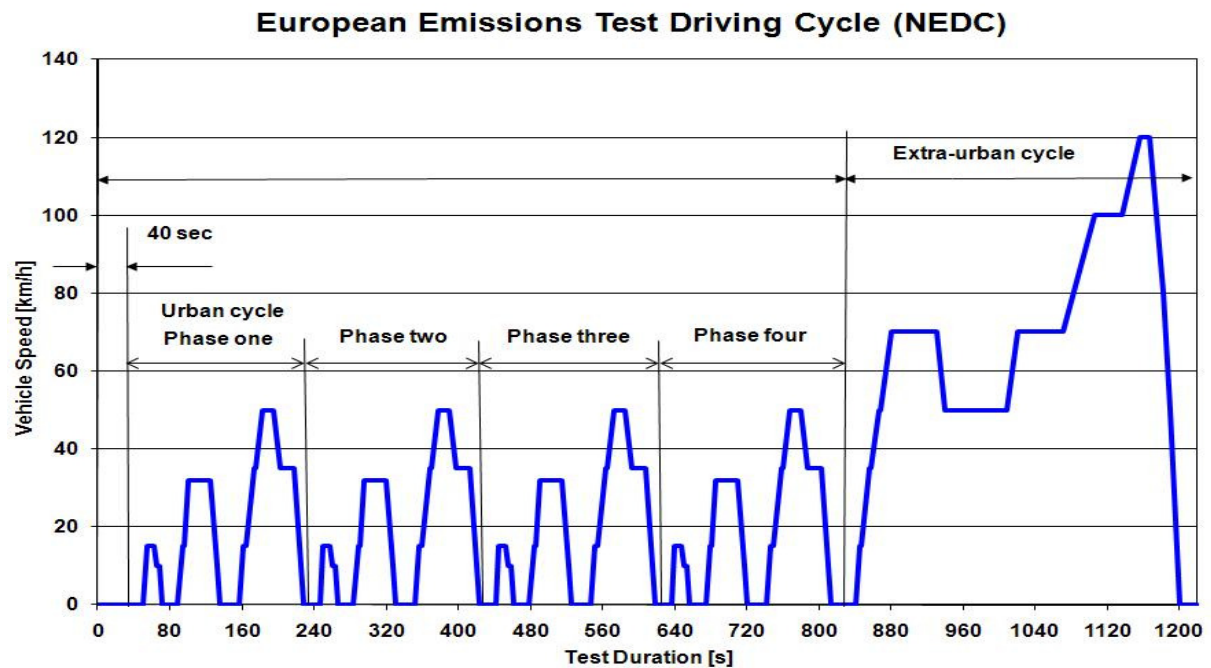


Figure 3. 3: ECE European test cycle (European Communities 2009)

Figure 3. 3 illustrates the New European Driving Cycle (NEDC), which is divided into two sections namely the Elementary Urban and the Extra-urban operating cycles. The Elementary Urban operating cycle is 195 seconds long with a theoretical distance of 1.013Km. It can be seen in Figure 3. 3 from 0-195 seconds and is repeated four times during the NEDC test cycle. The Extra-urban driving cycle is 400 seconds long with a theoretical distance of 6.955Km. It represents the high speed component of the driving cycle and is visible in Figure 3. 3 from 780-1190 seconds. According to Bosch (2007) the exhaust gas is collected in bags during the two phases. The pollutant mass is then measured and analyzed using the content of the bag with reference to the distance covered by the test vehicle.

3.1.1.3 Japanese test cycle

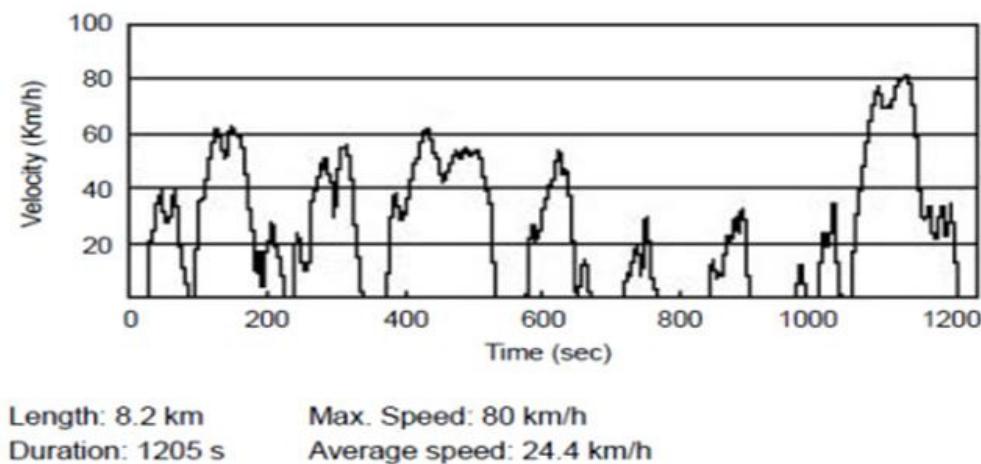


Figure 3. 4: Japanese JC08 test cycle (Delphi 2009: 46)

Bosch (2007) indicates that in 2008, a new Japanese test cycle, the JC08 would replace the existing 11-mode cycle as the cold start test which forms part of its two test cycles. In addition as of 2011 only the JC08 would continue to be used, thereby also replacing the existing 10·15-mode hot-start test cycle. Delphi (2009) states that an Amendment that occurred in November 2007, legislated the JC08 as the replacement cycle for both existing cycles as of October 2009. Figure 3. 4 illustrates the Japanese JC08 emissions test cycle.

3.1.1.4 Light duty cycle application

Bosch (2007) indicates that the methods used to test a vehicle's emissions on a chassis dynamometer are defined to simulate actual vehicle operation on the road as far as possible. "The driven wheels of the vehicle under test are placed on rotating rollers. This means that the forces acting on the vehicle, i.e. the vehicle's moments of inertia, rolling resistance and aerodynamic drag, must be simulated so that the trip on the test bench reproduces the emissions comparable to those obtained during an on-road trip" (Bosch, 2007). Furthermore, more modern chassis dynamometers use flywheel simulation while older test benches use real flywheels of different sizes to simulate the vehicle mass. "The test cycle is repeated by a driver in the vehicle. The required and current vehicle speeds are displayed on a driver control-station monitor. In some cases, an automated driving system replaces the driver to increase the reproducibility of the test results".

The SANS (2009) states that in the case of a dynamometer with a fixed load curve, the accuracy of the load settings at 80Km/h shall be $\pm 5\%$ per cent. In the case of dynamometers with adjustable load curve, the accuracy of matching dynamometer load to the road load shall be ± 5 per cent at 120, 100, 80, 60, 40Km/h and ± 10 per cent at 20Km/h. It continues with "A tolerance of ± 2 Km/h shall be allowed between the indicated speed and the theoretical speed during acceleration, steady speed, and deceleration when the vehicles brakes are used. The Standard indicates that gear changes are made at specified points in the cycle and that the

cycle allows 2 seconds in which a change must occur. Vehicles with more gears than explicitly specified in the cycle can still be tested; however the driver may only shift up through the additional gear/s at selected specified points in the cycle. Automatic transmission vehicles may also be tested although the test must be conducted with the transmission in its highest gear (Drive) and must operate as it would be under normal driving conditions. “Vehicle which does not attain the acceleration and maximum speed values required in the operating cycle shall be operated with the accelerator control fully depressed until they once again reach the required operating cycle” (SANS, 2009). The National standard dictates that the tyre pressure be set to the manufacturer’s specification but may be increase by up to 50% for a two-roller dynamometer. The airflow over the vehicle must be simulated via a variable speed fan or blower with an operating range of 10Km/h to 50Km/h with a tolerance of ± 5 Km/h.

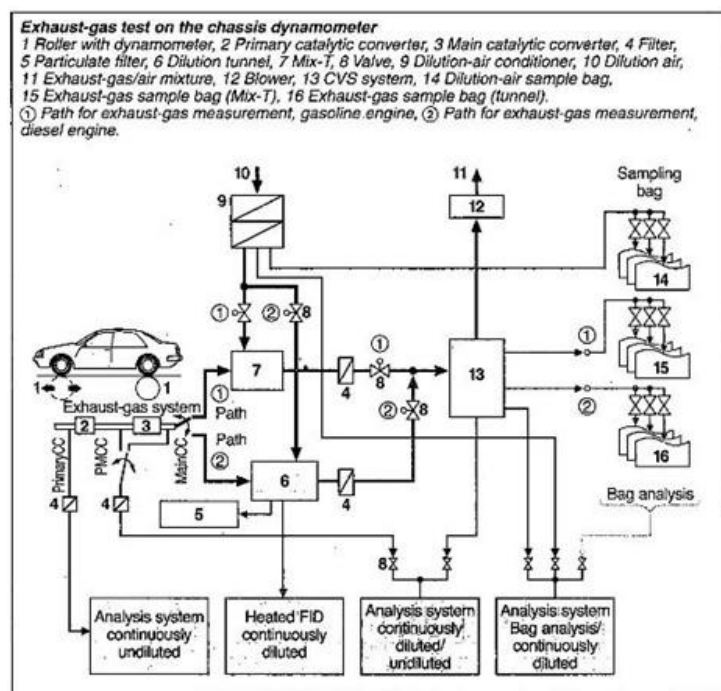


Figure 3. 5: Light duty vehicle emissions test set-up (Bosch 2007)

From SANS (2009) the connecting tube between the vehicle and the emissions measurement dilution system should be as short as possible with a maximum length of 6.1m if heat insulated. After the exhaust gas has been diluted in the dilution tunnel, the intended sample gas is stored in bags using a CVS method until analyzed. This test system layout is depicted in Figure 3. 5. Analysis must occur within 20 minutes of being sampled. “The EU standards specify emission limits for the following pollutants” (Bosch, 2007):

1. Carbon Monoxide (CO)
2. Hydrocarbons (HCs)
3. Nitrogen oxides (NO_x)
4. Particulates, although these limits are initially restricted to diesel vehicles.

To measure the exhaust emissions from a diesel engine, some changes or additional measurements are required over and above the requirements for gasoline engines. “The complete sample-taking system including the exhaust-gas measuring device for hydrocarbons must be heated to 190°C” states Bosch (2009) with reference to diesel emissions measurement. It is indicated that this heating requirement was needed to prevent the condensation of hydrocarbons, which have high boiling points, as well as to evaporate the hydrocarbons that may have already condensed in the diesel exhaust gas.

3.1.2 Heavy duty vehicle emissions testing

Heavy commercial vehicles have been tested on an engine test bench in a transient driving scheme since 1987. As with light duty vehicle emissions testing, the most commonly referred to heavy duty test cycles are those of the USA, the European community and Japan. The following sections will discuss these three heavy duty test cycles and will conclude with an overview of the test cycles application and implementation.

3.1.2.1 FTP test cycle

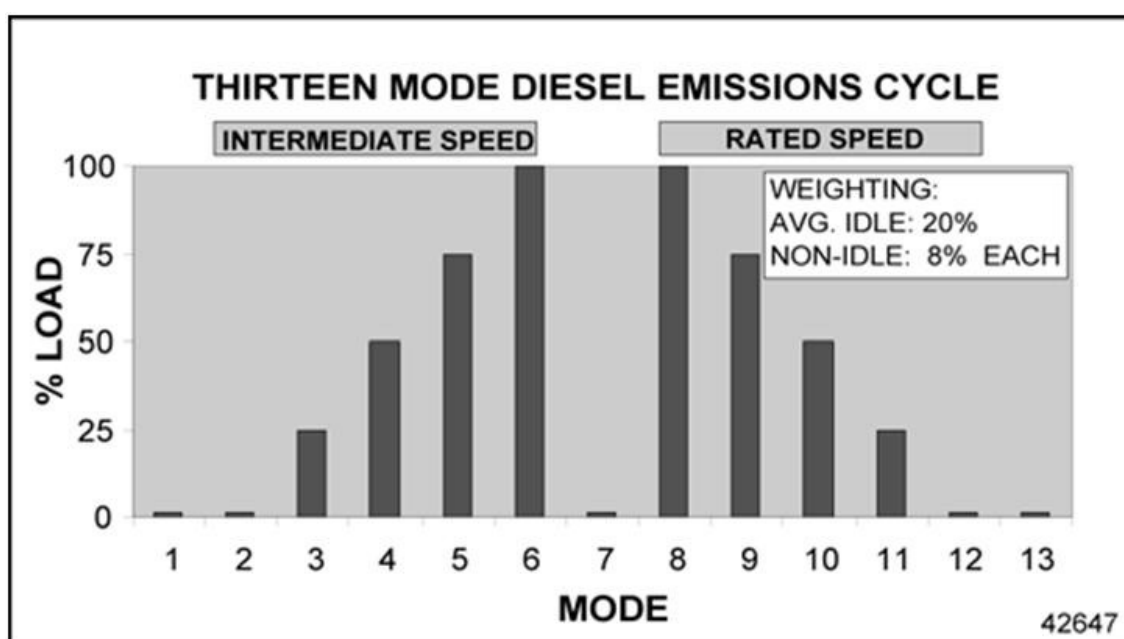


Figure 3. 6: Thirteen mode diesel emissions steady state test cycle (Merrion 2003)

According to Merrion (2003) heavy duty transient engine testing replaced steady state testing conducted using the existing thirteen-mode steady state cycle shown in Figure 3. 6. The thirteen-mode steady state cycle was first adopted by the EPA in 1974. This was four years after the EPA was formed to enforce the Federal Air Qualities Act that was enacted in 1970 in the USA. The reason for the continuous change to transient testing is that the engines speed and torque combinations found in a steady-state test have little relationship to actual patterns of use. Furthermore, steady-state tests only sample selected operating modes and are therefore easier to defeat than transient tests.

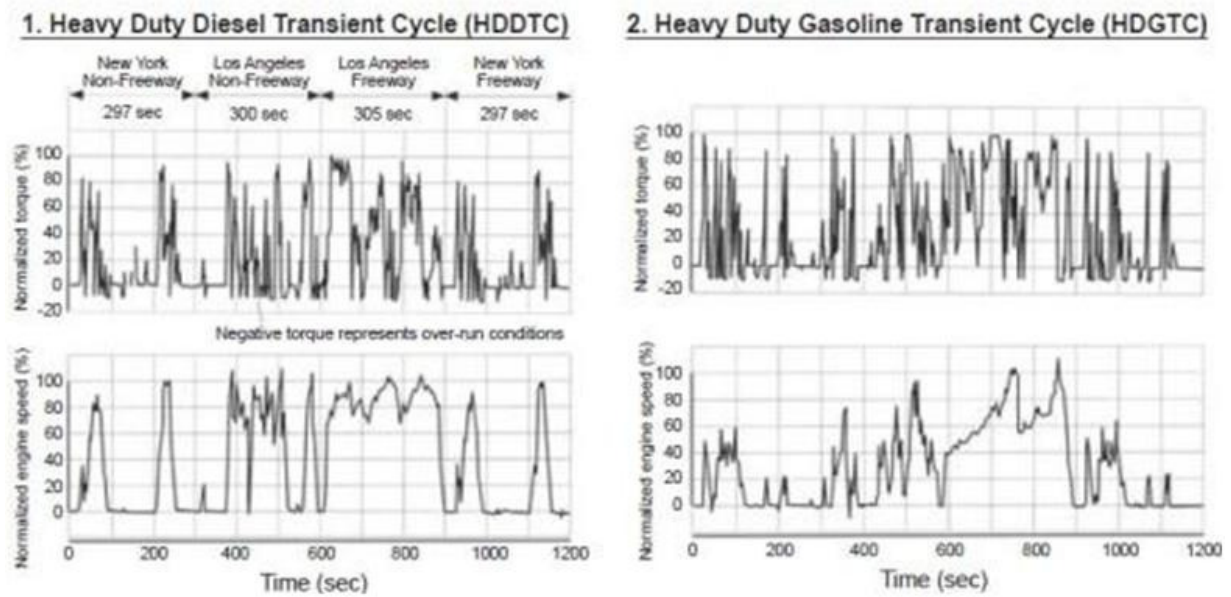


Figure 3. 7: FTP transient driving schedule for diesel and gasoline heavy duty engines (Delphi 2008)

According to Bosch (2007) the American FTP test cycle is the simulation or basic equivalent to operating an engine under realistic road-traffic conditions. Delphi (2009) says the test cycle comprises of four phases representing different driving conditions. The FTP also has different HD transient cycles for diesel engines and gasoline engines, as shown in Figure 3. 7. There is an additional cycle, the Federal Smoke Cycle that is used to test exhaust-gas opacity under dynamic and quasi steady-state conditions. Bosch (2007) explains that vehicles models from the beginning of year 2007 that are intent on meeting US emission limits must also comply with the European Community 13-stage test (ESC).

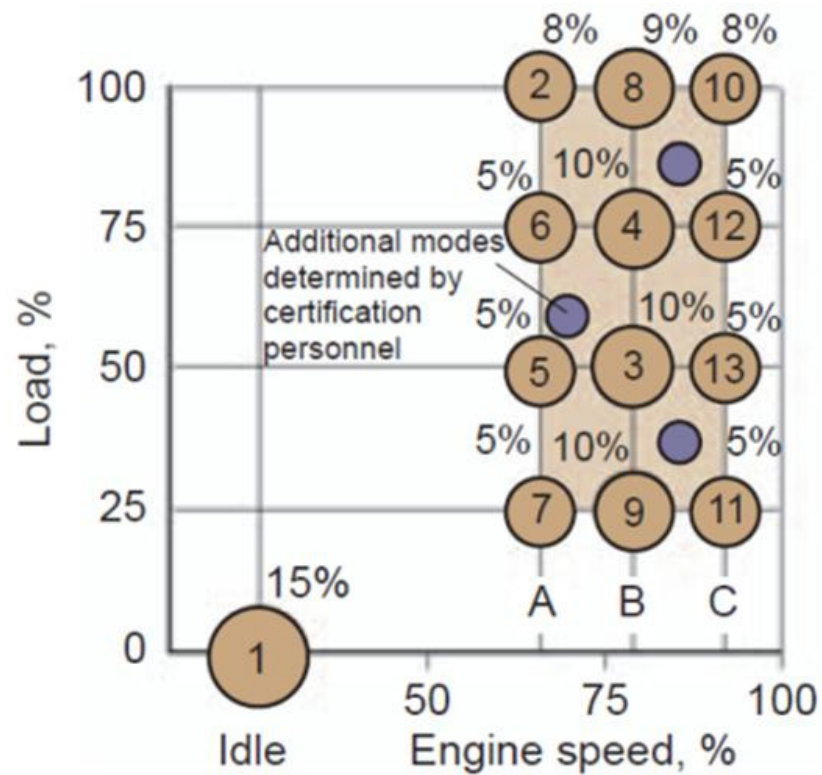


Figure 3. 8: European Communities 13-stage steady state heavy duty emissions test cycle (Delphi, 2008)

The 13-mode test cycle consists of thirteen different loads versus speed stages as can be seen in Figure 3. 8. There is one idle stage at the beginning of the test and three random test points within a set range. The engine's gaseous emissions are tested with varying amounts of load at three speed points calculated using the engine speed values where maximum power and torque occur.

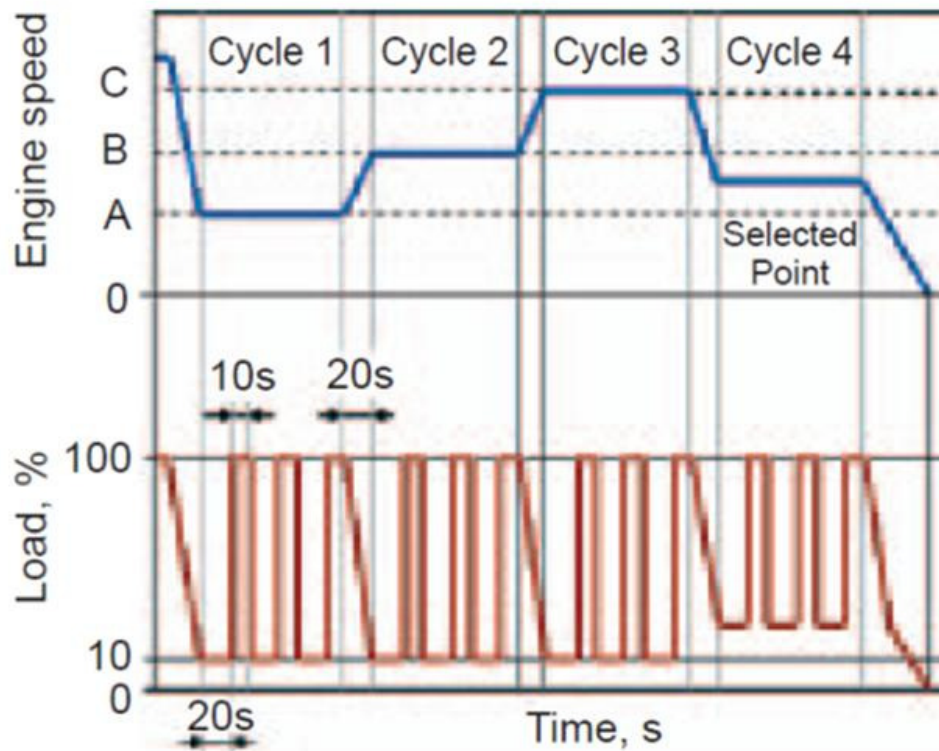


Figure 3. 9: Load response heavy duty emissions test cycle (Delphi, 2008)

According to Delphi (2009) the load response test as applied in the USA by the FTP (seen in Figure 3. 9) is a steady state test where diesel smoke opacity is measured. There are 3 engine test speeds and 2 load points which are altered during each stage (10% and 100% loads). There is also a random 4th stage present set at a random speed and initial load.

3.1.2.2 ECE test cycle

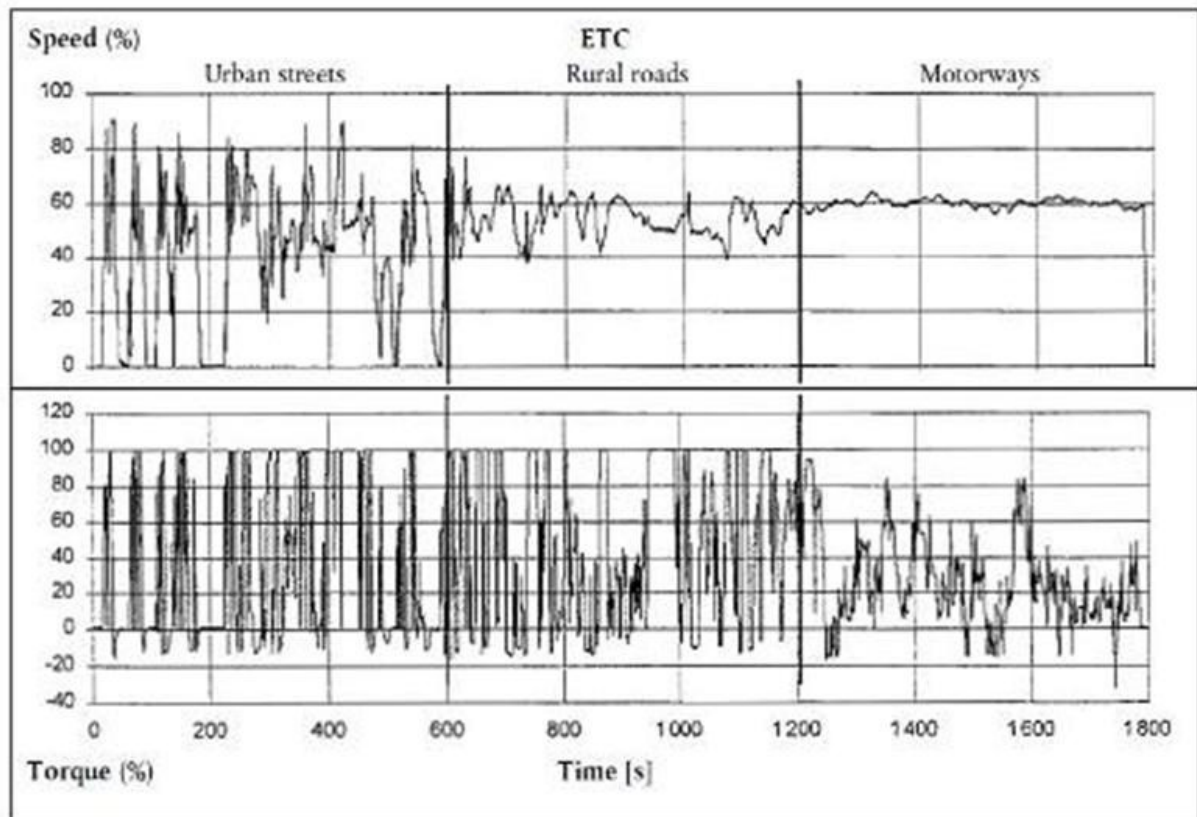


Figure 3. 10: European Transient diesel and gasoline heavy duty emission test cycle (European communities, 1999)

The European heavy duty transient cycle is divided into three stages; 1/3 urban, 1/3 rural and 1/3 motorway sections. “The cycle consists of a second-by-second sequence of transient modes. It is based on road-type-specific driving patterns of HD engines installed in trucks and busses” (Delphi, 2009). Load and engine speed are stated as a percentage function of the maximum engine speed and torque output of the test engine, as can be seen in Figure 3. 10. This will therefore result in different test set points for engines with varying steady state outputs. Opposed to the strategy of varying diesel and gasoline transient tests adapted by the FTP, the European Community use the ETC cycle for emissions testing of both diesel and gasoline engines.

As with the FTP legislation, vehicle attempting to comply with EU legislation is also required to pass European Communities defined 13-stage test cycle as is show in Figure 3. 8.

3.1.2.3 Japanese test cycle

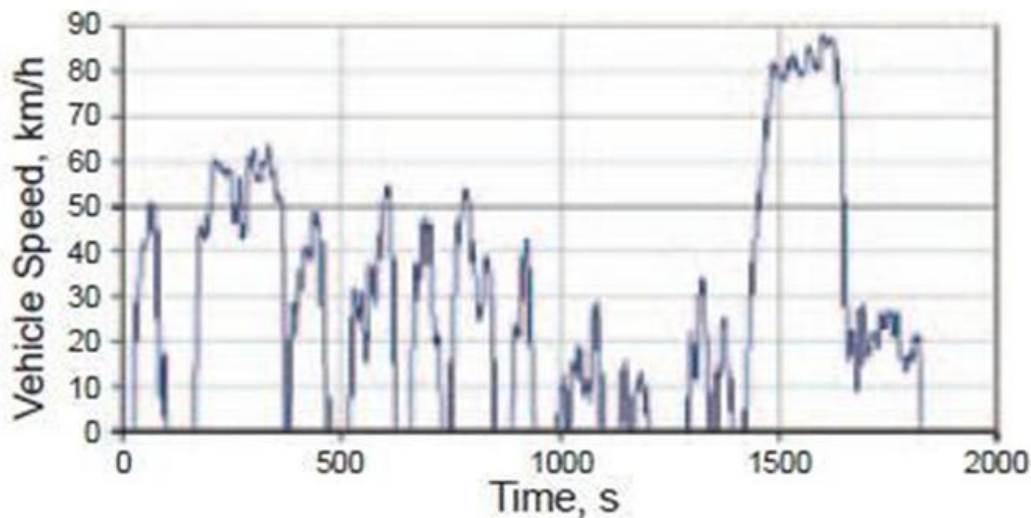


Figure 3. 11: (Delphi, 2008) Japanese JC05 transient emissions cycle for diesel and gasoline vehicles

Delphi (2009) states that the Japanese JE05 cycle became effective in 2005 for both diesel and gasoline applications. It continues to state that the cycle was based on Tokyo driving conditions and that the cycle is defined through vehicle speed versus time points that require conversion to engine conditions unlike the European and US cycle which are already defined by engine speed. The JE05 transient cycle is supplementary to the Japanese 13-mode diesel cycle or the Japanese 13-mode gasoline cycle.

3.1.2.4 Heavy duty cycle application

Bosch (2007) states that all test cycles for heavy commercial vehicles are run on an engine test bed. "For generating the ETC on a test cell, the engine needs to be mapped prior to the test cycle for determining the speed vs. torque curve" (European Communities, 1999). It continues to state that the determined values then undergo an unnormalization procedure thereby providing the values for the driving cycle.

The emissions measurement procedure has been described as follows "During the prescribed transient cycle of warmed-up engine operating conditions, which is based closely on road-type-specific driving patterns of heavy-duty engines installed in trucks and buses, the above pollutants shall be examined after diluting the total exhaust gas with conditioned ambient air. Using the engine torque and speed feedback signals of the engine dynamometer, the power shall be integrated with respect to time of the cycle resulting in the work produced by the engine over the cycle. The concentration of NO_x and HC shall be determined over the cycle by integration of the analyzers signal. The concentration of CO, CO_2 , and NMHC may be determined by integration of the analyzer signal or by sample bag. For particulates, a proportional sample shall be collected on a suitable filter. The diluted exhaust gas flow rate shall be determined over the cycle to calculate the emission value of the pollutants. The mass

emission value shall be related to the engine work to get the grams of each pollutant emitted per kilowatt hour” (European Communities, 1999).

The European Communities (1999) require that the engine speed and torque command set points be issued at 5Hz (10Hz recommended or greater). Feedback engine speed and torque are required to be recorded at least once every second during the test cycle, although the signals may be electronically filtered.

Bosch (2007) states that for non-stationary test cycles, the exhaust gases be collected and analyzed using the CVS method.

3.1.3 Emissions test equipment

Emissions measurement and quantification of internal combustion engines is a demanding exercise. Plint (1999) states that where emissions measurements are concerned, one is required to move into a totally different and very sophisticated field of instrumentation engineering. The apparatus makes use of subtle and difficult techniques borrowed from the field of physics. The following sections describe the fundamental equipment currently used for emissions measurement.

3.1.3.1 Emission chassis dynamometer

Plint (1995) while discussing chassis dynamometers used for light duty emissions testing states that standard emissions tests developed in the USA in the 1970’s were based on a rolling road dynamometer developed by the Clayton Company. These dynamometers have twin rollers of 220mm diameter and this became a de facto standard despite its limitations. Further more recent legislation by the US Environmental Protection Agency has called for machines having a single pair of rollers of diameter 122cm and electronic inertia simulation.

According to SANS (2009) dynamometer for light duty testing shall be capable of simulating road load with one of the following classifications:

1. Dynamometer with a fixed load curve, i.e. a dynamometer whose physical characteristics provide a fixed load curve shape.
2. Dynamometer with an adjustable load curve, i.e. a dynamometer with at least two road load parameters that can be adjusted to shape the load curve.

The standard continues to state that electronic inertia simulation may be used and that a dynamometer with one or two rollers is acceptable as long as the front roller is directly or indirectly coupled to the inertial mass and the power absorption unit.

SANS (2009) states that in the event that the dynamometer cannot reproduce the total resistance to progress on a chassis dynamometer between the vehicles speeds of 10km/h and 120km/h, the load absorbed by the dynamometer between the speeds of 10km/h and 120km/h should be as follows:

$$F = (a + b \cdot U^2) \pm 0.1 \cdot F_{80}$$

3-1

The value of F should not be negative.

Where:

F	=	total load absorbed by the dynamometer (N)
a	=	value equivalent to rolling resistance (N)
b	=	value equivalent to coefficient of air resistance ($\text{N}/(\text{km/h})^2$)
U	=	vehicle speed (km/h)
F_{80}	=	load at 80 km/h (N)

The Standard continues to specify the following restrictions:

1. It should be possible to measure, read and indicate load to an accuracy of ± 5 per cent.
2. The total inertia of the rotating parts (including the simulated inertia where applicable) shall be known and shall be within $\pm 20\text{Kg}$ of the inertia class for the test.
3. The speed of the vehicle shall be measured by the speed of rotation of the roller. It shall be measured within an accuracy of $\pm 1\text{Km/h}$ at a speed above 10Km/h .

3.1.3.2 Gaseous-emission measurement instrumentation

SANS (2009) states that a full flow dilution tunnel shall be used for emissions measurement of light duty vehicles. The European Communities (1999, which is the same standard used by South Africa for the regulation of heavy duty vehicle emissions measurement, states that the determination of gaseous and particulate emissions while conducting a European Transient Cycle may only be measured using a full flow dilution system. A partial flow system may be used, if its equivalence to a full flow system can be determined by a technical service. However, the full flow tunnel will be regarded as the reference. Bosch (2007) states that the most commonly used method of collection of exhaust gas from a dilution tunnel is by the CVS (Constant Volume Sampling) dilution procedure. The objectives of the elaborate exhaust sampling process are as follows:

1. The prevention of water vapor from condensing which may result in a loss of nitrogen oxides.
2. The prevention of secondary reactions from occurring in the collected exhaust gas.

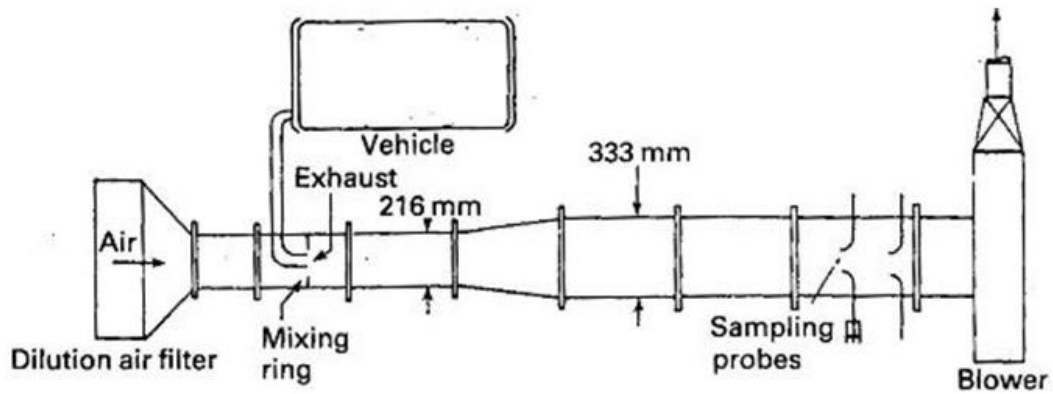


Figure 3. 12: Exhaust gas dilution tunnel (Plint, 1999)

Horiba's (2010) CVS system operates by allowing the exhaust gas to flow into a mixing tee where it is diluted with ambient air to prevent water condensation. After dilution the diluted-exhaust gas enters the sampling unit where its flow rate and volume are measured. Samples are then extracted proportionally before the critical flow venturi or the bulk stream venturi (depending on the type of dilution tunnel) and stored in sample bags. The mass of HC, CO, NO_x, CO₂ and CH₄ is then calculated from the gas concentrations in the bag.

In the Bosch system the vehicle exhaust gas is diluted with conditioned ambient air at a mean ratio between 1:5 and 1:10. The diluted gas is extracted in such a way that the total volumetric airflow composed of exhaust gas and dilution air is constant. The admixture of dilution air is therefore dependent on the momentary exhaust-gas volumetric flow. The volumetric flow during sampling remains constant during the bag filling phase.

Plint (1999) provides a table expressing gas emissions analysis techniques, as shown below:

Table 3. 3: Techniques of emissions analysis (Plint, 1999)

Gas	Technique	Typical range	90% Response time
CO	Non-dispersive Infra-red (NDIR)	0-3000ppm	2-5s
CO ₂	Non-dispersive Infra-red (NDIR)	0-20%	2-5s
NO _x	Chemiluminescence	0-10000ppm	1.5-2s
Unburned hydrocarbons (UHC)	Flame ionization Detector (FID) Fast FID	0-10000ppm	1-2s 1-2ms
Hydrocarbon species, CH ₄ , SO ₂ , acids, etc	Infra-red (FTIR)		5-15s

According to Bosch, particulates are measured for diesel engines. AVL (2010) states that EURO 5 and 6 legislation requires the mass and the number of particles in the vehicle exhaust emissions to be measured. According to Plint this measurement must be done using the CVS

measurement method. This is due to the fact that the makeup of a smoke particle in the exhaust pipe differs from that of the same particle after it has left the exhaust pipe and enters the atmosphere.

Bosch explains that legislation dictates that the gravimetric process should be the method used to measure the emissions particulate mass. This method entails removing a sample of diluted exhaust gas from the dilution tunnel during the driving test. This sample is then channeled through a particulate filter which is weighed before and after the test. The particulate emission is then determined using this loading, the total volume of diluted exhaust gas, and the partial volume channeled through the particulate filter.

The following explanation to a particulate counting method is given: “After a first hot dilution at 150°C, the sample is transported to an evaporation tube, where the remaining volatile components are transferred into the gaseous phase. After a secondary dilution, the particles are detected and counted using the light-scattering method” AVL (2010).

3.2 Road Load and Vehicle Simulation

Mathematics has been used to model vehicles actions and responses since the invention of the automobile. “A part-load power level useful as a reference point for testing automobile engines is the power required to drive a vehicle on a level road at a steady speed. Called road-load power, this power overcomes the rolling resistance which arises from the friction of the tyres and the aerodynamic drag of the vehicle” (Heywood, 1988). The power demands from an automotive engine depend on a large number of factors. These factors are based on driving conditions and are unique to any particular vehicle (Plint, 1999).

From Heywood (1988):

$$P_r = (f_r M_v g + 0.5 \rho C_D A_v V^2) V \quad 3-2$$

Plint (1995) explains that the road load equation describes the performance of the modeled vehicle and specifies the engine torque in terms of the following parameters:

1. Total mass of the vehicle + load
2. Rolling resistance
3. Wind resistance
4. Slope

Plint (1999) provides the following equation:

$$P_r = a_0 + a_1 + a_2 V^2 + M \frac{dV}{dt} + M g \sin \theta \quad 3-3$$









Where:

a_0 = Constant component of rolling resistance, N

$a_1 V$ = Speed dependant component, N
 $a_2 V^2$ = Aerodynamic resistance, N
 M = Mass of vehicle, kg
 θ = Slope of road surface

The total running resistance of a vehicle is the sum of the rolling resistance, the aerodynamic resistance and the climbing resistance (Bosch, 2007). This statement concurs with the previous statement made by Plint (1999).

3.2.1 Aerodynamic drag force

	Coefficient of aerodynamic drag C_{dr}	Aerodynamic drag in kW, mean values for $A = 2 \text{ m}^2$ and at various speeds ¹⁾			
		40 km/h	80 km/h	120 km/h	160 km/h
 Open convertible	0.33...0.50	0.70	5.3	18	42
 Offroad vehicle	0.35...0.50	0.71	5.5	19	44
 Notchback sedan (conventional shape)	0.26...0.35	0.50	3.8	13	31
 Station wagon	0.30...0.34	0.52	4.1	14	33
 Wedge shape, headlamps and bumpers integrated in body, wheels covered, underbody paneling, optimized flow of cooling air	0.3...0.4	0.58	4.6	16	37
 Headlamps and all wheels enclosed within body; underbody paneled	0.2...0.25	0.37	3.0	10	24
 Reversed wedge shape (minimal cross-section at tail)	0.23	0.38	3.0	10	24
 Optimum streamlining	0.15...0.20	0.29	2.3	7.8	18
Trucks, truck-trailer combinations	0.8...1.5	—	—	—	—
Motorcycles	0.6...0.7	—	—	—	—
Buses	0.6...0.7	—	—	—	—
Streamlined buses	0.3...0.4	—	—	—	—

¹⁾ No headwind ($v_0 = 0$).

Figure 3. 13: Coefficients of aerodynamic drag and associated power requirements for various body configurations (Bosch, 2007)

“The drag on a body in a moving fluid is a difficult quantity to determine, since it will be seen soon to depend on things such as the location of the transition from laminar to turbulent flow in the boundary layer as well as the location of separation, to name just two difficulties” (Shames, 2003). Bosch (2007) provides the following equation defining a vehicle’s aerodynamic drag.

$$F_A = C_D A_v \frac{\rho V^2}{2} \quad 3-4$$

C_D , the coefficient of drag is usually determined empirically in a wind tunnel with a measured drag force, calculated frontal area and a known fluid/gas density and fluid/gas velocity. Other empirical and theoretical methods of calculating the coefficient of drag do exist. Bosch (2007) provides a simple empirical method of determining the aerodynamic resistance of a vehicle.

As can be seen in Equation 3-4, aerodynamic drag force increases proportionally to the square of the vehicle's velocity, therefore the higher the simulated vehicle velocity, the more critical this component.

3.2.2 Rolling resistance

"In a sense, the most important of the resisting forces is the rolling resistance. While other resistances act only under certain conditions of motion, the rolling resistance is present from the instant the wheels begin to turn" (Taborek, 1957). Sources of the rolling resistance on pneumatic tyres are:

1. Work performed by flexing of the tyre body as it passes the ground contact area.
2. Work performed by the wheel penetrating or compressing the ground.
3. Work performed by frictional motion due to tyre slip.
4. Friction caused by air circulation inside the tyre and the fan effect of the rotating wheel on the outside air.

The first two of these factors account for the greater part of the rolling resistance while the remaining two only have secondary effects. Rolling resistance is defined by:

$$F_r = f_r W \cos \theta \quad 3-5$$

where the f_r component is the coefficient of rolling resistance and $W \cos \theta$ is the normal-to-ground component of the vehicle weight.

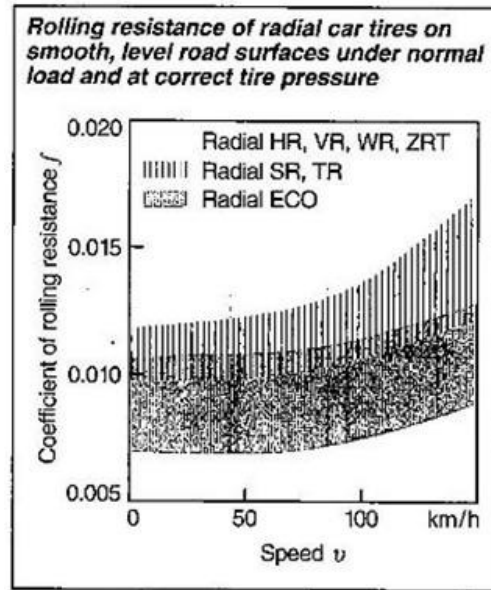


Figure 3. 14: Rolling resistance of radial car tyres on a road surface (Bosch, 2007)

According to Tamborek (1957) the coefficient of rolling resistance expresses the effects of complicated and interdependent physical properties of the tyre and ground. The coefficient cannot be simply calculated due to the vast amount of factors influencing it. Some of the most influential factors affecting rolling resistance are:

1. Ground-Surface Structure
2. Ground Elasticity
3. Tyre material and construction
4. Pressure and load
5. Temperature
6. Rotational velocity
7. Tyre geometry

It is virtually impossible to devise a formula that takes all the above factors into account. Even so, several equations have been developed for passenger-car tyres rolling on concrete surfaces.

“Relatively accurate values of f_r for concrete surfaces can as a function of speed be calculated from the following equation developed at the Institute of Technology in Stuttgart” (Taborek, 1957):

$$f_r = f_0 + 3.24f_1 \left(\frac{V}{44.704} \right)^{2.5} \quad 3-6$$

The constants f_0 and f_1 are derived from the following graph:

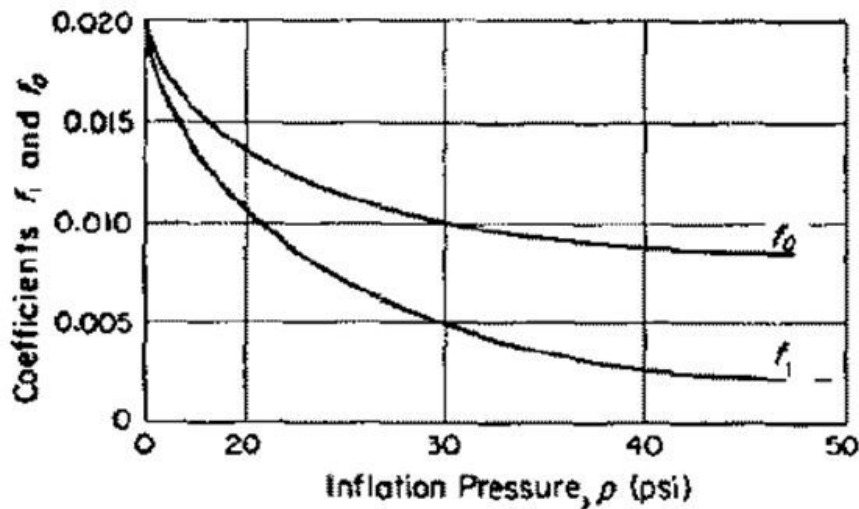


Figure 3. 15: Determination of f_0 and f_1 (Taborek 2005)

Although this equation is developed for concrete, the coefficient of rolling resistance is similar to that for tarmac. It is safe for the purpose of this model, to use this equation for use on tarmac surfaces.

3.2.3 Vehicle and rotating component Inertia's

Most transient testing is concerned with confirming the performance of a given vehicle rather than with detailed development of engines or transmissions (Plint, 1999). The most obvious way of dealing with (reducing) large acceleration terms is by the use of flywheels which are added to rolling road dynamometer to bring the inertia up to the required level. Disadvantages caused by the use of flywheels for vehicle inertia simulation, are provided below:

1. The flywheel may be quite massive and must be mounted very accurately if vibration is to be avoided.
2. The large amount of energy involved when the flywheels are running at speed must be contained with safety. Specially designed shut-down and alarm trips are required.
3. The use of flywheels render the dynamometer unsuitable for testing requiring rapid load changes and to deal with this problem there is a move towards computer simulation of inertia by rapid manipulation of the dynamometer load.

From Newton's second law:

$$F = Ma \quad 3-7$$

Plint (1999) provides the following term in his road load equation to account for vehicle inertia:

$$F = M \frac{dV}{dt} \quad 3-8$$

Using the overall drivetrain ratio and wheel diameter, this force can be calculated into a torque load at the engine flywheel.

Conradie (2001) provides the following relationship:

$$J_v = J_{vl} + J_{dt} \quad 3-9$$

In addition a means of determining equivalent vehicle inertia based on the overall gear ratio as well as a defined mass factor has been provided. The effective vehicle rotational inertia as seen at the clutch could be calculated from the effective mass and wheel radius by:

$$J_{vl} = \frac{f_m M R^2}{G_{ft}^2} \quad 3-10$$

The mass factor is defined as:

$$f_m = 1 + 0.04 + 0.0025 G_{ft}^2 \quad 3-11$$

The drive-train inertia is defined as follows:

$$J_{dt} = J_c + \frac{1}{G_t^2} \left\{ J_t + J_{dr} + \frac{1}{G_f^2} (J_f + J_w) \right\} \quad 3-12$$

The equivalent vehicle/dynamometer inertia of a rolling road dynamometer is defined as follows by SANS (2009):

$$I = I_m + (F_l / \gamma) \quad 3-13$$

where

I	=	Total inertia of the dynamometer (Equivalent inertia of the vehicle stated in Kg)
I_m	=	Inertia of the mechanical masses of the dynamometer (can be measured on the dynamometer or calculated by traditional methods)
F_l	=	Inertia force
γ	=	Tangential acceleration of roller surface

Equation 3-13 is derived from the rotational analog of the linear Equation 3-7:

$$T = I \alpha \quad 3-14$$

The rotating components of the drivetrain also contribute to the overall vehicle inertia however they are not simulated on a rolling road dynamometer as their contribution is the same on the rolling road as it would be on the actual road. Using traditional methods during vehicle component development, the inertia of the various powertrain components would be determined. Although not done on rolling roads, the load effect of a powertrain during transient running can be simulated using Equation 3-14 in conjunction to the individual component inertia.

3.3 Real-Time Computing

Hailperin (2007) defines an operating system as software that uses the hardware resources of a computer system to provide support for the execution of other software. He indicates that an operating system provides the following services:

1. The Operating system allows multiple computations to take place concurrently on a single computer system. It divides the hardware's time between the computations and handles that shift the focus between the computations.
2. The operating system controls interaction between the concurrent computations.
3. The operating system can provide support for controlled interaction of computations spread among different computer systems by using networking.

Hailperin (2007) explains that not all systems require an operating system. Some embedded systems make use of a single program directly executed by the embedded processor. More sophisticated embedded systems run multiple cooperating programs and use operating systems.

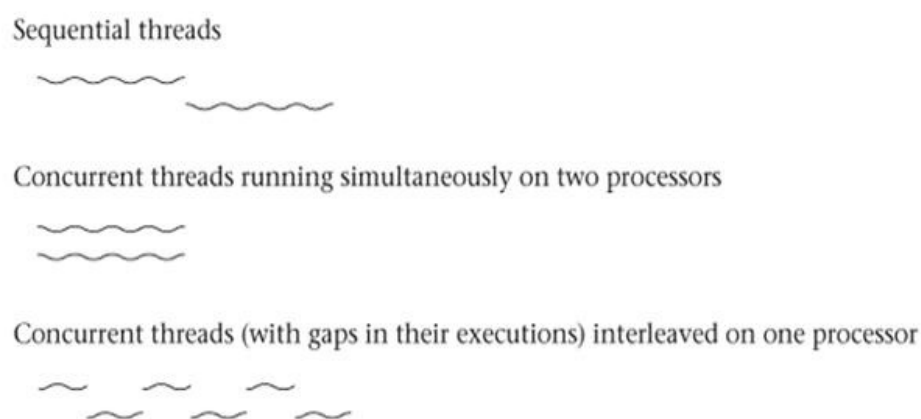


Figure 3. 16: Sequential and concurrent threads (Hailperin, 2007)

According to Hailperin (2007) a thread is the fundamental unit of concurrency. Any one sequence of programmed actions is a thread. A thread's lifetime extends from the time its first instruction executes until the time of its last instruction execution. If two threads have overlapping lifetime they are said to be concurrent.

Regular operating systems make use of concurrent threads to allow multiple programs or in the case of a single program; multiple processes to appear as though they occur at the same time. A single core PC can only process one thread at a time but may have many active threads in waiting.

“Cooperative multitasking, that is, where each thread's program contains explicit code at each point where a thread switch should occur. However, more realistic operating systems use what

is called Preemptive multitasking, in which the program's code need not contain any thread switches, yet thread switches will nonetheless automatically be performed from time to time" (Hailperin, 2007). Preemptive multitasking makes use of interrupts to stop a running thread and swap out the running thread for a thread with a higher priority. To stop a high priority thread from using all the processing time until the threads completion, the priority of waiting threads is continuously reassessed and increased until one of the waiting threads has a higher priority than the running thread at which stage the running thread is stopped via interrupt. Threads are also allocated time slices which are the maximum time a single thread can run without giving another waiting thread processing time.

Although this is just one example of a multithreading strategy, these types of employed strategies are effective for the day-to-day user but do not allow for deterministic running of a specific set of threads. A simple example of this is a time critical thread not being completed on time due to it being preempted by a higher priority thread of a non deterministic nature e.g. a key stroke or mouse click.

Sommerville (2004) defines a real-time system as one where the correct functioning of the system, depends on the results produced by the software and the time at which these results are produced. A soft real-time system is a system whose operation is degraded if results are not produced according to the specified timing requirements. A hard real-time system is a system whose operation is incorrect if results are not produced according to the specification.

Sommerville (2004) continues to explain that real-time computers interact directly with hardware devices and require embedded real-time software that must react to events generated by the hardware and issue control signals in response to these events. Event stimuli fall into two classes:

1. Periodic stimuli: These occur at predictable time intervals
2. Aperiodic stimuli: These occur irregularly. They are usually signaled using the computer's interrupt mechanism

Sommerville (2004) indicates that programming languages used for real-time system development need to include facilities to access the system hardware and it should be possible to predict the timing of particular operations in these languages. The advantage of using low-level system programming languages such as C is that it allows the development of very efficient programs. "These languages do not include constructs to support concurrency or the management of shared resources. These are implemented through calls to the real-time operating system that cannot be checked by the compiler, so programming errors are more lightly" (Sommerville, 2004). Events rather than objects or functions should be the center to the real-time software design process. Six interleaved stages of the real-time software design process are listed below:

1. Identify the stimuli that the system must process and the associated responses

2. For each stimulus and associated response, identify the timing constraints that apply to both stimulus and response processing
3. Choose an execution platform for the system: The hardware and the real-time operating system to be used. Factor that influence these choices include the timing constraints on the system, limitations on power available, the experience of the development team and the price target for the delivered system
4. Aggregate the stimulus and response processing into a number of concurrent processes
5. For each stimulus and response, design algorithms to carry out the required computations. Algorithm designs often have to be developed relatively early in the design process to give an indication of the amount of processing required and the time required to complete that processing
6. Design a scheduling system that will ensure that processes are started in time to meet their deadlines

Sommerville (2004) suggests that a timing analysis be performed for real-time system however this may be difficult as aperiodic stimuli are unpredictable and therefore requiring designers to make assumptions about the probability of these stimuli occurring as well as their impact on a system. UML modeling of real-time systems as state machine models is a good, language-independent way of representing the design of a real-time system and is therefore an integral part of real-time system design method.

Sommerville (2004) states that all but the very simplest embedded systems now work in conjunction with real-time operating systems. The real-time operating system manages processes and resources allocation in a real-time system. All except the simplest systems usually include:

1. A real-time clock: This provides information to schedule processes periodically
2. An interrupt handler: This manages aperiodic requests for service
3. A scheduler: This component is responsible for examining the processes that can be executed and choosing one of these for execution
4. A resource manager: Given a process that is scheduled for execution, the resource manager allocates appropriate memory and processor resources
5. A dispatcher: This component is responsible for starting the execution of a process

According to Hailperin (2007), hard real-time operating systems make use of fixed-priority scheduling to enable multithreading which in turn allows for multiple tasks to be processed by a single processor. Fixed-priority scheduling is when each thread in a system is assigned a numerical priority by the system developer. The system then gives preference to threads with higher priority to those with lower priority. "Although there may be some way for the user to manually change a thread's priority, one speaks of fixed-priority scheduling as long as the operating system never automatically adjusts a threads priority" (Hailperin, 2007). Equally high priority threads can be run in a round-robin or first in first out method however it is the system developer's responsibility to ensuring that there is sufficient processing ability to ensure that a rate-monotonic fixed priority schedule will work as desired.

4 DEVELOPMENT OF THE ROAD LOAD SIMULATION PROGRAM

The final road load simulation model was developed after having confronted many technical issues hampering development. These issues were present in both the software development as well as in the integration of the new system with the existing test stand infrastructure.

The road load simulation model evolved through three different models. The adoption of a completely new structure for the second (third model adopted the same structure as the second) model was as a result of unsatisfactory results of the first model. This path resulted in the development of three separate software programs, one off-line software development program and two real-time programs.

Integration of the system with the existing CAE dynamic test stand posed many problems. The unfortunate failure of an engine to dynamometer shaft during the test engines characterization highlighted some potential weaknesses of the existing setup.

This chapter discusses the development of the road load simulation program as well as the various components that affected the development and test cell integration.

4.1 Existing CAE Test Stand and Infrastructure

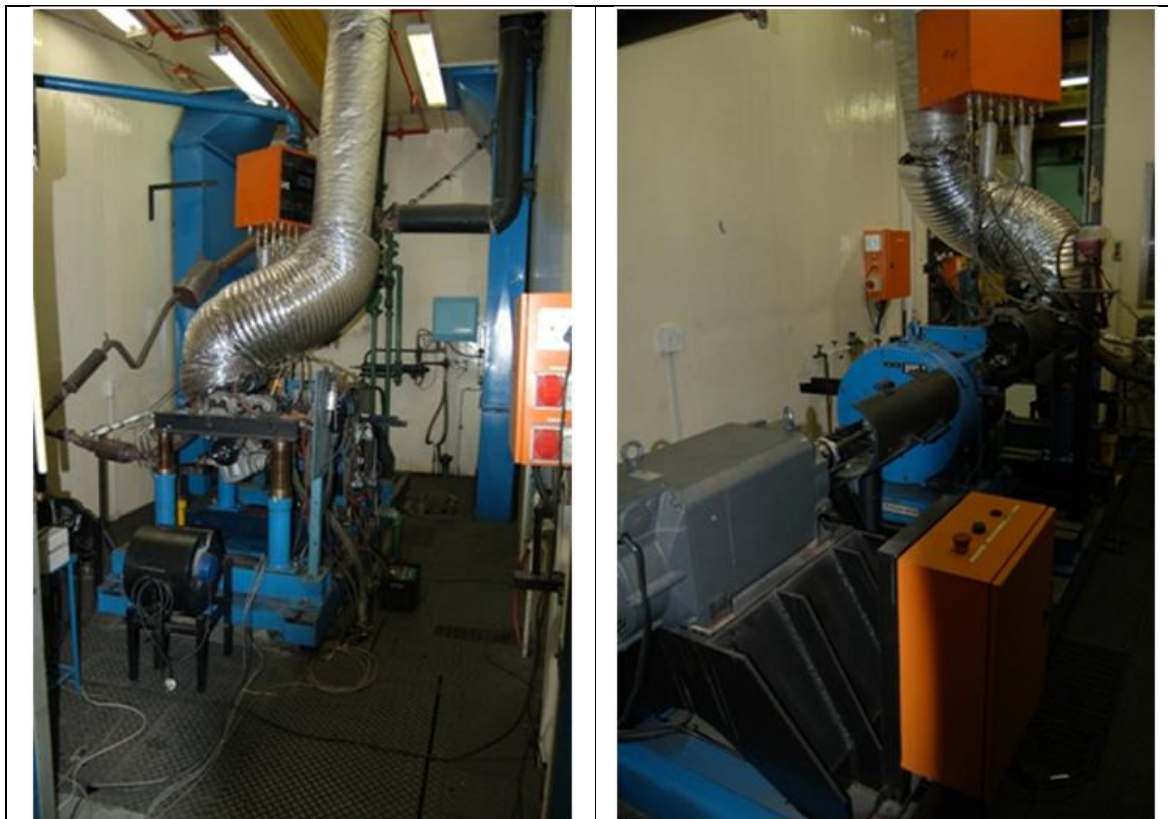


Figure 4. 1: Existing CAE Hybrid dynamometer test stand

An existing CAE test stand (Atl 07) was used for the development, testing and validation of the road load simulation system. The dynamometer was a combination of a Froude EC-38TA dynamometer, used for braking, and a Siemens servo motor coupled to the rear end, used to drive the engine, thus provided the ability to simulate over-run conditions. The servo motor was coupled to the rear of the dynamometer via a steel shaft and a one-way clutch. This allowed the Servo motor to drive but not brake the engine. The Siemens servo motor was controlled by an Allen-Bradley PowerFlex® 700 Variable Speed Drive. A test engine was coupled to the front of the dynamometer via steel shaft.

Table 4. 1: Froude EC 38 TA Specification

Froude EC 38 TA Eddy Current Dynamometer Specification	
Maximum power absorption:	165kW @3280-10000rpm
Speed Control Regulation:	±0.25% maximum rated dynamometer speed for a load change of 10% to 100% rated torque.
Torque Control Regulation:	±0.25% of maximum rated torque over a speed range of 5:1.
Supply voltage:	200-250 Volts 50-60 Hz single phase. This should be externally switched and rated 10Amp.
Output voltage max:	0.8 x supply Voltage
Output current max:	8 Amperes
Demand signal:	10 Volts negative
Moment of Inertia:	0.101kgm ²
Speed measurement:	60-tooth involute gear wheel

Table 4. 2: Siemens servo motor specification

Siemens Servo Motor Specification	
Maximum speed:	8000rpm
Maximum power output:	44.00 kW@2300rpm
Maximum torque output:	183N.m
Rated voltage:	398 Volts
Rated current:	85 Amperes
Power factor:	0.84
Efficiency:	0.911
Moment of Inertia:	0.228kgm ²
Speed measurement:	Encoder model No. H01 10245/R

Table 4. 3: Allen-Bradley drive specification

Allen-Bradley motor drive specification	
Input voltage:	400Volts
Normal duty power:	55kW
Heavy duty power:	45kW

Input, 3-phase frequency:	47-63Hz
Rated current:	100.5 Amperes
Output, 3-phase frequency:	0-400Hz
AC Voltage range:	0-400Volts
Base frequency:	50Hz
Continuous current:	105/85Amperes
1min overload current:	116/128Amperes
3sec overload current:	158/170Amperes

Engine torque was measured using a calibrated load cell attached to a torque arm. Engine speed was initially measured using the dynamometers 60-tooth inductance pick-up. Engine fuel consumption was measured using an AVL 415s dynamic fuel balance. Engine temperatures and pressures were measured using thermocouples and pressure transducers hung from an over-engine boom. Lambda values could be measured using an ETAS lambda scanner.

The test cell was automated and monitored with the use of ETA software which interacted with an Allen Bradley PLC. The PLC was used for data acquisition of data from the respective measurement devices. Speed and torque measurements were obtained from the dynamometer controller via the PLC.

The drive motor and the dynamometer were controlled by their respective drive and controller, however their set-point speeds were provided by ETA. Speed synchronization of the motor and the dynamometer were limited by the accuracy of their calibration with the analog set-point voltage provided by ETA via the PLC. Inaccuracies in this calibration resulted in the drive motor purposely being synchronized to revolve approximately 50rpm slower than the dynamometer at any speed set-point. The accuracies of this calibration were influenced by two main factors:

1. The dynamometer controller and motor drive both had their own physical speed measurement mechanisms with varying degrees of accuracy. The specifications of the dynamometer controller and the motors drive speed set-point acquisition card were also vastly different. The most evident of these differences was the resolution and voltage ranges of set-point acquisition of the controller and drive
2. The method of calibration/synchronization used

The speed offset of the drive motor was required to prevent the motor from driving the dynamometer and thereby resulting in an inaccurate engine torque measurement being produced by the dynamometers load cell due to the drive motors torque contribution. This was an unlikely scenario during steady state running, however it was of concern during transient running, where there was a change from increase in rotational speed to decrease or vice versa. Due to the physical/electrical properties of an AC motor it should be noted that if the AC drives set-point speed was set higher than the set-point speed of the dynamometer, torque transmitted between the two machines could increase at a rate limited by the current supplying ability of the motors drive. This could result in excessive loading of the mechanism coupling the dynamometer and drive motor occurring in a very short time period.

Many changes were made to the original setup of the CAE dynamic dynamometer. The operating principles of the added systems as well as its respective component selection will be discussed in the following section.

4.2 System Operating Principles

The intention of the system was to simulate any given vehicle and apply the respective vehicle loads to an engine on a test stand. The load would be applied in such a way that the loading experienced from the engine's point of view would be the same as it would be if the engine were in the original vehicle being simulated. To achieve the set out target, application specific software that integrated with the required data acquisition hardware would have to be developed.

To determine the system requirements and specification, a list of functional and non-functional requirements was generated. Sommerville (2004) defines functional requirements as a description of the services the system should provide, in detail. Non-functional requirements are developed as those which are not directly concerned with the specific functions delivered by the system. They may relate to emergent system properties such as reliability, response time and storage occupancy.

Functional requirements:

1. A user friendly interface must be provided.
2. The interface should at minimum display the engine speed, applied load, throttle position and simulated vehicle speed. Any other data required by the operator to ensure safe running of a cycle should also be displayed.
3. It should be possible for the operator to pause the cycle at any stage or transfer back to manual control at any stage in the test cycle.
4. The program must ensure that the maximum engine speed is not exceeded at any stage.
5. Various emissions cycle saved in a comma separated file should be importable thereby allowing the system to run in an automated style outputting loads onto the engine relating to their respective vehicle velocity values from the input file.
6. The input file should consist of a velocity profile (a column of time values and a column of speed values at the respective time value) with an optional gear selection input column.
7. The simulated vehicles properties should be supplied by the operator through the user interface. The following properties should be adjustable:
 - a) Air density
 - b) Vehicle drag coefficients
 - c) Vehicle frontal area
 - d) Vehicle mass
 - e) Rolling resistance coefficients
 - f) Wheel /tyre properties

- g) The inertia values of the rotational components
 - h) Effective vehicle inertia mass
 - i) Final drive gear ratio
 - j) The number of transmission gears
 - k) The gear ratios of the transmissions gears
 - l) Clutch properties
8. The following test engine properties associated with the simulated vehicle should be entered by the operator through the user interface:
 - a) Maximum engine speeds
 - b) Idle speed
 - c) Engine inertia
 - d) Maximum braking force
 9. At minimum, the engine speed, applied load, throttle position and vehicle speed should be recorded by the system. This data and any other data required for the validation of a cycle should be recorded at a rate equal to or higher than that required by the set emissions standards.

Non-functional requirements:

1. The system should comply with the regulations of the current light duty emissions regulations as far as possible. It should be noted that the developed system does not fully comply with the regulations. They will however, be followed as closely as possible.
2. The system must be able to record data at 100 Hz or higher.
3. Data should be recorded in real-time. Timing and data integrity must be ensured.
4. The system should be designed with a fail-to-safe methodology as far as possible.
5. The data displayed by the user interface should be real-time and free from any lag or jerk as this can often unsettle the operator especially when engines are operating under heavy loads and high engine speeds.
6. The system should be capable of functioning with various types of driven dynamometer configurations.
7. The control loop of the system should operate at a minimum of 200 Hz.

With the functional and non-functional requirements defined, the overall architecture of the system would under normal circumstances then be defined. However, in real-time and data acquisition dependent systems, the designed architecture may be dependent on the selection of software compiler and hardware components. This was the case with the system being reported upon and as such, the selection of a software compiler and hardware components were selected before the complete architecture was determined. Insight, research and in the unavoidable circumstances assumptions about software, hardware and system architecture had to be made to allow for what was believed to be suitable components to be selected at this early stage.

The process of selection of the software compiler, data acquisition hardware and a basic overview of the selected components integration with the existing CAE test stand will be discussed below.

4.2.1 Software and hardware selection

The selection of a software compiler and programming language was the first significant decision that needed to be made as this would affect the development and final outcome of the system. For the type of system defined by the requirements above, three compilers/programming languages were identified to be most suitable language to be used for the development:

1. Borland C++: This is a low level programming language commonly used in electronic applications for the programming of microprocessors and controllers. Its low level compiler enabled it to produce effective and efficient machine code allowing for high processing loads. C++ was also commonly used in industry to develop commerce based application with the use of user interface driven tools and packages.
2. Matlab: The Math-scripting and Simulink tools would have created an ideal development environment for the creation of a mathematical based model. Its compiler was developed with the aim of processing large amounts of complex numbers using efficient method.
3. LabVIEW: This is the highest level programming level language of the three considered but was specifically targeted at data acquisition based systems. It was intended to integrate with data acquisition hardware seamlessly and efficiently.

During the final selection of a suitable programming compiler/language, a list of the critical and desired attributes of the respective compilers was tabulated. It was determined that the most important factors influencing the choice of the software development environment were as follows:

1. Ease of integration with hardware devices.
2. High data processing speed (high through-put rate).
3. The ability to function in a real-time environment.
4. Mathematical manipulate and modeling ability.
5. Signal processing and manipulation ability (e.g. filtering).
6. Knowledge of the chosen development environment and its functionality.
7. Cost/accessibility.

Using the above listed factors, The Kepner-Tregoe method as explained by Lussie (2006) was used to determine the most suitable software development environment. This method was based on the weighting of critical and beneficial criteria. Each of the options was judged on a one through ten scale based on their ability to fulfill the various criteria. These results were then multiplied by the weighting factors to yield a total value of which the highest scoring would be the most appropriate solution.

Table 4.4: Kepner-Tregoe Method applied to the determination of a software compiler

Must Criteria		LabVIEW	C++	Matlab
Is a license available or obtainable		Yes	Yes	Yes
Real-time ability		Yes	Yes	Yes
Want Criteria	Meets Criteria			
	Weighting	LabVIEW WS	C++ WS	Matlab WS
Ease of hardware integration	7	7 \Rightarrow 49	4 \Rightarrow 28	4 \Rightarrow 28
Data processing speed	8	6 \Rightarrow 48	9 \Rightarrow 72	7 \Rightarrow 56
Mathematical manipulation	6	8 \Rightarrow 48	7 \Rightarrow 42	10 \Rightarrow 60
Experience with programming language	10	6 \Rightarrow 60	4 \Rightarrow 50	2 \Rightarrow 20
Software supplier support	3	8 \Rightarrow 24	2 \Rightarrow 6	4 \Rightarrow 12
Student support	4	8 \Rightarrow 24	2 \Rightarrow 8	6 \Rightarrow 20
Total weighted score		233	196	200

The Kepner-Tregoe method culminated in the selection of National Instruments LabVIEW 8.6 development environment. The most compelling attributes of the LabVIEW environment was its hardware integration ability as well as its seamless ability to integrate with real-time operating system.

As it was necessary to develop a time deterministic solution, a real-time system was required. Two solutions for time deterministic data acquisition and processing were found to be most prominent in industry. These two systems were:

1. Field Point Gate Arrays with integrated data acquisition: This system commonly appears in the form of a PCI card or a separated chassis mounted device. The data acquisition component acquires the data while the FPGA chip would be used for deterministic processing of the data. The software program installed onto the FPGA determined what processing or manipulation would be done on the acquired data and at what rate.
2. Real-Time Desktop Computer with a PCI-DAQ device. These are regular desktop computers running real-time operating systems. Data is acquired using a PCI DAQ card that has real-time functionality. Data is then processed using the PC's processor. The real-time operating system ensures that the processing required by the installed program occurs in deterministic method.

Both FPGA as well as RT operating systems had advantages and disadvantage and for the purpose of this dissertation both were believed to be workable solutions. Current trends in the automotive testing industry seem to encourage the use of FPGA technology as this technology could be found in devices such as ETAS ETK ECU interface and devices such as an ETAS ES1000. However the number of real-time operating system developers and companies offering real-time computing solutions was on the increase and it appears that for larger projects, RT PC solutions were commonly used.

Table 4.5: Advantages and disadvantages of Real-time operating systems and FPGA's with respect to their implementation of this dissertation

	Real time operating system	FPGA
	Advantages	
1.	Makes use of an off-the-shelf PC as a target.	Hardware level implementation of real-time system.
2.	Program size only limited by processing ability.	High operating frequency.
3.	Allows for multicore processors.	True parallel processing.
4.	Processing power and memory expandable.	Processing power and memory fixed.
	Disadvantages	
1.	Hardware drivers are only provided for a limited set of chipsets.	High cost of hardware.
2.	Software level implementation of real-time system.	Size of real-time program implementable limited by the physical size of the chip (number of gates, multipliers, and memory built into the chip).
3.	Lower operating frequency.	Not easy to determine the correct size FPGA required.
4.	Makes use of Multithreading on cores that are allocated more than one thread.	

One of the targets of this dissertation was to create a cost effective vehicle simulation program that could be used in South Africa. This requirement implied that it was beneficial to have a higher development cost with the advantage of a reduced per-head capital cost required for the hardware infrastructure of the rolled-out system. The use of a RT OS on a desktop computer would have ensured a lower rolled-out cost, as this was not a commercial cost and development cost would not have affected the rolled-out cost. However it was believed that the additional challenges faced during development would affect development time required which in the case of a commercial project, would have affected the roll-out cost.

The reality of every project is that it has an assigned budget which does not always allow for the best, most efficient or simplest solution, but for the most cost effective solution. This project

was no exception when considering the limited budget and as such, it was elected that a RT operating system running on a desktop computer be used.

To follow will be an explanation of operating principles of the selected RT operating system running on a desktop computer.

4.2.2 LabVIEW RT operating principles

The vehicle simulation software program was developed using National Instruments LabVIEW compiler. The following software packages were used during the development of the system:

1. NI's LabVIEW 8.6 graphical programming compiler was used for code generation. This was the core compiler used with all LabVIEW programming applications.
2. NI's LabVIEW Real-Time Module was used to integrate LabVIEW with the real time operating system. The LabVIEW Real-Time Module also allowed LabVIEW to create an application with deterministic timing that would be ran on a real-time target.
3. LabVIEW Real-Time deployment license for standard PC's using Pharo's ETS real-time operating system.

The LabVIEW real-time development environment required a host PC and a target PC. The host PC was the primary development platform on which the simulation program was developed and was the display and control panel for the target PC once the developed software was deployed to the target PC.

Together with the developed software, hardware was also required to integrate the software into the CAE test stand. The following section discusses the various aspects of integration of the hardware with the existing CAE test stand.

4.2.3 System integration and hardware interfaces

Changes needed to be made to the CAE dynamic test stand that would allow for the development and testing of the vehicle simulation program. These changes together with the developed system would advance the existing test stand from a dynamic test stand to a transient test facility.

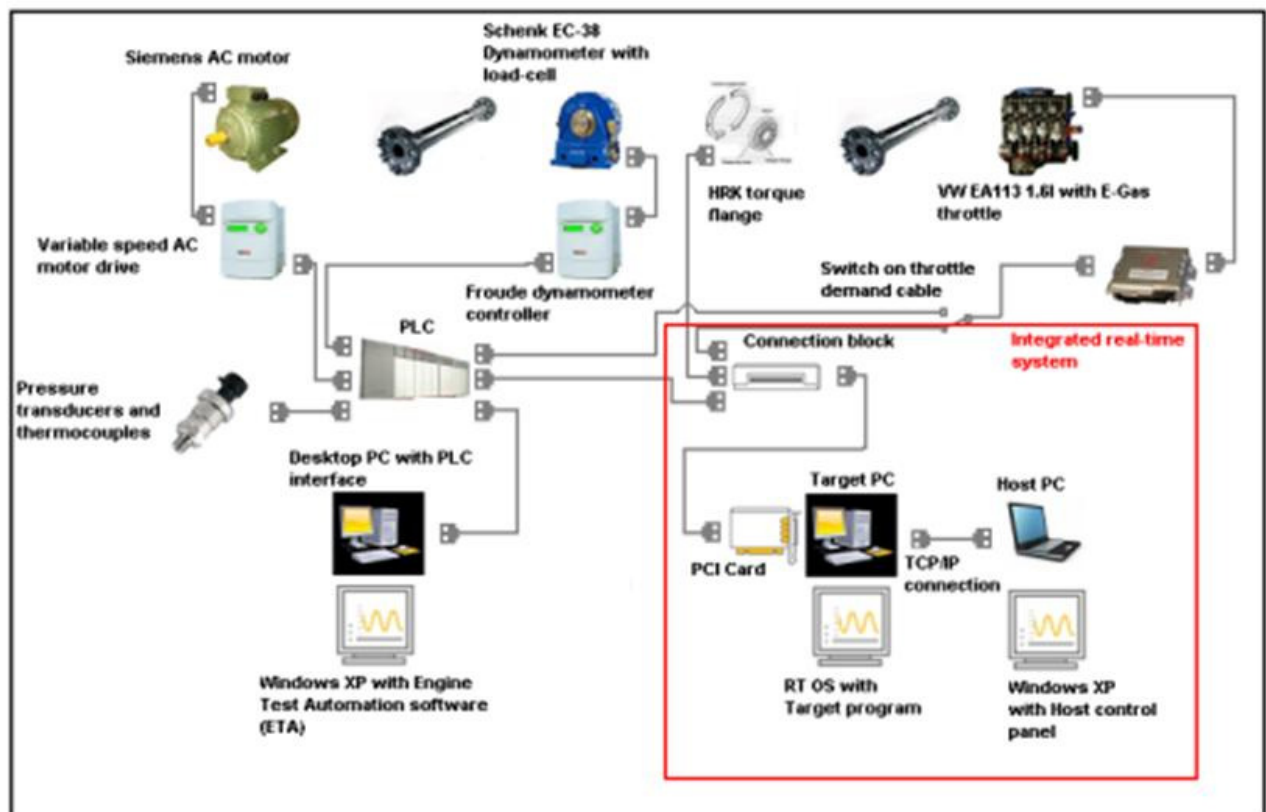


Figure 4.2: Target PC integration with the existing test stand equipment

The physical interface between the existing test stand equipment and the installed simulation system was the electronic connection block for the National Instruments DAQ card installed in the target PC. The DAQ card used the following channels to generate and measure signals to and from the existing equipment:

Table 4. 6: Target PC data acquisition interface channels

	Channel name	Channel type	Input/output relative to target PC
1.	Torque (Flange)	Analog (-10 - 10V)	Input
2.	Engine speed	Counter (TTL)	Input
3.	Throttle position	Analog (0 – 5V)	Input
4.	Engine speed	Analog (0 - 5V)	Output
5.	Throttle position	Analog (0 - 5V)	Output

The torque flange was installed between the dynamometer and the shaft connecting it to the engine. This would allow for the measurement of the load applied across the load cell which in turn was used to determine the load applied to or generated by the engine.

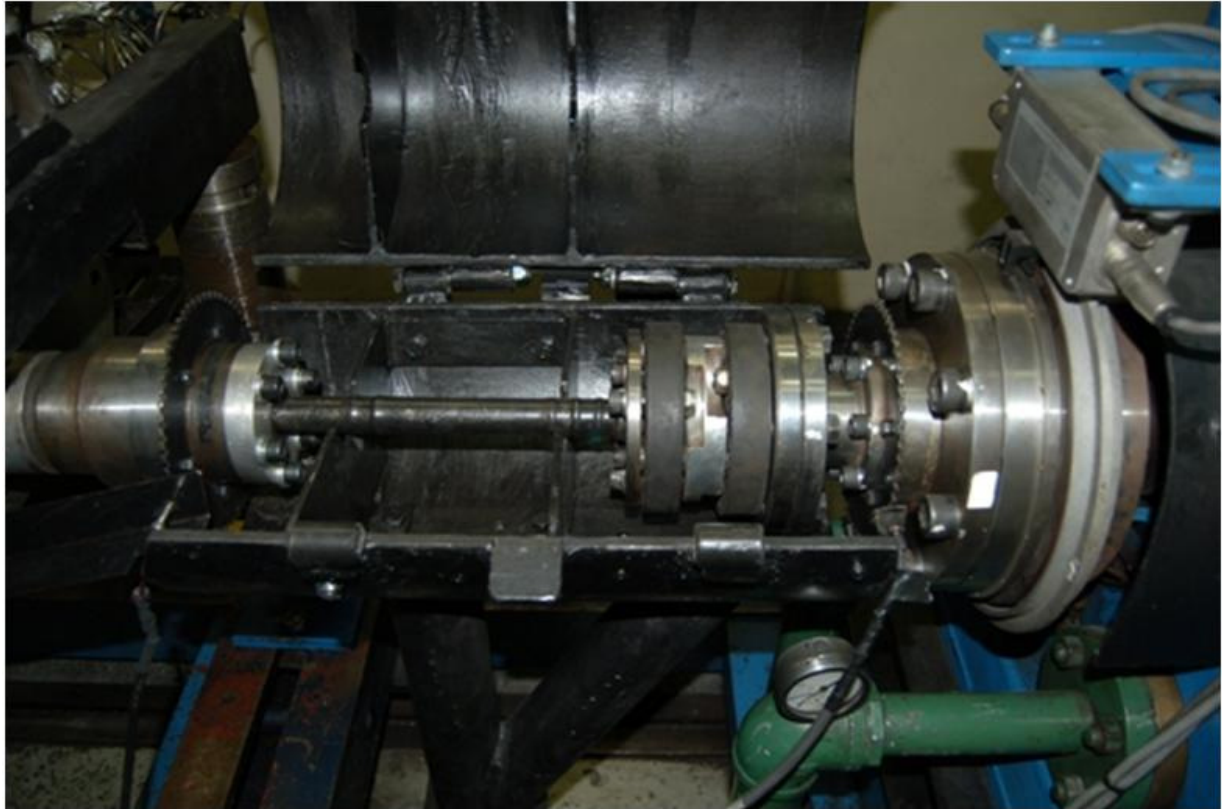


Figure 4. 3: The C.V adapter flanges with 60-tooth disks and the torque flange.

Engine speed measurement was initially obtained using an analog voltage (0 – 10V) provided by the dynamometer controller but this method was later replaced by an independent system after a shaft failure occurred (see Appendix C). A universal C.V. joint adaptor flange (see Appendix B) was designed that could be mounted on either side of the engine to the dynamometer shaft without any modification to the existing shaft. The designed adaptor flange had a 60-tooth wheel attached to it. A digital magnetic pick-up which provided a digital pulse output was used in conjunction with a TTL counter onboard the DAQ card to determine engine speed. An adaptor flange together with its respective measurement equipment was installed at each end of the shaft although the simulation program that was developed only required a single speed measurement. The two speed pick-ups were used for the shaft investigation that was run concurrently with the simulation program development as a result of the shaft failure that occurred on the test stand.

An engine throttle position was obtained by the target PC's DAQ card from the PLC which in turn measures this value from the potentiometer on the engines throttle actuator or more commonly known as an E-GAS throttle body.

As ETA (the existing Engine Test Automation system) was a tried and tested system, it was decided that it would remain the primary test cell control system (this was decided as a safety precaution). ETA monitored all signals provided by the developed system as well as all sensors

from the engine test stand. ETA's alarms were left to function as normal, with the intent of preventing an incident should something have gone wrong during the development and testing. ETA was only monitoring and recording during the development of the new system and had no influence on the setpoint values sent to the dynamometer, drive motor or engine unless an alarm was triggered. For safety reasons it was decided that the setpoint values used by the dynamometer, drive motor and engine should be switchable between those provided by ETA and the developed system. The ability to switch control between the two programs required the switching of the throttle, engine speed and motor setpoints between the two systems. A selector button was placed in ETA that was used to select whether ETA or the developed systems setpoints would be used.

The target PC's speed and throttle output setpoints were read into ETA using analog input channels on the PLC. This was done so that the operator could ensure that the difference between the developed system's and ETA's setpoints were not too large when switching between the two software systems.

The safest method of switching from the transient simulation to ETA was to set the ETA throttle position to 0%, the dynamometer setpoint speed to a high value (higher than the current engine speed) and the drive motor below engine idle speed. When switching systems, the engine throttle would close and the engine would coast down to idle under the test stands rotational inertia. This method also worked when switching from ETA to the simulation as the simulation default was a stationary vehicle which would result in both systems requesting an idle condition at the switch and thus a safe switching condition.

ETA used an analog output channel from the PLC to the dynamometer controller and another analog output channel from the PLC to the variable speed drive to provide speed setpoints. This allowed the setpoint speeds of the drive and brake to be set independently. The target PC's DAQ card had two analog outputs, one of which was required for engine throttle actuation thus only allowing for a single speed setpoint output. As the dynamometer and motor drive had different set-point input voltage ranges, a single channel could not provide the setpoint to both devices. The solution was to measure the target PC's analog speed setpoint with the PLC and then use the PLC to recalibrate this signal and output them onto the same two channel that would normally be used by ETA. The switching between the two speed setpoints was therefore conducted by the PLC with the switching being activated by a button placed in ETA. This button was further connected to a digital output on the PLC which was used to switch an electronic relay which in turn switched between the two throttle demand setpoints.

The developed system recorded the engine speed, load, throttle position and simulated vehicle speed at 100 Hz. ETA was used to log all engine and test stand parameters but at a slower 10 Hz, which was the fastest it could log reliably. A calibration ECU (SIMOS 7.6 CCP) was used during the system development there by allowing ECU data to be logged using ETAS ECU interface software, INCA. This logging was done via CAN bus (using ETAS CAN-Link PCMCIA Typell) with different ECU parameters being logged at different rates (the default recording speed were used).

4.3 Data Acquisition

All interaction between the developed system and the existing infrastructure was done through the data acquisition card that was installed in the target PC. Based on the selected development environment and real-time operating system it was convenient to select a DAQ card from the National Instruments range. As the card would be used in the real-time environment on the target PC, it had to be capable of supporting the LabVIEW RT module. Before a data acquisition card was selected, a basic specification was drawn up based on the anticipated requirements. Listed below are the minimum requirements that were used to compile a basic specification that was used to select the data acquisition card:

1. A minimum of two analog outputs.
2. A minimum of two analog inputs.
3. DAQ card must be LabVIEW RT compatible.
4. The highest speed the test engine was expected to reach was 6000rpm, thus:

$$6000rpm = 100rev/sec = 0.01 \frac{sec}{rev} = 100Hz \quad 4-1$$

The Nyquist sampling theorem states: "A continuous signal can only be properly sampled, only if it does not contain frequency components above one-half of the sampling rate" (Smith, 1999). Thus the minimum sampling frequency required to be able to correctly reconstruct the sampled signal would be 200Hz.

5. The voltage range of 0 to 10 Volts or -10 to 10Volts was to be used. Thus the change in voltage per rpm deviation would be:

$$\frac{10}{6000} = 0.0016 V/rpm = 1.6mV/rpm \quad 4-2$$

Or if the full 20 Volt range was used:

$$\frac{20}{6000} = 0.0033 V/rpm = 3.3mV/rpm \quad 4-3$$

6. Based on the 10 Volt range as used in Equation 4-2, the change in voltage per Newton meter deviation (2939N.m is the minimum positive calibration value from the torque flange) would be:

$$\frac{10}{2939} = 0.0034 Volts /rpm = 3.4mV/rpm \quad 4-4$$

From point five and six it is noted that the card required a sensitivity of less than 1.6mV thus allowing for accurate measurements.

When the DAQ card was selected, the specification drawn up and used to select the card was based on the assumption that the speed and torque inputs would be analog voltage input and the throttle and speed outputs would be analog voltage output. This was not the solution used

in the final version of the system. This was what was proposed as a solution at the time of DAQ card selection. Thus a National Instruments PCI 6221 (37-Pin) DAQ card was selected. The specification of this card can be found in Appendix A. Although this data card was well above the required specification it was the most cost effective card available that could provide the required functionality. The Real-time support was the only limiting factor.

Additional information on the various devices that the DAQ card interacted with, as well as the data acquisition techniques used are discussed below.

4.3.1 Engine torque measurement

The existing test stand measured the torque produced by the engine using a load cell attached to a lever arm which in turn was connected to the shaft-bearing housing. This housing was supported on the trunnion-bearings. The shaft-bearing housing extended through the rear trunnion-bearing and further formed part of the housing for the stator coils of the Eddy current dynamometer. Thus, when the dynamometer was in speed control mode and the engine produced enough torque to reach the set-point speed, the dynamometer produced a resistive force there by generating a reaction force. This force acted concentrically to the load cell with a known distance from the center of the rotation of the applied force thus resulting in the ability to convert the force measured by the load cell into a torque measurement or moment. However, when the engine was being driven by the electric motor as was the case under over-run simulation, the dynamometer did not apply a braking force as the engine was not producing enough torque to exceed the dynamometer's set-point speed. This in turn resulted in no force being created (or required) on the stator coils and hence no force applied on the load cell and thus no negative torque or motoring torque was measured. This circumstance occurred as the electric motor was rigidly mounted to the test stand behind the dynamometer instead of on trunnion bearings with a connected load cell as was done with the dynamometer.

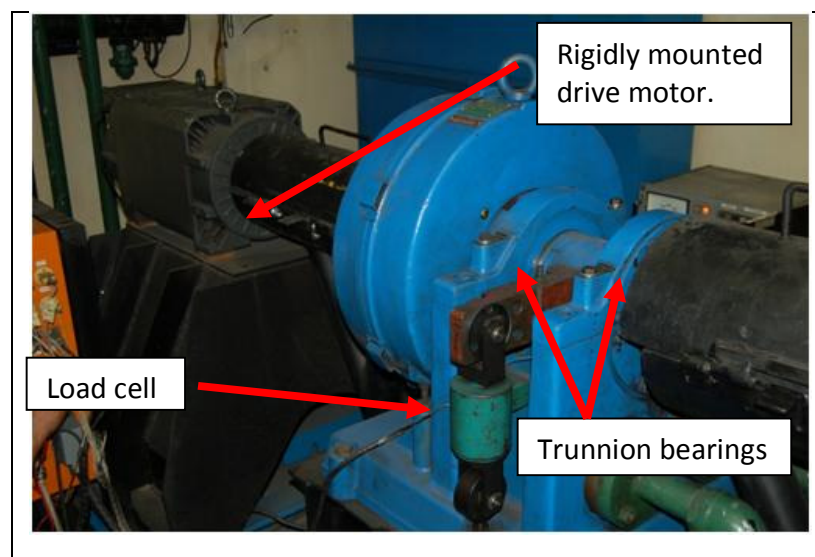


Figure 4. 4: Dynamometer and drive motor mounting and support

The solution to the measurement of both positive and negative torques in the described system was the measurement of the torque using a torque flange. This was not a cost effective solution in terms of a generic solution for a commercial project, however CAE possessed a torque flange that could be used at no additional cost to the project and as such, this was a suitable solution for development purposes. Table 4. 7 provides the specification and Figure 4. 5 a graphical representation of the torque flange that was used.

Table 4. 7: HBM Torque flange specification

HBM Torque Flange Specification	
Code number:	T10F-005R-SU2-G-7-W2-N
Nominal (rated) torque:	5kN.m
Nominal (rated) sensitivity (nominal signal range between torque = zero and nominal torque) Frequency output: Voltage output:	5kHz 10Volts
Characteristic tolerance (deviation of the actual output quantity from the nominal signal range at nominal torque: Frequency output: Voltage output:	±0.1% ±0.2%
Nominal rotation speed:	8000rpm
Torsional stiffness:	9900kN.m/rad
Torsion angle at nominal torque:	0.029degrees
Mass moment of inertia of the rotor:	0.11kg.m ²
Weight:	14kg

The torque flange was installed between the engine and the dynamometer on the dynamometer end of the connection shaft. The torque flange measured the strain in the rotor which, with the physical and material properties of the flange know can be used to determine the torsional stress in the flange. This stress can then be used to determine the force acting over a radius (a moment). This was necessary knowledge as this implied that the distortion (twisting) of the flange was measuring torque on one face of the flange relative to the opposing face while in rotation.

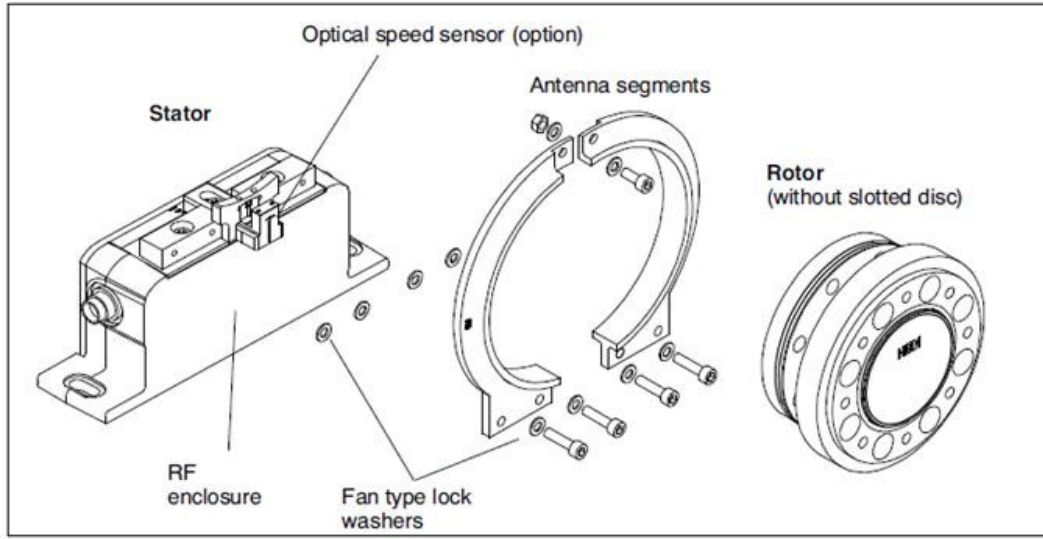


Figure 4. 5: HBM torque flange components (HBM 2007)

Thus, when the engine drove the dynamometer, the load applied to the flange by the engine was measured relative to the resisting load created by the dynamometer. When the electric motor drove the engine, the load applied to the engine by the motor was measured relative to the engine's resistance. Thus, the uncorrected (ECE correction) engine torque based on the torque measured by the torque flange was as follows:

Engine driving the Eddy-current dynamometer

Engine motored by the dynamometer (AC motor driving)

$$T = J \propto$$

$$T_T = -T_E + T_{TF} - J_D \propto_D \quad 4-5$$

$$T = J \propto$$

$$T_T = T_D - T_{TF} + J_E \propto_E \quad 4-6$$

If the system is viewed over an infinitesimally small time duration so that the system under transient conditions can be assumed to be a sequence of steady-state steps, then it could be assumed that $T_E = T_D$. If it is further assumed that the shaft connecting the dynamometer to the engine was completely rigid, then $\propto_E = \propto_D$. If the system is considered as a closed one with no energy loss e.g. heat transfer out the system, then $T_T = 0$.

$$0 = -T_E + T_{TF} - J_D \propto_E$$

$$T_{TF} = T_E + J_D \propto_E$$

$$T_E = T_{TF} - J_D \propto_E \quad 4-9$$

$$0 = +T_E - T_{TF} + J_E \propto_E$$

$$T_{TF} = T_E + J_E \propto_E$$

$$T_E = T_{TF} - J_E \propto_E \quad 4-10$$

In the equations above, the referred to actual engine torque was inclusive of all the internal losses within the engine with the exception of the torque required to overcome the engines inertia.

4.3.2 Engine speed measurement

Initially the engine speed measurement for the vehicle simulation system was obtained from the dynamometer controller. This signal was 0 to -20 Volts and was sent to the PLC where it was inverted and reduced to a 0 to 10 Volt signal that the DAQ card in the target PC could safely acquire. After an engine failure on the test stand, this speed acquisition method was reviewed and it was decided that this engine speed acquisition method be abandoned and an independent engine speed acquisition system be implemented.

The engine speed acquisition system that was developed consisted of a 60-tooth rotor and a magnetic pick-up that produced a digital signal. A C.V. adaptor flange was designed that had a 60-tooth rotor to be mounted to it. The adaptor flange in turn could be installed between the torque flange and the connecting shaft as well as between the connecting shaft and the engine bell-housing intermediate shaft. Two of these adaptor flanges can be observed in Figure 4. 3 located in their working positions.

Table 4. 8: Digital magnetic pickup specification

TSI digital magnetic pickup	
Model number:	RS-304-172
Output signal max. rise time:	1000ns
Output signal max. fall time:	50n.s
Max. gap between the rotor and the pickup:	1.905mm
Actual gap between the rotor and the pickup:	1mm
Supply voltage:	5.0Volts DC. $\pm 10\%$
Ground connection:	Common to the low side of the signal and the negative side of the power source.
Rotor	
Pitch:	60 teeth
Outer Diameter:	170mm
Tooth depth/amplitude:	5mm
Rotor thickness:	3mm
Rotor surface speed @ 800rpm:	7.103m/s
Rotor surface speed @ 6000rpm	53.407m/s
Further details on the specification can be found in the appendix.	

The adaptor flange was designed to allow different diameter toothed rotors to be fixed to it. This was advantageous as the magnetic pickups that were used had a specified measurable surface speed range. The surface speed of the rotors and thus the measurable engine rpm range could be varied by changing the diameter of the rotors fixed to the flange.



Figure 4. 6: Torque-flange side engine speed magnetic pickup and 60-tooth disk

The distance between the magnetic pickup and the toothed wheel was critical to the functionality of the pick-up and affected the measurement range when incorrectly set. The flange was inserted on the engine side of the shaft and as such could move with the engine in a plane perpendicular to the shaft axis. When the pickup was mounted to a static object (in this case the shaft guard), the required gap could not be maintained due to the engines movement. The solution was to mount the magnetic pickup statically relative to the engine as was done and can be seen in Figure 4. 7.



Figure 4. 7: Engine side engine speed magnetic pickup, 60-tooth disk and sensor mounting bracket relative to the engine.

During the software evaluation a fundamental problem was caused by the magnetic pickup. At unpredictable intervals a high frequency spike in the amplitude of the digital magnetic pickup

was generated. Three separate sensors were tested with all exhibiting this characteristic. When the spike from the pickup output signal occurred, an implausible signal error was generated by the DAQ card which in turn halted the data acquisition and the program from running. Relocating the signal cable and improving the cables shielding had no effect. It was found that through the software interface of the DAQ card, a filter limiting the minimum detectible pulse width could be implemented. The filter was set to have a minimum detectable pulse width of 6.425E-6 seconds and resulted in the spike being filtered out and allowed engine speed to be acquired up to 6000rpm.

4.3.3 Throttle demand signal

The VW EA113 engine made use of a drive by wire throttle commonly referred to as an E-Gas throttle. This type of throttle differed from the conventional cable drawn throttle as it had an electronic throttle demand. This electronic demand signal consisted of two signals that were generated by potentiometers within the throttle pedal. The first signal was a 1 to 5Volt D.C. signal and the second was half the voltage of the first signal. The two signals formed part of a fail-to-safe system whereby, if the voltage of the second signal did not maintain its value at half that of the first signal line or vice-versa, an error was registered within the ECU and the throttle actuator would return to its idle position until the error code was cleared.

The simulated full voltage signal was generated using an analog voltage output of the DAQ card. The half voltage signal was generated by dividing the full voltage signal using a voltage divider constructed using two equal resistors in a series configuration. The half voltage was generated at the node between the two resistors. The resistors were both 470Ω and required the following driving current from the DAQ card:

Table 4. 9: Throttle demand driving current required from DAQ card.

At 1 Volt	At 5 Volt
$V = IR$	$V = IR$
$I = \frac{1}{940}$	$I = \frac{5}{940}$
$I = 1mA$	$I = 5mA$

The specified upper limit of the drive current from the DAQ card was 5mA. Thus from the calculations above, the required current range was just within the limits of the DAQ card (the required current could be adjusted by installing larger or smaller resistors). If the required current exceeded the specified maximum output current, it could have had adverse effects on the delivered output voltage (a drop in the requested output voltage every time the maximum drive current was exceeded). If the required current was significantly low, the developed voltage could have been susceptible to voltage drift as the signal current could easily be affected by magnetic interference.

4.4 Engine Characterization

Engine characterization is the process of defining or relating an engine's input to its output. In the specific case, defining what ECE corrected torque would be produced by an engine under a given throttle position and engine speed.

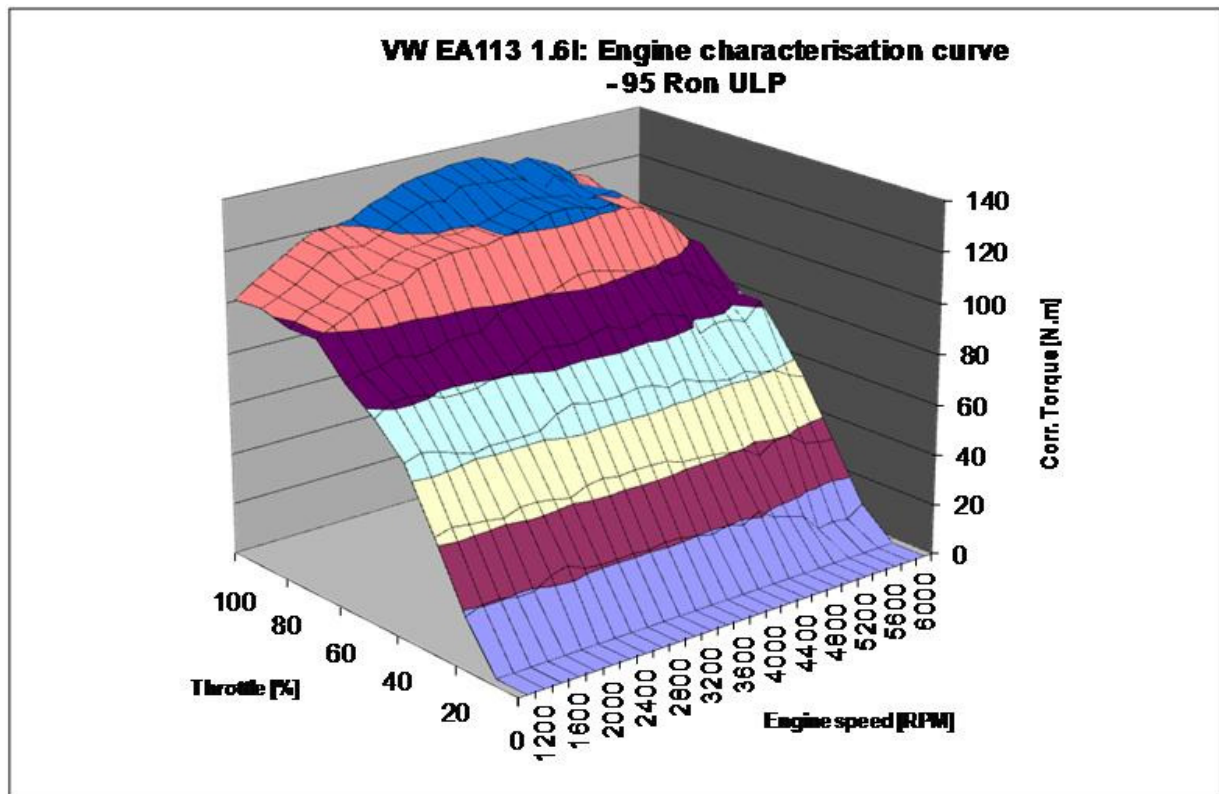


Figure 4. 8: Steady-state engine characterization of a Volkswagen EA113, 1.6l engine.

At the end of the software planning and the start of development, it was realized that an accurate engine characterization curve would be required. This characterization was to be used to simulate the engine's response during offline software (discussed later) testing and development, as well as to determine throttle positions for the first developed online model (also to be discussed later).

To acquire the data required to generate the engine characterization, 10 engine performance curves were run, with a 10% variance in throttle demand between each. The first performance curve was run at 100% throttle demand and last curve at 0% throttle demand.

For each individual curve the engine was run through a standardized warm-up cycle. Once warm, the engine speed was increased to 6000rpm where control over the engine and test cell equipment was shifted to an automated test procedure programmed into ETA. Measurements were taken at decrements of 200rpm down to and including 1000rpm. Each recording stage was sampled at a 10Hz frequency.

A driven dynamometer was required to complete the curves as at low throttle demand values (normally less than 20% demand) the engine would not produce enough torque to overcome its internal resistance (friction, inertia). Therefore the engine could not reach high speed without assistance. For example at 10% throttle the engine would not reach 6000rpm without having been driven as it would only produce enough torque to overcome its own internal resistance up to 3000rpm.

The failure of the shaft connecting the engine to the dynamometer occurred while increasing the engine speed up to the performance curve start speed of 6000rpm at 10% throttle demand. The engine characterization curve could thus not be completed. During the shaft failure, the engine block and the bell-housing cracked. A comprehensive incident report conducted for CAE as well as VWSA can be found in Appendix F. A replacement test engine was generously provided by VWSA to allow the continuation of the project. It was decided however that the characterization curve could not be completed or redone in its entirety until the cause of the failure was diagnosed and clearly understood. The characterization curve data obtained up to the engine failure was complete and sufficient.

4.5 First Simulation Program

The first simulation program was subdivided into two sections. Each of the two sections was developed as a Virtual Instrument (VI) and consisted of further nested VI's to create the logic. The first section processed the velocity profile and calculated the values required by the dynamometer to perform the simulation on the test stand. Once calculated the first section saved the data in a file that was used by the second section of the program. The second section of the program was integrated with the test stand and used the file generated by the first section of the program to run the simulation on the test stand.

The first section of the program that generated the simulation data was sub-divided into the following three VI's that performed the processing:

1. The terrain VI.
2. The driver VI.
3. The vehicle VI.

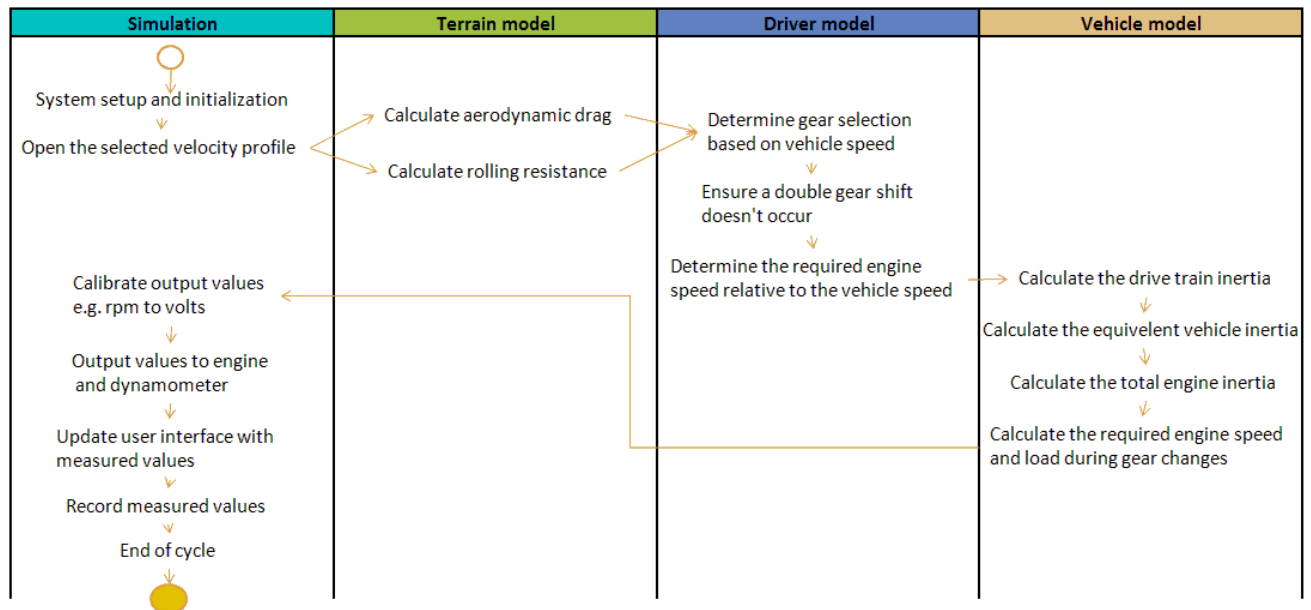


Figure 4. 9: Simulation program 1 process overview block diagram

When a simulation was to be run, the user would create a velocity profile in a comma-separated file that contained two columns. The first column was the timing and the second was the required simulated vehicle speed. The file that was created together with other physical properties of the simulated vehicle would be read and processed by the simulation program prior to running on the dynamometer. The following properties of the simulated vehicle would be required to run a simulation:

1. Vehicle weight.
2. Frontal area.
3. Air Density.
4. Aerodynamic drag coefficient.
5. Rolling resistance coefficients.
6. Number of gears and gear ratios of all gears.
7. Final drive gear ratio.
8. Wheel radius.
9. Gear shift, engine speed points.
10. Engine idle speed.
11. Maximum engine speed.
12. Engine and power train inertia values.
13. Engine characterization.

During the processing, the various loads on the modeled vehicle would be calculated from the entered properties as well as the velocity profile. Gear changes would occur at preselected engine speeds and with the required vehicle speed known as well as the selected gear ratio, the relating engine speed was calculated. With the engine speed prior to and after a gear change

known, the required engine speed and load values were manipulated to simulate a gear change. The required engine load and speed was then used to determine the throttle angle relating to the required engine speed and torque values. This was done using the engine characterization curve that was previously created. The preprocessing resulted in the creation of a new file containing the required engine speeds and throttle positions.

When the simulation was run on the test stand, the preprocessed data was sent to the target PC from the host PC where the preprocessing occurred. While the engine was running, control over the test stand was then transferred from ETA to the simulation program. The required engine speeds and throttle positions would then be calibrated into transmittable values and output to the dynamometer (including A.C. drive) and engine respectively. While the simulation was running, the actual engine load, speed and throttle position were measured and calibrated in real-time on the target PC where it was recorded and saved to a binary file. The calibrated measured values were also sent to the host PC where they were displayed on trend graphs. Upon the completion of a simulated run, the recorded data was processed to determine the accuracy of the run.

The functioning of the components of the first simulation program are discussed below. The results of a simulated run using this program will also be discussed.

4.5.1 The terrain VI

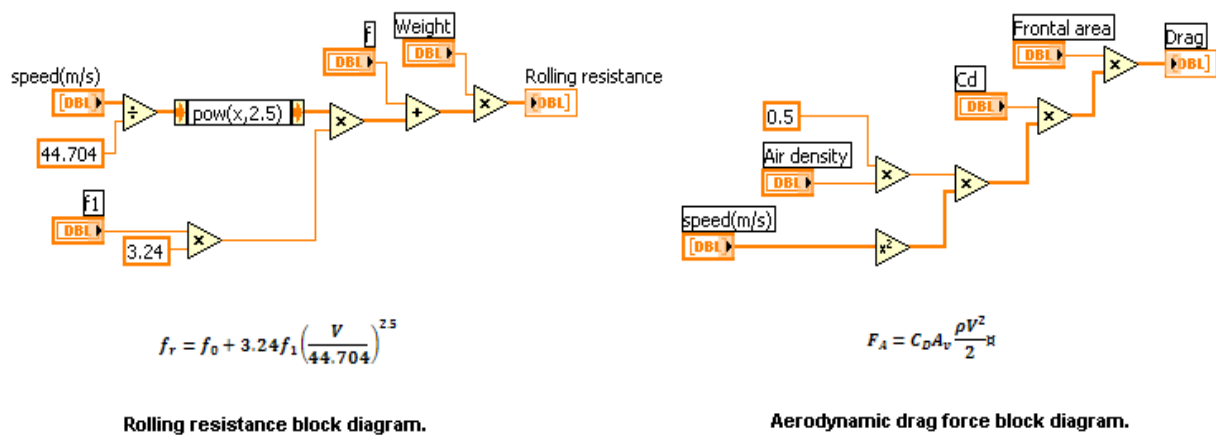


Figure 4. 10: Rolling resistance and aerodynamic drag VI block diagrams.

The terrain model as its name indicated was responsible for the calculation of all the loads associated with the simulated terrain. The calculated terrain loads consisted of the vehicle's aerodynamic resistance and rolling resistance. Road gradient was not accounted for in the simulation as it was not required for the running of an emissions cycle simulation. However, it could easily have been accounted for using the following equation:

$$F_1 = W \sin \phi$$

4-7

Where ϕ is the angle of inclination.

The terrain VI received the velocity profile from its parent VI simulation in an array format where the vehicle speed in km/h had been converted to meters per second. This array was then processed using the code depicted in the block diagrams shown in Figure 4. 10 and the rolling resistance and aerodynamic drag force were calculated for each of the vehicle's speed value in the array. The resistive forces were then added together and multiplied by the wheel radius to create a torque at the wheel axle. These values were then inserted into an array and returned to the calling VI, simulation. The aerodynamic drag force and the rolling resistance were determined using Equation 3-4 and Equation 3-6.

4.5.2 Driver VI

The driver VI was conceptually intended to calculate all values associated with a real driver in an automobile. The intended tasks of the VI included the determination of the gear selection, throttle demand and clutch actuation (the amount of torque that was transferred between the engine and powertrain). This concept created many program structuring hurdles and as a result the driver VI's responsibility were reduced to the determination of the gear selection and the engine speed relative to the vehicle speed and gear selection.

Gear change points were determined using up and down gear change setpoints based on engine speed. The engine speed relative to the current gear and requested vehicle speed (from velocity profile) was determined. When the gear shift setpoint engine speed reached the upper limit, the transmission ratio was swapped to that of the next higher gear ratio. If the lower limit was reached, the transmission ratio was switched to the next lower gear ratio. This gear shift methodology created the equivalent of a sequential transmission where a gear could not be skipped during down or up shifting. This was not ideal but was believed to be suitable for the intended application as no gears were skipped during gear shifts in an emissions cycle. Neutral transmission gear was simulated by removing all loads from the engine (the equivalent of depressing the clutch in a vehicle). This too was not ideal as even in neutral the engine in a vehicle would experience some load. However engine load resulting from a neutral transmission gear would have been minimal and as such, it was believed to be adequately accurate.

A complication was encountered during the development of the driver VI. Depending on the transmission gear shift setpoint selected, a double gear change would occur under certain conditions. While simulating a gear shift, the gear selection algorithm would change the selected gear back to the original gear before the first simulated gear change was complete. This would occur when a given gear change setpoint correlated to a vehicle speed in the vehicle speed profile where an increase and then a decrease in vehicle speed occurred. The program would select a higher gear near the end of the vehicle speed acceleration period and then at the start of the deceleration, the original gear would be selected before the gear up shift was

complete. This would result in unrealistic engine loading condition being calculated as well as high rate of change in the engine speed. To prevent this from happening, the software code was edited stopping gear changes from occurring within one second of one another. This meant that deliberate gear changes could also not be set to occur less than one second from one another. Gear changes occurring in close succession were not an explicit requirement nor was this situation anticipated during runs and thus, limiting the time duration between gear shifts by one, was not viewed as a concern.

4.5.3 Vehicle VI

The vehicle VI computed the vehicle's inertia, summed the inertial loads with the terrain torques and determined the engine load based on the clutch actuation. The vehicle VI also manipulated the required torque and engine speed during simulated engine gear changes.

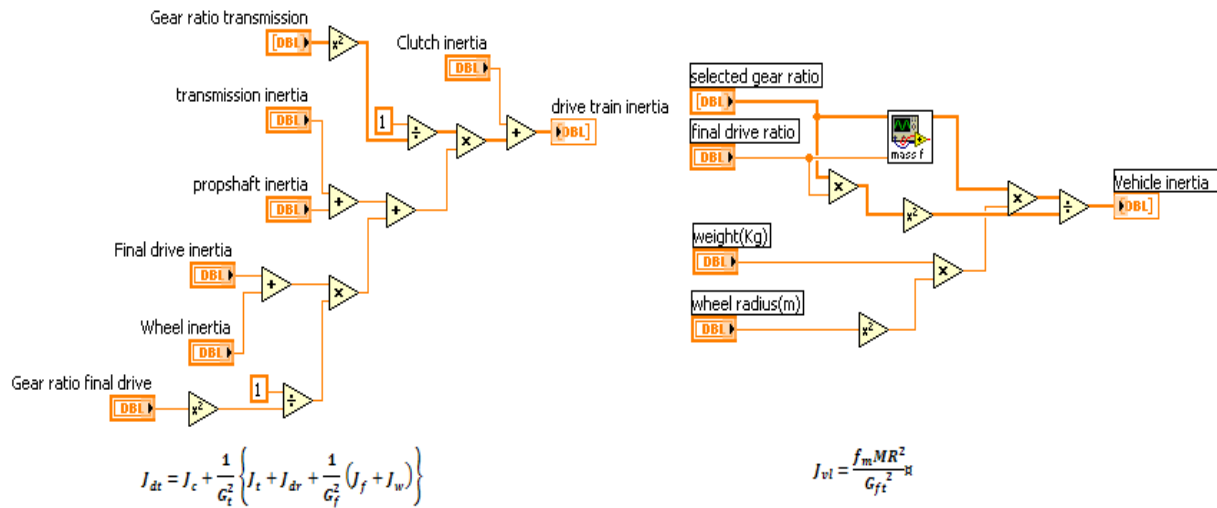


Figure 4. 11: Powertrain (left) and vehicle (right) inertia VI block diagrams.

The vehicle and powertrain inertias were calculated for every simulated vehicle speed using Equation 3-10 and Equation 3-12 respectively. According to Equation 3-14, the torque at the clutch as a result of the effective rotational inertia could be determined by multiplying the equivalent vehicle and powertrain inertia by the angular acceleration of the powertrain at the clutch. Therefore, the total torque loading applied to the engine at the clutch was:

$$T_c = F_a R G_{tf} + F_R R G_{tf} + I_v \alpha_e \quad 4-8$$

Before attempting a realistic gear change simulation it was decided that a simplistic model would be implemented first. Once this model functioned correctly while running on the test stand, a realistic simulation of a gear change would be attempted. The simplified gear change used a second order quadratic equation curve fit to ramp-up or ramp-down the engine speed to the speed required by the newly selected gear. The throttle demand was set to zero during the simplified gear change to simulate the throttle let-off during an actual gear change. This was not an accurate simulation of a gear change; however it provided insight into the loads that

could be anticipated on the test stand during gear change simulation. Few gear changes occurred during an emissions cycle simulation, and each of these gear change simulations had a short duration in comparison to the full cycle length. This indicated that no dramatic effects on the overall accuracy of the model were expected due to the implementation of the simplified gear changes.

The simulation of gear changes in the cycle concluded the preprocessing of a velocity profile. The resulting output file was then used to run the simulation on the dynamometer. This file contained the required engine speed, throttle position and engine load. Engine speed and throttle positions were used during test stand running while the engine load values were used for post run processing and cycle accuracy validation. Engine speed and throttle positions were output through the target PC's DAQ card as analog voltages as discussed previously. Values were output at a rate of 400Hz. Engine speed measurement was obtained using an analog voltage from the dynamometer controller, throttle position was measured at the EGAS throttle potentiometer as an analog voltage and the engine torque was measured as an analog voltage obtained from the torque flange. These measured values were recorded at a rate of 100Hz by the target PC.

For reasons that will be discussed in Chapter 5, further development on this program was abandoned. The intention was to pursue a real-time hardware in the loop processing model as opposed to a preprocessing model as was used with this program.

4.6 Second Simulation Program

The second simulation model was intended as an offline software development program. It was used to test a new structure for the revised program and ensure correct software functionality before implementation on the test stand. Offline testing was required as all computations were to be done in real-time, thus the setpoints could not be reviewed prior to being sent to the components of the test stand. This meant that all possible scenarios required testing prior to running of the system on the test stand to minimize any risk to the equipment.

The program was developed using the standard LabVIEW development environment as opposed to the real-time development environment. Once the second program was developed, it was transferred to the real-time environment so that it could be integrated with the test stand in the form of the third simulation program.

As with the first program, the second program could conceptually be divided into three sub-VI's as displayed in Figure 4. 12. However when coding the system, it was realized that this scenario created an unnecessary amount of data processing. Although this model was conceptually retained, the programming was abandoned. Instead all sub-VI's code was brought directly into the parent VI.

The second program was developed as an iterative computational model that would process data at simulation time during testing. For development purposes, the previously generated

and discussed engine characterization was used to simulate the response of a real engine to engine speeds and throttle positions provided.

The program initiated with the entering of engine and vehicle parameters of the simulated vehicle. The second program required the following additional properties:

1. Maximum clutch transfer torque.
2. Target vehicle pull-away acceleration rate.

Once the required parameters were entered, the intended driving cycle or velocity profile was selected. The program would then begin. Many of the original sub-VI's from the first simulation program were re-used, however, the structure and overall method and functionality had changed significantly.

As the second simulation program did not run on the target PC (real-time OS), deterministic timing was not possible. For offline development purposes, this was of no concern. The focus was to obtain a correctly functioning model i.e. the ability to calculate the engine speed and load based on the vehicle parameters and velocity profile. The input velocity profile used during development was a 100 Hz file and as such it was convenient to run the program at one loop or iteration per input value. It would further have been frivolous to increase the loop frequency of the developed simulation program while running on a normal desktop PC as this did not have a deterministically timed OS and would render no additional information but would increase the processing time.

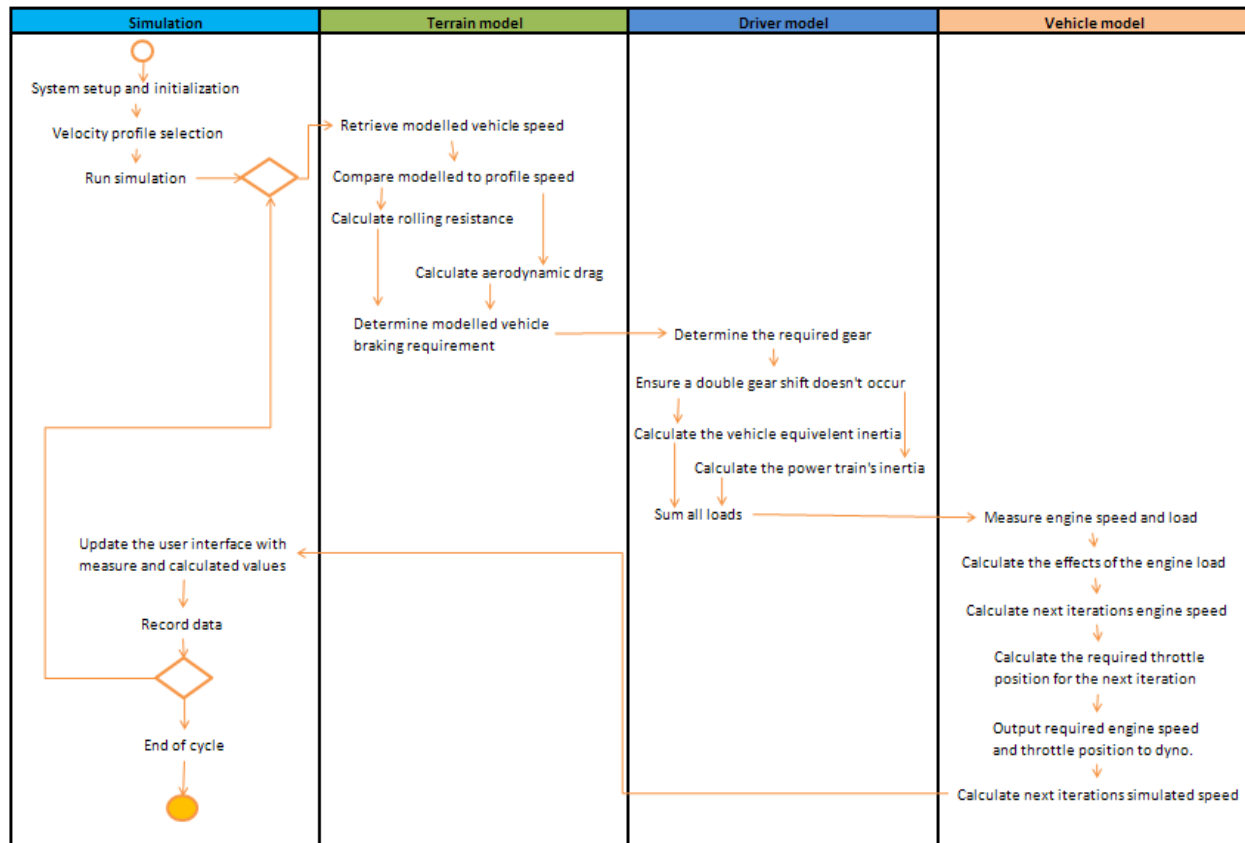


Figure 4. 12: Simulation program 2 process overview block diagram

The simulation would begin using a default simulated vehicle speed. Gear selection was made using the same principles as were used in the first simulation program. In the first program, however, engine speed was used to determine gear shift points and in this program vehicle speed was used. This change made no difference to the functionality just the method used to obtain the result. The ECE emissions cycle quoted vehicle speeds at which gear changes were required to occur during a test cycle and as such, it was a logical decision that gear changes would occur at user defined vehicle speed setpoints.

Once the required gear was determined, the aerodynamic drag and rolling resistance was calculated based on the current simulated vehicle speed. The drivetrain rotational inertia as well as the effective vehicle rotational inertia were also calculated. The coded VI's from the first simulation model were those used to calculate the aerodynamic drag, rolling resistance, drive train rotational inertia and effective vehicle rotational inertia. These were also used in the second program as no changes to their calculations were required. The block diagrams for these VI's are visible in Figure 4. 10 and Figure 4. 11. The calculated loads and inertias were then used to determine a total load and effective rotational inertia at the engine.

With the simulated vehicle loads determined, the required vehicle speed was compared to the simulated vehicle speed. If the latter was higher than that required, and other set requirements were met, a braking simulation algorithm was implemented.

The most complex VI of the second program was the simulation of the torque transferred to/from the engine via the simulated clutch. Unlike the first program, this model was intended to accurately model the engine loading that occurred during a real gear change. This VI was divided into two coded models; the first model was the locked-up clutch model which was used to simulate normal driving conditions. The second was the clutch-slip model which was used to simulate all conditions where clutch slip was present.

To determine whether the clutch should have been in the locked-up or slip mode, three parameters were evaluated:

1. The selected gear ratio in the previous iteration loop was compared to that of the selected gear ratio in the current loop. When the ratios were not equal, it indicated a gear change had occurred in the current iteration. If these two values were equal, it would have indicated that no gear change had occurred and the lock-up model would have been implemented. Alternatively it may have indicated that an earlier gear change was still being simulated and the slip-model was still implemented to complete the clutch slip modeling until clutch lock-up occurred.
2. The mode of the clutch model in the previous iteration of the loop. The mode was either in locked-up clutch mode or in clutch-slip mode which was set in the loop's previous iteration. This was required in the circumstance where a gear change had occurred in a previous iteration to the last (n-2) and the model was still simulating that gear change's clutch-slip.
3. The neutral gear variable was used to indicate that the clutch-slip model was required as the simulated vehicle was in the neutral gear, which was simulated by removing the load from the engine.

When the locked-up model was selected, as was the case under normal driving conditions, the simulated vehicle speed was controlled by the vehicle speed setpoint using a PID controller. The output of the controller was a throttle demand value. This value together with the current engine speed (determined using the current vehicle speed and the selected gear ratios) was then sent to the simulated engine, which used the previously measured engine characterization data to calculate the simulated torque output of the engine based on the provided engine speed and throttle demand value.

If the slip model had been selected, the throttle position, engine rpm, drivetrain rpm as well as the torque transferred to the drivetrain via the slipping clutch would be calculated using developed algorithms. The calculated throttle position and engine rpm was then sent to the simulated engine, which used the previously measured engine characterization data to calculate the simulated torque output of the engine from the provided engine speed and throttle demand value.

The produced engine torque or in the case of a slipping clutch, the engine torque transferred to the drivetrain side of the clutch, would have the previously calculated load torque (terrain

torque) subtracted from it. This would yield the 'excess torque' or torque available to accelerate the vehicle. If the engine torque produced was less than the load torque, the vehicle would decelerate. This torque would then be manipulated using Equation 3-14 to yield the drivetrains angular acceleration which was further manipulated to yield the vehicle and engine acceleration. This acceleration was multiplied by the loops period to yield the increase in engine and vehicle speed that occurred during the loops current iteration. These changes in speed were then added to their respective current speeds. This would result in the end of the current iteration. The engine and vehicle speed and other calculated values would then be sent to the next iteration of the loop as initial values. This process would continue until the entire velocity profile had been run.

4.6.1 Simulated vehicle braking VI

One of the newly added VI that was neither present nor required in the first simulation program was a vehicle braking algorithm and controller. The simulated vehicle speed used by the first program was always equivalent to the speed setpoint (engine speed was a product of the required vehicle speed and transmission ratios) and as such did not require a braking algorithm as braking force was all ready accounted for, but as an unknown quantity. With the second program, the vehicle speed was dependent upon the calculated throttle demand signal's effect on the engine torque output and its ability to overcome the terrain loads. The simulated vehicle speed was therefore decoupled from the required vehicle speed with the only link being the required vehicle speed which was the setpoint for the simulated vehicle speed PID controller.

An implication of the decoupling of the simulated speed from the required speed was that if the required speed was reduced rapidly, without a braking algorithm, the only forces that would yield in a reduction of the vehicles speed were those of the simulated rolling resistance, the aerodynamic resistance, engine braking and the effects of the vehicle and drivetrains effective rotational inertias. These forces were found to be capable of reducing the simulated vehicle's speed, but only at low rate of change of speed (especially at low vehicle speeds) and as such, the need for the braking algorithm was evident.

The braking algorithm made use of a PID controller to regulate the simulated vehicle speed to the required vehicle speed. The output of the controller was a force applied at the wheels in the direction opposite to that of the vehicle's travel. This force added to the terrain induced forces which were used to create the load on the engine, and indirectly determine the vehicle speed. The range of the force could be adjusted, but it was intended that the range of this force would simulate the range of the actual vehicle braking ability. To prevent the braking PID from 'fighting' or counteracting the effects of the throttle PID (both controllers attempting to control the simulated vehicle speed) the gains of the braking PID were set to values resulting in a slower controller. Thus the throttle controller would act as the primary means of controlling the vehicles speed and the braking PID as a slower secondary means of controlling or reducing the simulated vehicle speed. To further prevent the controllers from counteracting one another as

well as to ensure that the braking controller was only active when intentionally required, the following condition had to be met before the braking controller was enabled:

1. The current throttle demand from the throttle PID had to be less than 15% for the braking controller to be activated. This prevents the braking controller from counter-acting the throttle PID while it was controlling the vehicle speed under normal driving conditions. This also prevented a situation which would result in a full throttle demand, full braking demand scenario or the real life analogy of driving while holding the brakes on.

As well as complying with the above condition, one of the following conditions also had to be met:

1. The simulated vehicle speed needed to exceed the vehicle speed setpoint by 1.5km/h while in normal driving mode. This allows the throttle PID controller to have a small steady state error as well as a small margin to stabilize the vehicle speed without the braking controller counter-acting the throttle PID's efforts to control the vehicles speed. This condition also fell within the speed tolerance allowed by the ECE cycle specification of $\pm 2\text{km/h}$ tolerance.
2. The program was required to simulate a downward gear shifting or a stopping scenario. This allowed for the real life analogy of reducing the vehicle's speed while gearing down.

4.6.2 Simulated clutch locked-up VI

The simulated clutch lock-up VI was intended to determine the amount of load transferred from the drivetrain to the engine or the amount of torque transferred from the engine to the drivetrain. However, as the torque transferred to or from the engine was dependent on the torque output of the engine, it was a convenient location in the code to determine the throttle demand required to achieve the vehicle setpoint speed.

The clutch lock-up VI was used in all situations when there was no clutch slip modeling required. With no clutch slip present, all the torque generated by the engine was transferred to the drivetrain and the entire load associated with the vehicle was transferred to the engine. A further task of the model was that of controlling the simulated vehicle speed by balancing the torque output of the engine with the vehicle load under steady state or transient vehicle speed conditions. Under these conditions, the throttle controller would increase the engine output torque to yield a positive net torque output (more torque produced by the engine than load caused by the vehicle) in order to accelerate the vehicle and a negative net torque output in order to decelerate the vehicle.

The throttle controller made use of a PID controller. The required vehicle speed was used as the setpoint, with the simulated vehicle speed as the process variable. The output of the controller was a throttle position demand, which was then sent with the current engine speed to the simulated engine.

The clutch plate rotational velocity was determined by the manipulation of the simulated vehicle velocity using the drivetrain transmission ratios. With the clutch in a locked-up model, the rotational velocities of clutch the plate and the pressure plate/flywheel were equivalent and thus the engine speed could be directly determined from the simulated vehicle velocity.

As previously discussed, the output from the engine simulation model was the simulated engine torque relative to the provided throttle demand and engine speed. The simulated engine torque in combination with the vehicle load and the system's effective rotational inertia were then applied to the simulated vehicle velocity, and the change in vehicle velocity was then determined.

As previously defined, the actual engine torque output on a test stand under transient conditions with the load measured using a torque flange was determined as follows:

For the engine driving the dynamometer:

$$T_E = T_{TF} - J_D \alpha_E \quad 4-9$$

For the dynamometer motoring the engine:

$$T_E = T_{TF} - J_E \alpha_E \quad 4-10$$

The angular acceleration of the engine was thus:

$$\alpha_E = \frac{T_E - T_C}{J_E} \quad 4-11$$

The angular acceleration of clutch plate or "vehicle" was:

$$\alpha_V = \frac{T_C - T_V}{J_V} \quad 4-12$$

As the clutch model was a locked-up model:

$$\begin{aligned} \alpha_E &= \alpha_V \\ \alpha_E &= \alpha_V = \frac{T_E - T_V}{J_E + J_V} \end{aligned} \quad 4-13$$

Thus, if Equations 4-9 and 4-10 are substituted into Equation 4-13 the following is obtained:

For the engine driving the dynamometer:

$$\alpha_E = \frac{(T_{TF} - J_D \alpha_E) - T_V}{J_E + J_V} \quad 4-14$$

$$\alpha_E = \alpha_V = \frac{T_{TF} - T_V}{J_E + J_V + J_D}$$

For the dynamometer motoring the engine:

$$\alpha_E = \frac{(T_{TF} - J_E \alpha_E) - T_V}{J_E - J_V}$$

$$\alpha_E = \alpha_V = \frac{T_{TF} - T_V}{2J_E + J_V} \quad 4-15$$

Conradies (2001) suggested that the Euler integration algorithm be used to determine the next iterations clutch angular speed. This was done by multiplying the calculated clutch angular acceleration by the control loop period and then added the current iterations simulated clutch speed. Mathematically stated:

$$\omega_{n+1} = \omega_n + \alpha_n \Delta t \quad 4-16$$

Using the rotational accelerations defined in equations 4-14 and 4-15, the vehicle and engine speeds were determined. For the development of this offline simulation, the load to be measured by the torque flange was simulated using an engine characterization curve. This was one of a number of compromises that had to be made to create the offline simulation, resulting in inaccuracies that existed in this program. The aim of this program however, was to develop a functional system intended for a test stand under circumstances in which most of the offline program inaccuracies would be removed during online operation.

The most evident of the included inaccuracies in this program was the J_D term. The inclusion of this term in equation 4-14 resulted in higher simulated rotational accelerations than would have realistically occurred. Logically this made sense as the inclusion of this term, was intended to compensate for the effects of the dynamometer under transient operation but in this simulation model no dynamometer model was present. This term was however included as any related error would be removed once this program evolved into the online program that was to be run on a test stand. Further inaccuracies were the values of torque provided by the engine characterization. These values were measured under steady state conditions while the simulation was of a transient nature. Thus, in this program, the simulated value provided by the engine characterization as the simulated measured torque flange was actually equal to the engine torque. Therefore, if a more accurate result was required from this program using the given engine characterization, equation 4-13 should have been used in place of equations 4-14 and 4-15. This was not done as this program was intended to run on a test stand where engine torque would have to be calculated as suggested above. The last of the known errors that would be corrected during the evolution from the offline model to the online model was the replacement of the time constant Δt that was programmed into Equation 4-16, with a measured value of the period between one iteration of the control loop to the next. This could be done as the online model would be running on a deterministic real-time PC.

4.6.3 Simulated clutch-slip VI

The clutch-slip VI controlled the engine and drivetrain interaction during all events in which clutch-slip was intentionally introduced under real world conditions. The clutch-slip VI was responsible for simulating:

1. Gear changes up.
2. Gear changes down.
3. The Vehicle-pull-away.
4. The Vehicle coming-to-rest.

Before any modeling occurred, it was important to determine which maneuver needed to be simulated. The intention was to produce a simulation of a human gear change and not necessarily an ideal gear change. This required a computer model of the mechanical components as well as the human interactions with these components. The components of a clutch have been well defined in many texts using Newton's laws; however the human control process of these components has not. Having considered the challenge of modeling this interaction, it was decided that it would be beneficial to focus efforts on simulating a gear change based on an individual's interaction with the mechanical components as opposed to using averaged data of a group of people's interaction. This would prevent the possible confusion developed by contradictory methods used by individuals in the group. Group normalized data could always be attempted at a later stage.

After having completed the literature study, PID controllers were found to be capable of controlling the simulated clutch. They were however less than ideal at controlling the simulated clutch in a manner emulating a human's control process. National Instruments view is that Fuzzy logic is a method of rule-based decision making and process control that emulates the rule-of-thumb thought process used by human beings.

In order to determine which clutch-slip scenario required simulating, a clutch-slip model was required. Each scenario had its own set of conditions that defined when its respective model was used. These conditions were as follows:

- 1) Gear change up or gear change down model: The gear change must have occurred on the loops current iteration or a gear change must already have been in the process of being simulated as a result of a gear change that occurred on a previous iteration. A gear change was detected by comparing the current iterations gear ratio to the last iterations. If the current ratio was higher than the previous iterations, it was a down-shift. If the current iterations gear ratio was lower than the previous iterations, it was an up-shift.
- 2) Vehicle pull-away model: The current simulated gear needed to be the lowest gear. The simulated vehicle needed to be stationary and the setpoint speed needed to be greater than 0km/h. All of these conditions needed to have been met on the current iteration or were met on a previous iteration with the pull-away simulation still occurring.

- 3) Vehicle come to rest model: The current simulated gear needed to be the lowest gear. The simulated vehicle speed needed to be less than 10km/h but the vehicle needs not be stationary. All of these conditions had to have been met on the current iteration or on a previous iteration with the “come to rest” simulation still occurring.

As each scenario listed above had its own conditions and limitation, each will be discussed separately:

4.6.3.1 Gear changes

The development of a gear change strategy started with the curve fitting in the first simulation program. In the second program (offline program), the curve was replaced with a more realistic gear change simulation that was developed. During a gear change the throttle demand value was set to zero in the first 10ms of the simulation while the vehicle’s effective rotational inertia and load were progressively removed from the engine over 20ms. During an up-change the engine speed would then fall until it came within 50rpm of the drivetrain or clutch the plate speed. At this stage, the vehicle load would begin to be re-applied to the engine while simultaneously increasing the throttle position to that which it was before the gear change simulation. The PID throttle controller would re-activate and take control of the throttle demand.

To produce the clutch-slip modeling, equations 4-14 and 4-15 were re-defined to from equations 4-16 and 4-17. These two equations enabled the simulation of clutch-slip, thereby making it possible to simulate the discontinuity between the engine and drivetrain during a gear change. While the clutch was locked-up, all torque produced by the engine minus its internal losses were transferred through the clutch and into the drivetrain. During the disconnection of the drivetrain, a reduction in the vehicle’s load on the engine could be simulated by subtracting a percentage of the engine output torque from the full torque output of the engine. This was done in equations 4-17 and 4-18 using the clutch transfer constant R.

The engine angular acceleration equation is derived for the engine driving the dynamometer on the test stand.

$$\begin{aligned}\alpha_E &= \frac{T_E - T_V}{J_E + J_V} \\ \alpha_E &= \frac{(T_{TF} - \alpha_E J_D) - R(T_{TF} - \alpha_E J_D)}{J_E + R(J_V)} \\ \alpha_E &= \frac{T_{TF} - RT_{TF}}{J_E + J_D + R(J_V + J_D)}\end{aligned}\tag{4-17}$$

The engine angular acceleration equation is derived for the dynamometer, motoring the engine on the test stand.

$$\begin{aligned}\alpha_E &= \frac{T_E - T_V}{J_E + J_V} \\ \alpha_E &= \frac{(T_{TF} - \alpha_E J_E) - R(T_{TF} - \alpha_E J_E)}{J_E + R(J_V)} \\ \alpha_E &= \frac{T_{TF} - RT_{TF}}{2J_E + R(J_V - J_E)}\end{aligned}\tag{4-18}$$

The simulated effective vehicle rotational inertia was also manipulated using the clutch transfer constant R . Thus when the gear change simulation started and the full vehicle load was present, the clutch transfer constant was equal to one and thus all engine torque produced by the engine was being transferred to the vehicle side of the clutch. The effective vehicle rotational inertia was also present, thus giving Equation 4-13. Once the gear change simulation progressed to the point of full clutch-slip, the clutch-slip constant was reduced to zero which yields Equation 4-11 and thus the engine slip mode.

On the drivetrain side of the clutch, a similar process was followed. Equation 4-12 was used to evolve equation 4-13 so that the vehicle's reaction to the disconnection of the engine could be simulated. This was done using the same clutch transfer constant. This resulted in equations 4-19 and 4-20.

The vehicle angular acceleration equation is derived for the engine driving the dynamometer on the test stand.

$$\begin{aligned}\alpha_V &= \frac{T_E - T_V}{J_E + J_V} \\ \alpha_V &= \frac{R(T_{TF} - \alpha_E J_D) - T_V}{R(J_E) + J_V}\end{aligned}\tag{4-19}$$

The vehicle angular acceleration equation is derived for the dynamometer motoring the engine on the test stand.

$$\begin{aligned}\alpha_V &= \frac{T_E - T_V}{J_E + J_V} \\ \alpha_V &= \frac{R(T_{TF} - \alpha_E J_E) - T_V}{R(J_E) + J_V}\end{aligned}\tag{4-20}$$

However, Shigley (2003) proposes the following two equations for the amount of transferable torque through a clutch:

1. Uniform Wear

$$T_{Cmax} = \frac{Ff}{4}(D + d)\tag{4-21}$$

2. Uniform Pressure

$$T_{Cmax} = \frac{FfD^3 - d^3}{3D^2 - d^2} \quad 4-22$$

These equations show that the torque transferable through a clutch was not dependant on the engine torque output but on the physical properties of the clutch. The maximum transferable torque of a new clutch (uniform pressure model which produces a higher value then uniform wear model) fitted to an automobile would be well in excess of the engine's maximum output. This was easily demonstrated by the ability to stall an engine on the test stand using the dynamometer to brake the engine through the clutch while at wide open throttle. As equations 4-17 through 4-20 calculate the transfer torque as a percentage of the engine's produced torque, the scenario of stalling the engine on the test stand would not be possible based on these equations. Thus, the model required the input of a maximum clutch torque transfer value, T_{Cmax} to produce a realistic model. Thus the final equations used to model the clutch were as follows:

The engine angular acceleration equation is derived for the engine driving the dynamometer on the test stand.

$$\alpha_E = \frac{T_{TF} - RT_{Cmax}}{J_E + J_D + R(J_V + J_D)} \quad 4-23$$

Engine angular acceleration equation is derived for the dynamometer motoring the engine on the test stand.

$$\alpha_E = \frac{T_{TF} - RT_{Cmax}}{2J_E + R(J_V - J_E)} \quad 4-24$$

Vehicle angular acceleration equation is derived for the engine driving the dynamometer on the test stand.

$$\alpha_V = \frac{R(T_{Cmax}) - T_V}{R(J_E) + J_V} \quad 4-25$$

Vehicle angular acceleration equation is derived for the dynamometer motoring the engine on the test stand.

$$\alpha_V = \frac{R(T_{Cmax}) - T_V}{R(J_E) + J_V + J_D} \quad 4-26$$

4.6.3.2 Vehicle Pull-away

The vehicle pull-away mode functioned on a similar principle to the gear change strategy. Equations 4-23 through 4-26 were the fundamental equations used to determine the engine and vehicles response to throttle and clutch actuations (change in R value) that were made. The control strategy of the simulated clutch as well as the throttle demand were done using a fuzzy

logic based control strategy. Although not a true fuzzy logic controller in the traditional sense, the fundamental principles were followed.

In the developed control structure, the normal Fuzzification process did not occur. Instead, input variable were directly evaluated by rules based upon linguistic conditions. These rules underwent a Defuzzification process or translation into mathematical expressions which were set out in a nested IF statement format. The rules used in the control of the pull-away simulation were based on broken down human rule of thumb techniques to pulling a vehicle away. The final output was an alteration in the throttle demand and simulated clutch transfer constant R

National Instruments (1997) states that Fuzzy set theory differs from traditional Boolean (or two-valued) set theory in that partial membership in a set is allowed. Membership of each real variable based on the fuzzy set theory was determined in a second set of nested IF statement after the initial rule based evaluation that occurred in the first set of nested IF statements. The control could only adjust the throttle and simulated clutch transfer constant by one unit (one percent of throttle demand or clutch actuation) per iteration and as such a control structure with a non-Boolean type output was created. This meant that the output did not have to be yes or no as is done with Boolean operations. Instead an output could consist of partial membership.

4.6.3.3 Vehicle come to rest and idle

Once a simulated vehicle's speed was reduced below a set speed designated by the operator and the vehicle setpoint speed was less than the simulated vehicle speed or equal to zero, the "come to rest" algorithm was initiated. At this stage, if the throttle position was not already equal to zero percent throttle demand (the vehicle would already have been slowing and hence the throttle could have been zero), it would have been set to zero percent. Simultaneously the clutch transfer constant would have been reduced to zero thereby simulating clutch disengagement. During the clutch disengagement, Equations 4-23 through 4-26 were used.

Once the simulated clutch was disengaged and the engine would simulate an idle condition where Equations 4-23 through 4-26 were used to determine the engine idle speed with the throttle demand set to zero percent and clutch transfer constant set to zero. Idle speed was determined using the above mentioned Equations and was therefore dependent upon the torque output of the simulated engine with no load applied. Ideally, the simulated engine would have idled at the point when the simulated torque output from the engine was nil. However due to the previously discussed problems with the engines characterization, idle was exceptionally difficult to achieve. The extrapolated values at low load and speed values were not ideal. To achieve using this data and as such, the simulated engine idle speed was set to a minimum engine speed input by the program operator.

4.7 Third Simulation Program

The third simulation program also reused the code developed during the second simulation program. It was the real-time engine test stand implementation of the software developed in the second simulation program. The evolution required the splitting of the second simulation program into two components: the user interface on the host PC and the simulation processing component on the real-time target PC.

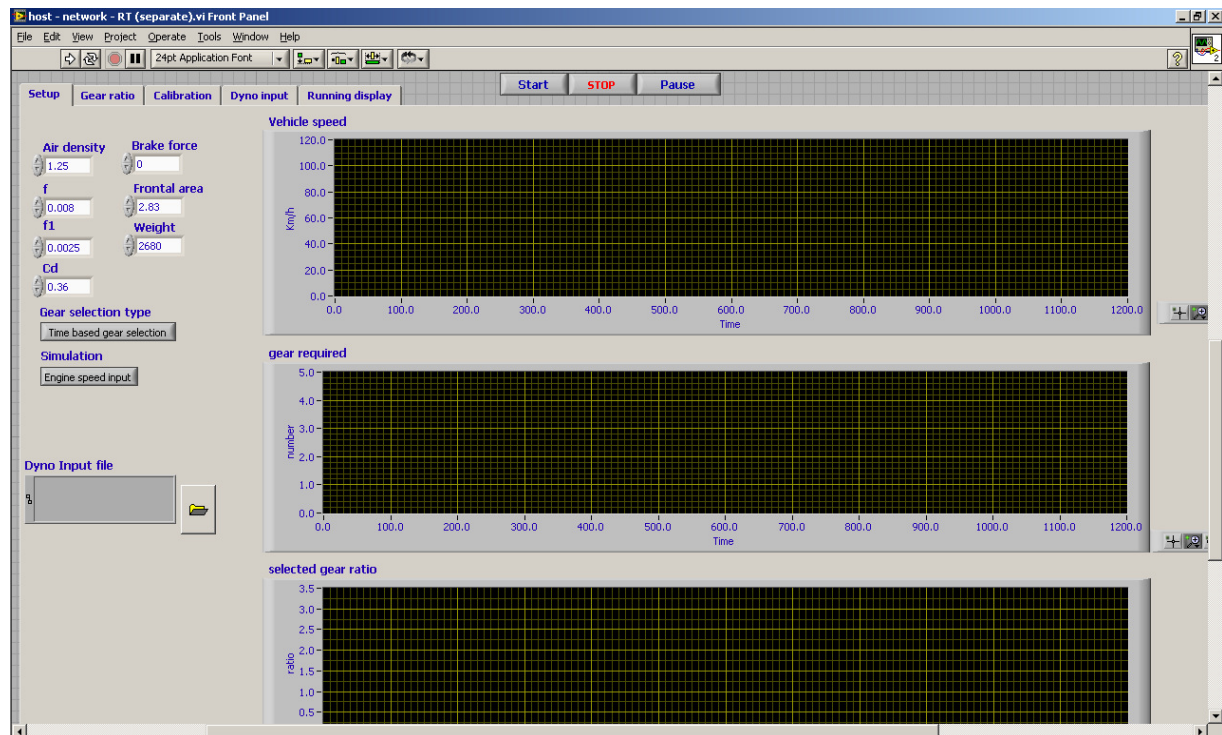


Figure 4. 13: Host PC user interface screen shot showing the five tabs

The host PC was responsible for running the user interface as well as providing the target PC with all the data the simulation algorithms required. The host PC user interface consisted of five tabs (similar to multiple sheets in a Microsoft excel spreadsheet), as follows:

1. Setup: This was where most of the simulated vehicle parameters served as input to the program. It was also where the velocity profile to be simulated was selected
2. Gear ratio: This tab was where the number of gears to be simulated was selected with their respective gear ratios. The final drive ratio, wheel diameter, minimum engine speed and maximum engine speed were also selected on this tab. To assist the user, the program would use the input data to determine the vehicle speed relative to engine speed for each gear and plot it on a graph.
3. Calibration: The calibration window was used to calibrate the DAQ card input and output channels from their intuitive units to their respective electronic units or vice versa e.g. torque to voltage. The three input and three output channels could be calibrated, as well as an additional spare channel.

4. Dynamometer input: This tab plotted the selected velocity profile or the predetermined engine speed and throttle position that were to be provided to the test stand. The engine speed, throttle position and estimated torque would be plotted so that the values could be visually confirmed before running on the test stand.
5. Running display: The running display plotted trend graphs of the engine speed, throttle position, measured torque and the spare channel. This was a useful tool for trouble shooting.

When the required vehicle parameters were selected, the simulation could be run. In addition to being able to start and stop a simulation, it could be paused at any time except during pull-away and gear change simulation. Pausing was achieved by repeating the simulated vehicle setpoint speed that was sent to the speed PID controller.

The simulation software that was developed was run in real-time on the Target PC. To allow for the real-time processing, some structural changes needed to be made to the code developed for the second program. The target PC's software consisted of a program initialization portion and four concurrent loops. Each loop ran at a different deterministic speed which was dependant on the nature of the content of the loop. The four loops were as follows:

1. Host PC communication loop. This loop was responsible for all data transfer to and from the user interface. The loop was set to run at 50Hz as this was the maximum refresh rate of the display. The loop accessed measured values from the DAQ card, converted them to a suitable format and then sent them across the network to the user interface on the host PC. A similar principle applied for data transferred from the host PC to the target PC with the exception of the data initially being accessed from memory opposed to the DAQ card.
2. Engine speed measurement loop. This loop ran at 30kHz and using measured values from the DAQ card, calculated the engine speed. This loop was intended to run at 400Hz, however it was previously discussed that the intended speed acquisition system was unsuccessful and as such the engine speed was measured using a digital TTL magnetic pickup and a counter on the DAQ card. In compliance with the Nyquist sampling theorem, the minimum sampling rate required was 12kHz, thus the 30kHz used was more than sufficient for accurate measurement.
3. Real-time data recording loop. This loop recorded the measured engine speed, torque, throttle position, simulated vehicle speed and their respective time stamps. These measurements were accessed from the DAQ card, recorded to a binary file on the target PC and recovered after a simulation was runs. The data was then converted to a comma separated file so that it could be processed. The data was recorded into a binary file as it had a higher storage rate than a CSV file and thus require less processing power. The loop ran at a rate of 100Hz and as such the recording rate was set to 100Hz.
4. The simulation loop. This loop was responsible for calculating the simulated vehicle properties based on the values provided by the simulation of the engine and the parameters measured from the engine. The simulation loop was the real-time implementation of the vehicle simulation code from the second simulation program and

as such incorporated all the vehicle simulation code. Some changes were made to the existing code to integrate it with the test stand.

5 SIMULATION PROGRAM TESTING AND EVALUATION

A total of 96 hours of testing was conducted under engine running conditions. This time was spent obtaining data for the engine characterization, checking the hardware installation, PID controller tuning and overall system evaluation. Testing of the data acquisition system and other test stand installed equipment was conducted during the development of the first simulation program. Once the first system was evaluated, the development of the second simulation program began. During the development of the second program, dynamometer input response, engine rotational inertia and dynamometer rotational inertia were concurrently measured for the specific test stand. Once the second simulation program was completed it was converted to a real-time system and implemented on test stand hardware as simulation program 3.

The final simulation program evaluation was conducted on the CAE dynamic engine test stand. Testing was conducted using a Volkswagen EA 113 engine simulated in a Volkswagen Polo chassis. The vehicle specifications are as follows:

Table 5. 1: Test vehicle technical specification.

Engine	
Engine model	EA 113
Capacity	1598cc
Number of cylinders	4
Combustion process	4-stroke, petrol
Compression ratio	11.5:1
Coolant type	Water
Bore	76.5mm
Stroke	86.9mm
Maximum Power	76kW @ 5700rpm
Maximum Torque	148N.m @ 4500rpm
Chassis	
Type	Polo
Weight	1145kg
Width	1650mm
Height	1467mm
Frontal area	2.23m ²
Drag co-efficient	0.32
Tyre running radius	0.308m
Transmission	
Number of gears	5 forward, 1 reverse
1 st gear ratio	3.45
2 nd gear ratio	1.95
3 rd gear ratio	1.28
4 th gear ratio	0.88
5 th gear ratio	0.67
Final drive	4.533

Factory claimed fuel consumption	
ECE urban cycle	9.2l/100km
ECE extra-urban cycle	5.3l/100km
ECE combined cycle	7.0l/100km

A discussion on the testing conducted on the three simulation programs that were developed as well as the supplementary testing conducted, is given below.

5.1 First Simulation

During the development of the first simulation program much testing was conducted on the deterministic data acquisition and recording components (hardware and software). As these components were the foundations of the entire system, it was crucial to ensure their correct functioning. To allow the data acquisition code to be tested under transient engine running conditions without using the vehicle simulation code, an additional code was developed that enabled engine speed and throttle position values to be read from a file and output to the test stand. This allowed the running of the engine test stand in a transient manner thereby enabled the independent evaluation of the deterministic DAQ and the simulation code.

Figure 5. 1 plots the results of a test conducted on the DAQ system while the engine was running under transient conditions. The figure depicts a setpoint velocity profile and the recorded velocity profile. The figure highlights the initial problems that were experienced with the real-time software and had to be overcome to ensure that the system was deterministic. The recorded engine speed profile depicted in Figure 5. 1 appears to be a stretched version of the setpoint profile. Initial investigations suggested problems with the method of recording data, however in this specific case, the cause was poor coding techniques which lead to excessive load on the target PC's processor and as such deterministic timing could not be maintained. Once the processor load was reduced using code optimization techniques, additional fail safe procedures were implemented to notify the user in the event that processor load became excessive and thereby threatened the deterministic timing of the program.

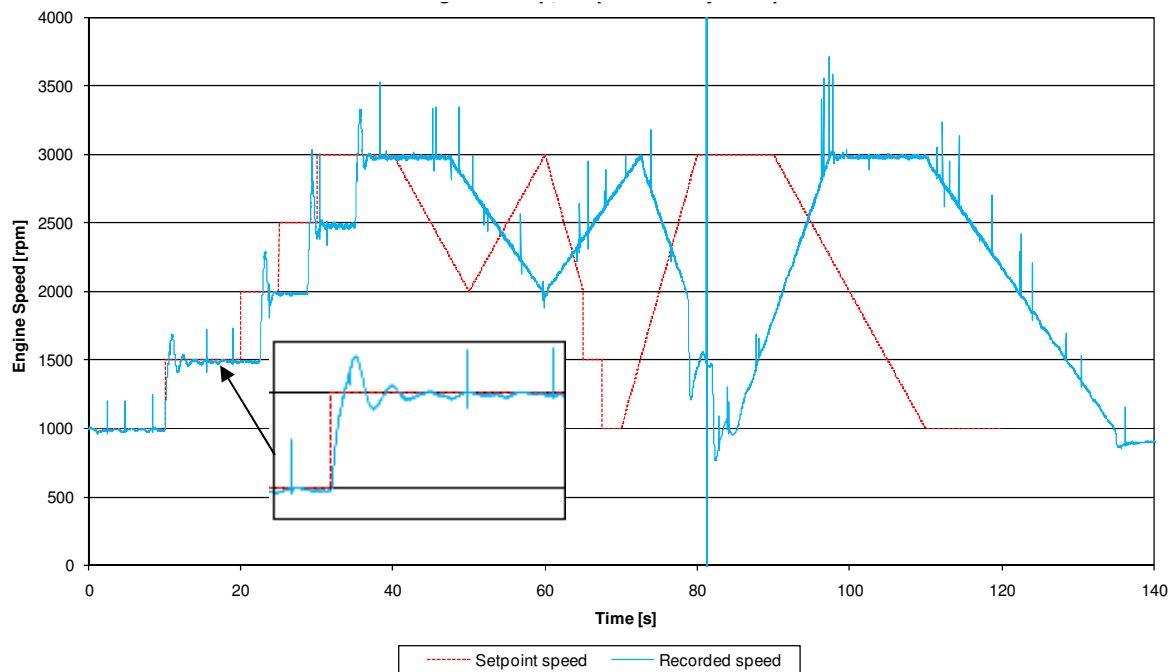


Figure 5. 1: Engine speed versus time for Simulation program 1, test 7. Recorded engine speed following a step, ramp and steady state input.

The enlarged image within Figure 5. 1 was placed to show the immediate advantage of the high recording rate that was sustainable using the developed system. The enlarged portion was of the dynamometer PID controller controlling the engine/dynamometer speed after having received a step change input. This oscillation (overshoot) in the dynamometer's control response had not been clearly recorded previously.

Figure 5. 1 also depicts the high frequency noise produced by the magnetic engine speed pick-up. These spikes could be recorded as speed measurement which at this stage, was done using an analog channel (unfiltered) and not a counter channel as was used for the third simulation program. These spikes resulted in the implementation of a digital filter in the third simulation program.

Once the faults highlighted in Figure 5. 1 were corrected, the simulation part of the system was developed. When the first system's development was completed, a review was conducted on the calculated engine speed and throttle demand setpoints as well as the anticipated engine torque output generated by the first simulation program. The conclusion of the review was that the anticipated engine torque did not appear to relate to the required engine speed and throttle positions calculated by the first simulation program. It was however decided that the simulation would be run on the engine test stand and the results would then be re-evaluated.

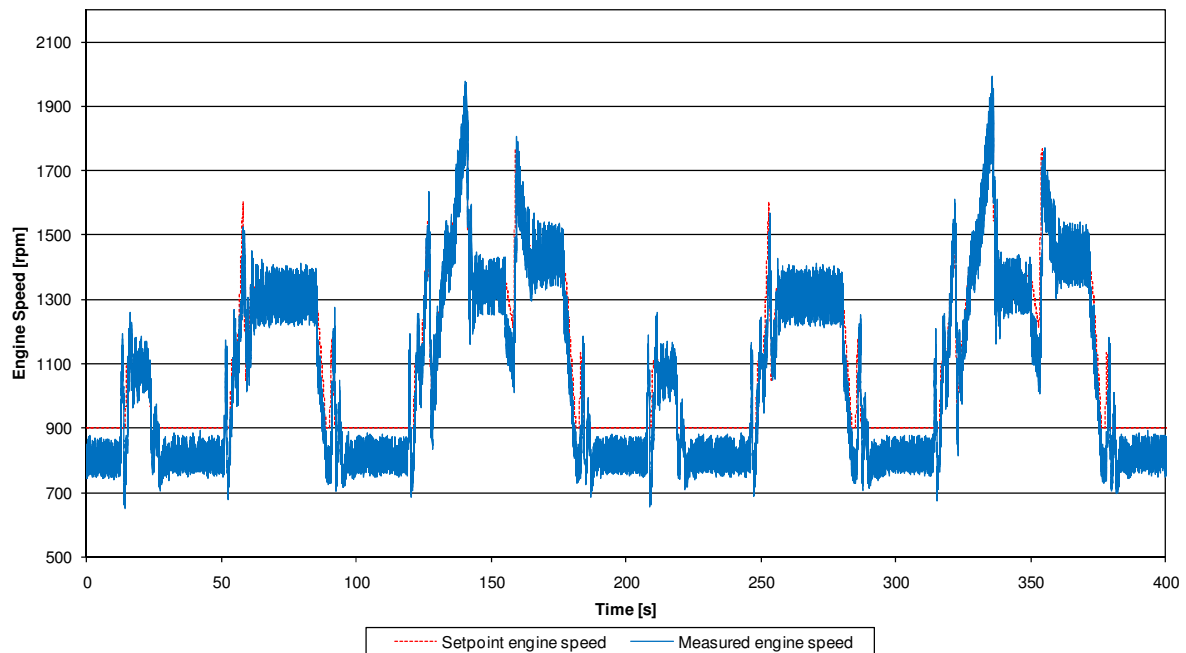


Figure 5. 2: Engine speed versus time for Simulation program1, test1. Measured engine speed while simulating two ECE urban cycles.

Figure 5. 2 displays the recorded engine speed in comparison to the engine speed setpoints when run on the test stand. The setpoints were calculated for the simulation of two continuous ECE urban cycles by the first simulation program. As can be seen, the setpoint profile was correctly traversed, however it was evident that the simulation program's idle speed was set at a higher engine speed than the actual idle speed. Figure 5. 2 further displays a continuous high frequency oscillation in the recorded engine speed. This oscillation had amplitude of approximately 100rpm and started when the speed measurement system was changed from the analog signal received from the dynamometer controller to the developed system using the digital magnetic pickup. It was discovered that the oscillation was caused by the instantaneous engine speed sampling done using the magnetic pick-up. The engine speed was not measured by the simulation program at the same point in the engine's 4 stroke process each time it was sampled and thus the engine speed would vary between measurements. This was corrected by taking a running average of the engine speed over a duration of 720 degrees of engine rotation or 1 complete cycle. This correction was implemented in the third simulation program.

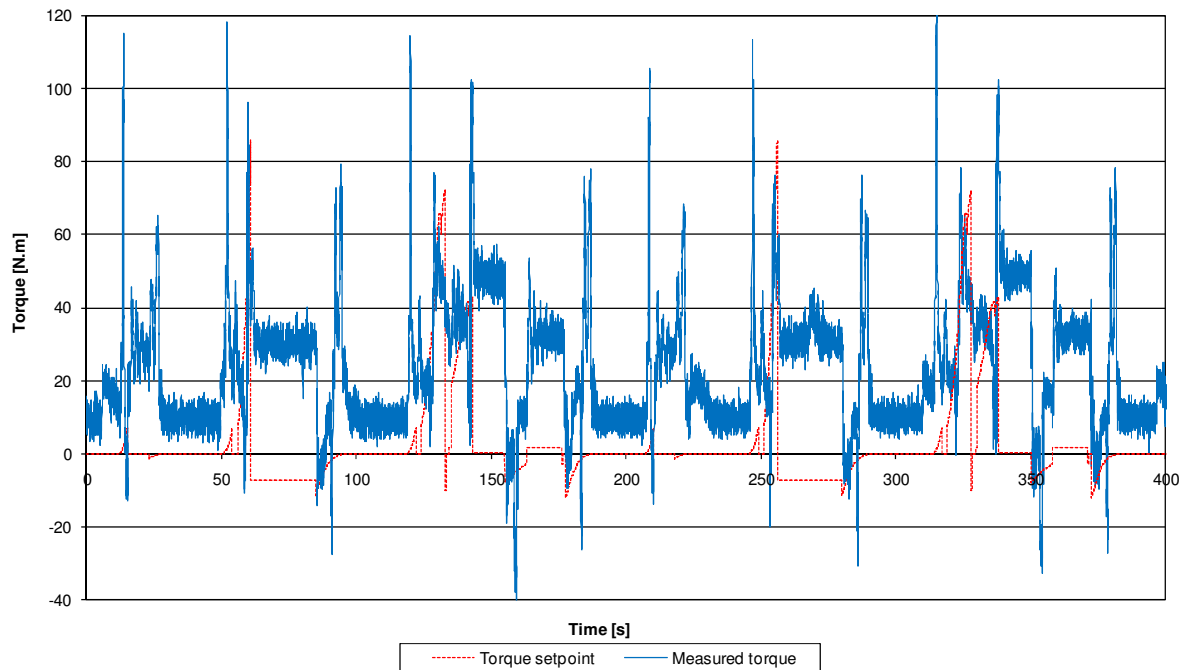


Figure 5. 3: Torque versus time for Simulation program1, test 1. Measured torque flange torque while simulating two ECE urban cycles.

Figure 5. 3 displays the plotted measured engine torque together with the anticipated engine torque calculated by the first simulation program for two consecutive ECE urban cycles. This data is relative to the engine speeds given in Figure 5. 2. From Figure 5. 3 it was immediately evident that the recorded engine torque and the simulation calculated anticipated engine torque did not correlate and as such, the result was that the ECE urban cycle had been incorrectly simulated. This led to a review of the entire first simulation program which highlighted many problems with both the program as well as the simulation. These problems were found to be extensive and spread throughout the program. After having attempted a vehicle simulation on the test stand using the method required by the first simulation program, it was recognized that this method provided no indication of how a simulation was progressing until the final results were processed after a simulation was run on the test stand. This was less than ideal for both the development of the software as well as for the intended use of the completed program. Thus it was decided that instead of implementing the required changes to correct the vehicle simulation code of the first simulation program, a new program would be developed that incorporated all the changes required to correct both the functionality and simulation faults present in the first program.

5.2 Second Simulation Program

The second simulation program was used to develop the software code required to correct the shortcomings of the first simulation program. This program was never evaluated on an engine test stand but was evaluated in real time through its user interface displayed in Figure 5. 4.

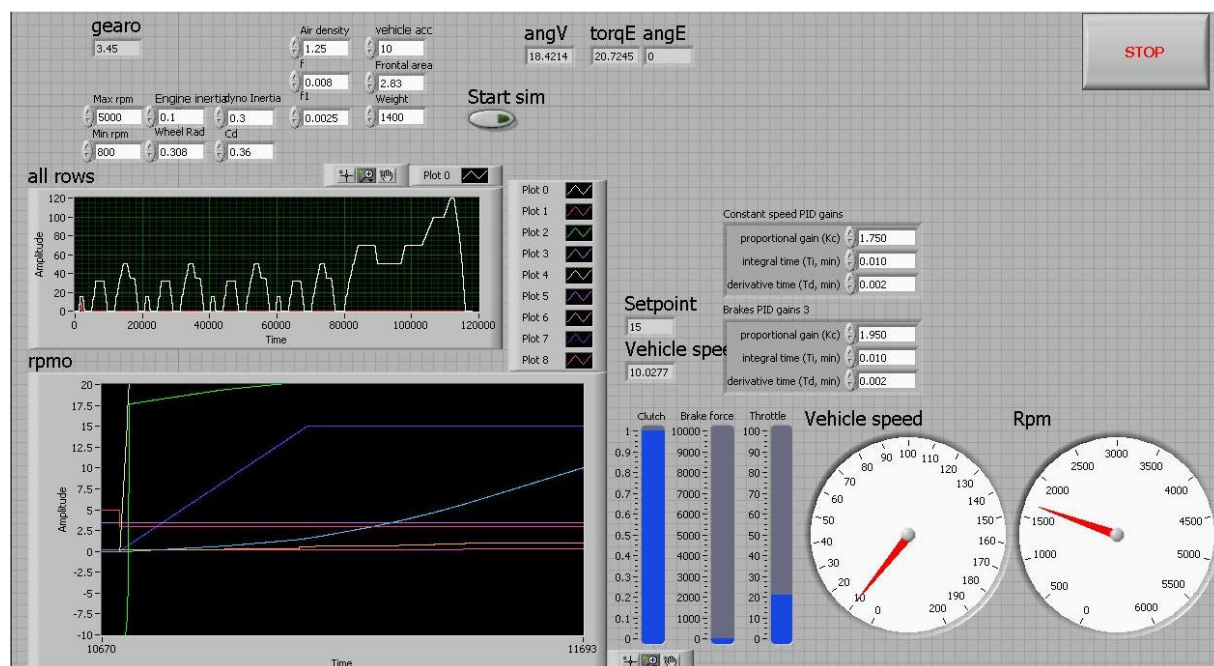


Figure 5. 4: Simulation program 2 trouble shooting user interface.

Data was not recorded during the development and testing of the second simulation program and thus no results can be displayed. The effectiveness of the developed code for this program can however be evaluated by the results of the third simulation program which was the real time test stand implementation of the code developed in the second simulation program.

5.3 Third Simulation Program

The final evaluation testing was conducted by means of the third simulation program. The following aspects were evaluated:

1. Simulation accuracy.
2. Ability to follow a provided cycle.
3. Repeatability and reproducibility of results.

Under ideal circumstances, the preferred method of conducting the final evaluation of the third vehicle simulation program would have been to conduct a series of ECE emissions tests using a real vehicle on a rolling road as prescribed by the ECE standard and then on an engine test stand simulating the same vehicle. The emissions and performance figures from the two data sets could then be compared and the simulation system evaluated on the three aspects listed above. This testing would have required access to a rolling road emissions facility as well as an engine test stand emissions facility. Neither of the two was accessible for the evaluation of the simulation system, and thus a comparison of the emissions as an evaluation of the simulation accuracy was not possible.

As an alternative, it was elected that system accuracy be evaluated based on the fuel consumption of an actual vehicle compared to that of a simulated vehicle over the duration of an ECE cycle. This would remove the need for the emissions test equipment. South African legislation requires vehicle manufacturers to publish fuel consumption data together with emissions data of the vehicles they produce, based on an ECE cycle. The simulation accuracy evaluation was thus based on the fuel consumption results of the ECE simulation and compared to that of the manufacturer's published fuel consumption results. This was recognized as an imperfect method of evaluation, however with the available resources, funds and time, it was the most reliable means of evaluation possible and would provide a clear indication of the system accuracy over an ECE urban cycle, ECE extra-urban cycle and a complete ECE cycle. It would, however, fail in providing instantaneous confirmation of accuracy.

The third simulation system was evaluated based on the above listed aspects through a series of eighteen attempted ECE emissions cycles. Eleven of the eighteen runs were successfully conducted with the other seven providing a clear indication of a limit to the programs ability. The eleven completed runs of the ECE cycle were used to evaluate the simulation accuracy, ability to follow a provided cycle and repeatability. The final four of the eleven cycles conducted were spent evaluating the system's ability to adapt to changes in the simulated vehicles properties. A summary of the results of the eighteen evaluation runs are given in Table 5. 2 with discussions of the various runs following under their appropriate evaluation criteria heading.

Table 5. 2: Summarized ECE run configurations and fuel consumption results

	Comments	vehicle mass (kg)	Rolling res. Cons. f0	Rolling res. Cons. f1	Drag coefficient Cd	Urban 1 [l/100km]	Urban 2 [l/100km]	Urban 3 [l/100km]	Urban 4 [l/100km]	Average urban [l/100km]	Extra-urban [l/100km]	combined [l/100km]
	Actual vehicle properties	1245			0.32	9.2	9.2	9.2	9.2	9.2	5.3	7
run 1	fuel flow meter refill in extra-urban	1245	0.0015	0.006	0.32	10.84	11.78	11.81	12.27	11.83	5.24	7.66
run 2	fuel flow meter refill in extra-urban	1245	0.0015	0.006	0.32	10.96	11.76	12.11	12.71	12.04	5.35	7.81
run 3	fuel flow meter refill in extra-urban	1245	0.0015	0.006	0.32	10.93	11.84	11.99	12.62	12.00	5.34	7.78
run 4	fuel flow meter refill in extra-urban	1245	0.0015	0.006	0.32	11.18	11.79	12.28	12.93	12.20	5.26	7.81
run 5	fuel flow meter refill in extra-urban	1245	0.0009	0.005	0.44	11.28	12.08	12.50	12.66	12.29	5.33	7.88
run 6	fuel flow meter refill in extra-urban	1245	0.0009	0.005	0.44	11.11	11.95	12.32	12.71	12.18	5.36	7.86
run 7	fuel flow meter refill in extra-urban	1245	0.0009	0.005	0.44	11.17	11.90	12.56	12.59	12.21	5.44	7.93
run 8	Incomplete run (incomplete dutch lock-up)	622.5	0.0009	0.005	0.44	-	-	-	-	-	-	-
run 9	Incomplete run (incomplete dutch lock-up)	622.5	0.0009	0.005	0.44	-	-	-	-	-	-	-
run 10	Incomplete run (incomplete dutch lock-up)	622.5	0.0009	0.005	0.44	-	-	-	-	-	-	-
run 11	Incomplete run (incomplete dutch lock-up)	622.5	0.0009	0.005	0.44	-	-	-	-	-	-	-
run 12	Incomplete run (incomplete dutch lock-up)	622.5	0.0009	0.005	0.44	-	-	-	-	-	-	-
run 13	Incomplete run (incomplete dutch lock-up)	622.5	0.0009	0.005	0.44	-	-	-	-	-	-	-
run 14	increase aero drag, decreased vehicle mass	830	0.0009	0.005	0.44	10.15	10.76	11.30	11.90	11.03	5.55	7.54
run 15	Incomplete run (incomplete dutch lock-up)	622.5	0.0009	0.005	0.44	-	-	-	-	-	-	-
run 16	actual vehicle properties	1245	0.0015	0.006	0.32	11.06	11.95	12.03	12.44	11.82	5.42	7.34
run 17	increase aero drag	1245	0.0009	0.005	0.44	11.12	11.85	11.44	12.37	11.78	5.89	7.68
run 18	increase aero drag, decreased vehicle mass	830	0.0009	0.005	0.44	10.03	10.90	11.13	11.89	10.94	5.67	7.24

5.3.1 Simulation accuracy

The simulations accuracy compared to the real vehicle was determined by measuring the fuel consumed by the engine on the test stand while conducting a simulated ECE cycle. It can be seen in the results provided for run one in Table 5. 2 that the simulation using the actual vehicles physical parameters had a fuel consumption in excess of 10% of that claimed by the manufacturer over a complete ECE cycle.

A fundamental component of the evaluation was the quantification and justification of any inaccuracies found in the simulation. After having reviewed run 1's results, it was determined that a further three runs would be conducted to validate the excessive fuel consumption shown in run 1. This was done as runs 2 through 4 and it was found that the mean fuel consumption of the simulation exceeded the manufacturer's claims by 30% on the urban cycle however the extra-urban cycle showed less than one percent inaccuracy. When the fuel consumption of the two cycles was averaged proportionally to the distance travelled in each cycle, the combined inaccuracy was 10%. As the extra-urban cycle was longer in distance, it had a larger influence over the two cycles combined fuel consumption.

As no obvious fault were found with the simulation program, the engine and vehicle loading methods as applied by simulation program 3 to the engine on the test stand and the load applied on an ECE specified chassis dynamometer were compared. The aerodynamic drag load and rolling resistance load applied to a vehicle on a rolling road that abides by the ECE emissions standard, applies a load according to the following equation:

$$F = (a + b \cdot U^2) \pm 0.1 \cdot F_{80} \quad 5-1$$

The upper and lower limits of the load applied at the wheels of the vehicle calculated using Equation 5-1, as well as the aerodynamic drag load and rolling resistance applied by simulation program 3 on to the engine on the test stand are visible in Figure 5. 5.

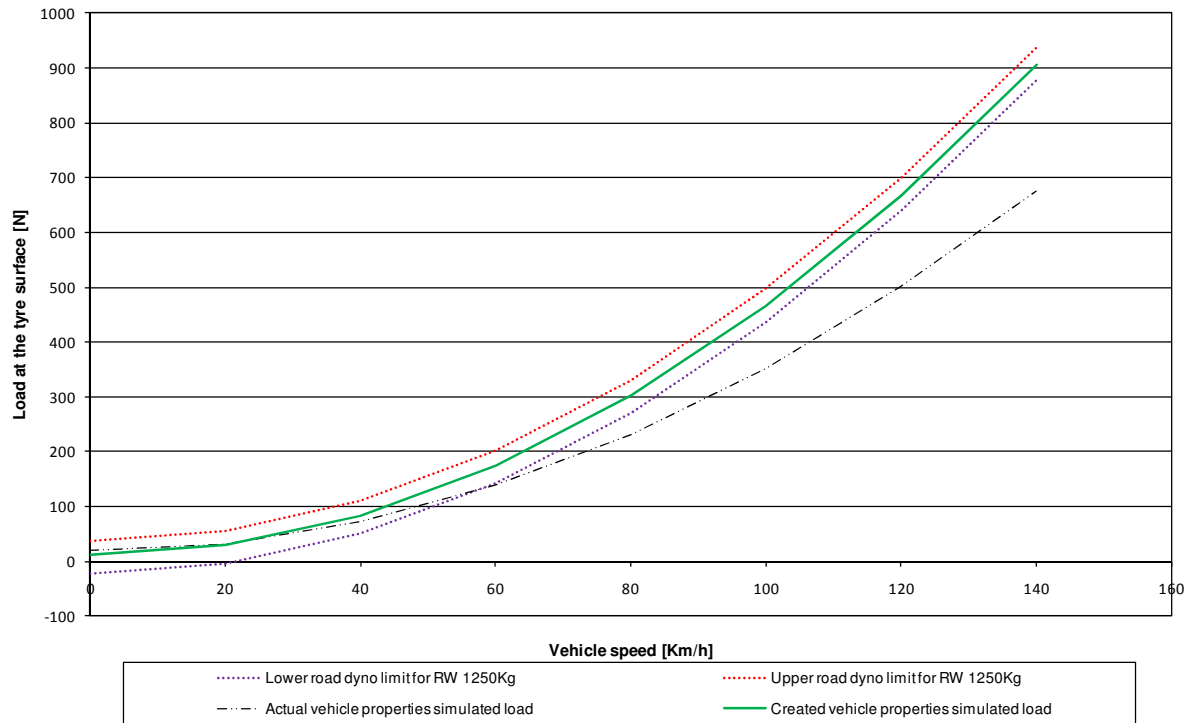


Figure 5. 5: Load at tyre surface versus vehicle speed.

The load applied by simulation program 3 was the composition of the aerodynamic drag load determined using the following equation:

$$F_A = C_D A_v \frac{\rho V^2}{2} \quad 5-2$$

The rolling resistance was calculated using the following equation:

$$f_r = f_0 + 3.24 f_1 \left(\frac{V}{44.704} \right)^{2.5} \quad 5-3$$

It can be seen in Figure 5. 5, that the two methods of determining the road loads correlated well at low speeds, however at speeds above 58 km/h the load applied to the engine on the test stand fell well outside the limits imposed by the ECE standard.

The impact of the differing vehicle road loads were evaluated by deriving alternative vehicle parameters that could be used with equation 5-2 and equation 5-3 to provide load on the engine test stand that would be consistent with those prescribed by the ECE standard.

With the altered loading profile constants input into simulation program 3, runs five through seven were conducted to evaluate any possible changes in the fuel consumption. After having processed the data from the runs, an increase in average fuel consumption over three runs was observed. The fuel consumption increase over the urban cycle was 2.5%, the extra-urban cycle

by 1.5% resulting in a combined additional increase of 2% to a value of 7.9l/100km. This increased fuel consumption in comparison to that obtained in runs 1 through 4 was anticipated due to the increased load and indicated that the different loading profile was not the cause of the already excessive fuel consumption.

It had been shown that the aerodynamic drag and rolling resistance loads were not responsible for the excessive fuel consumption, it was suspected that the simulated vehicle's inertia may have been the cause. The vehicle's inertia would only affect the fuel consumption when the vehicle accelerated and (assuming fuel cut-off during deceleration) result in an increase in the engine load. The error in the measured fuel consumption of the urban cycle was found to be significantly worse than that of the extra-urban cycle when compared to the vehicle manufacturers claims. It was also evident that there was significantly more periods of acceleration during the urban cycle than the extra-urban cycle. When these facts were considered concurrently, they highlighted the need for an investigation of the vehicle's simulated inertia.

Runs eight through thirteen represent unsuccessful attempts at half vehicle mass and increased aerodynamic drag and rolling resistance. It was intended that these runs show a disproportional reduction in the fuel consumption over an ECE cycle thereby confirming the incorrect vehicle inertia simulation. Due to the low mass of the simulated vehicle, periodic simulated clutch engagement problem occurred preventing a simulated clutch lock-up which resulted in incomplete ECE cycles. During the six runs various solutions to the simulated engagement were attempted but none corrected the intermittent problem. As the allocated engine test stand time was almost used up, another method of evaluating the vehicle's simulated inertia had to be found.

Appendix 6 and 7 of the South African National Standard (2009), [*Uniform provisions concerning the approval of vehicles with regard to the emission of pollutants according to engine fuel requirements*] prescribes a method for the verification of simulated inertias for rolling road dynamometers and a method for the measurement of vehicle road load. These two methods were applied resulting in the inertia of the simulated vehicle at the actual vehicle's mass being determined. The inertia was determined using a series of simulated vehicle ramp downs following the listed procedure:

1. Calculate the simulated vehicle speed at 3500rpm for each gear.
2. For the final deceleration zone of the extra-urban cycle starting at 120km/h and ending at 0km/h as in Figure 3.3, simulation program 3 was set so that the throttle demand was set to zero and the braking algorithm was deactivated. Thus resulting in a coast down situation.
3. Gear changes were set so that the gear to be tested would be selected at 3500rpm thereby allowing steady coast down from 3000rpm.
4. The simulated vehicle was then left to coast down to idle speed at which stage the test was concluded.
5. The procedure was repeated for all gears.

This process yielded the vehicle coast down speed profiles as displayed in Figure 5. 6.

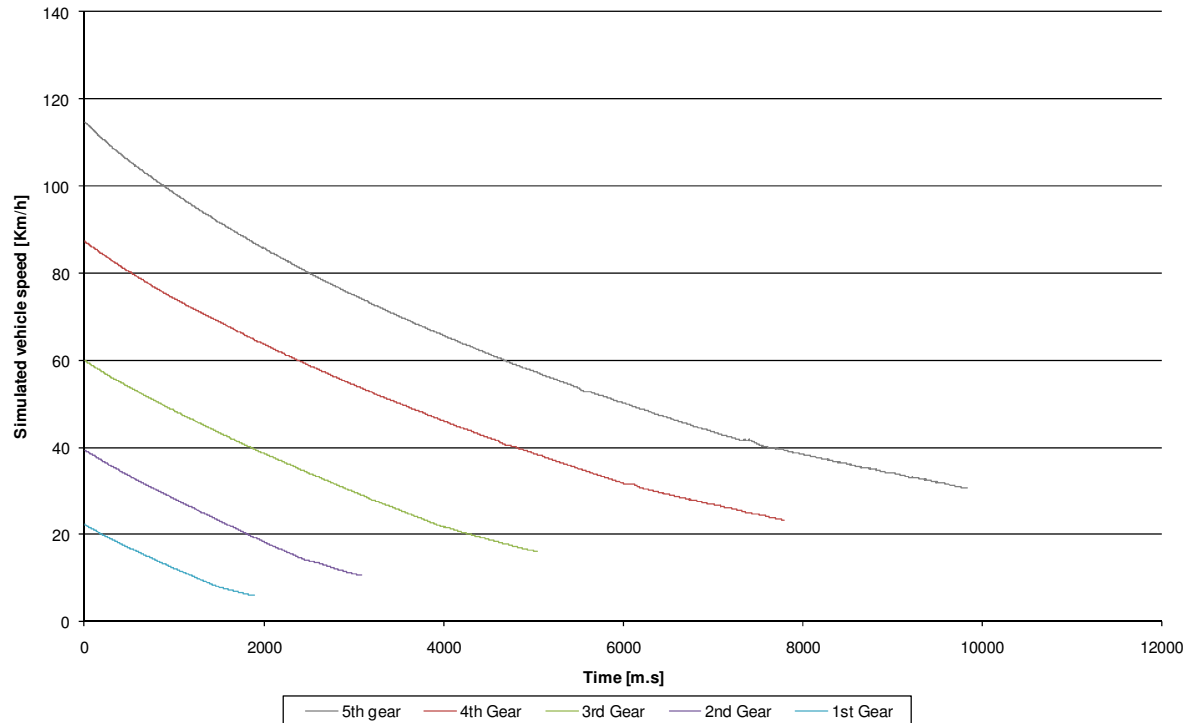


Figure 5. 6: Simulated vehicle speed versus time for gears 1 through 5.

From the trends recorded during the simulated coast down runs that are displayed in Figure 5. 6, the angular acceleration at the wheels of the vehicle could be determined. The engine torque measured on the dynamometer was also mathematically manipulated into an equivalent force at the wheels of the vehicle. These values could then be placed into equation 3-13 to yield equivalent vehicle inertia in kilograms or more commonly known in these units as the vehicle's mass.

$$I = I_m + (F_l/\gamma) \quad 5-4$$

Figure 5. 7 plots the calculated equivalent vehicle inertia as well as the force and acceleration derived from the simulated vehicle coast down data for the first gear.

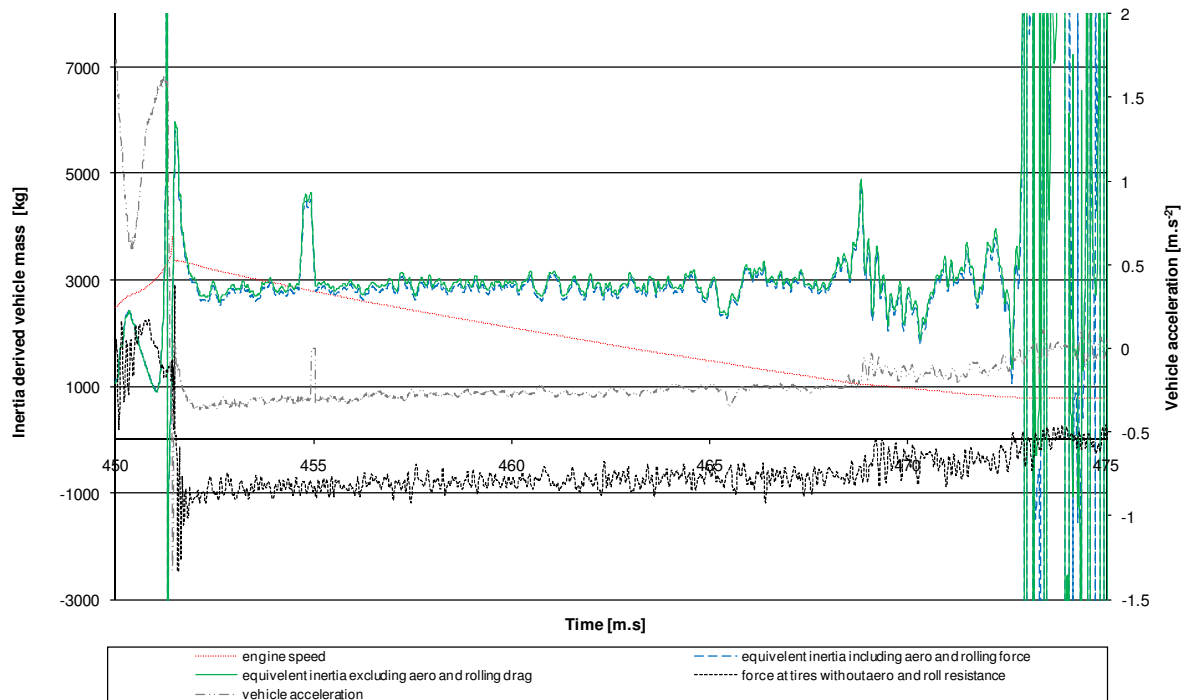


Figure 5. 7: Inertia derived vehicle mass versus time for first gear.

After having processed the recorded vehicle coast down data for gears two through five as was done for the first gear, the simulated equivalent inertias were plotted resulting in Figure 5. 8. This plot clearly indicated a significant problem with the method used to determine the simulated vehicle inertia. If the vehicle inertia had been correctly simulated, the correlation method used should have yielded the simulated vehicle effective inertia of 1250kg (the test vehicle weight) for all gears, however this did not occur. Simulated equivalent vehicle inertia ranged from 1250kg through 2900kg depending on the selected gear.

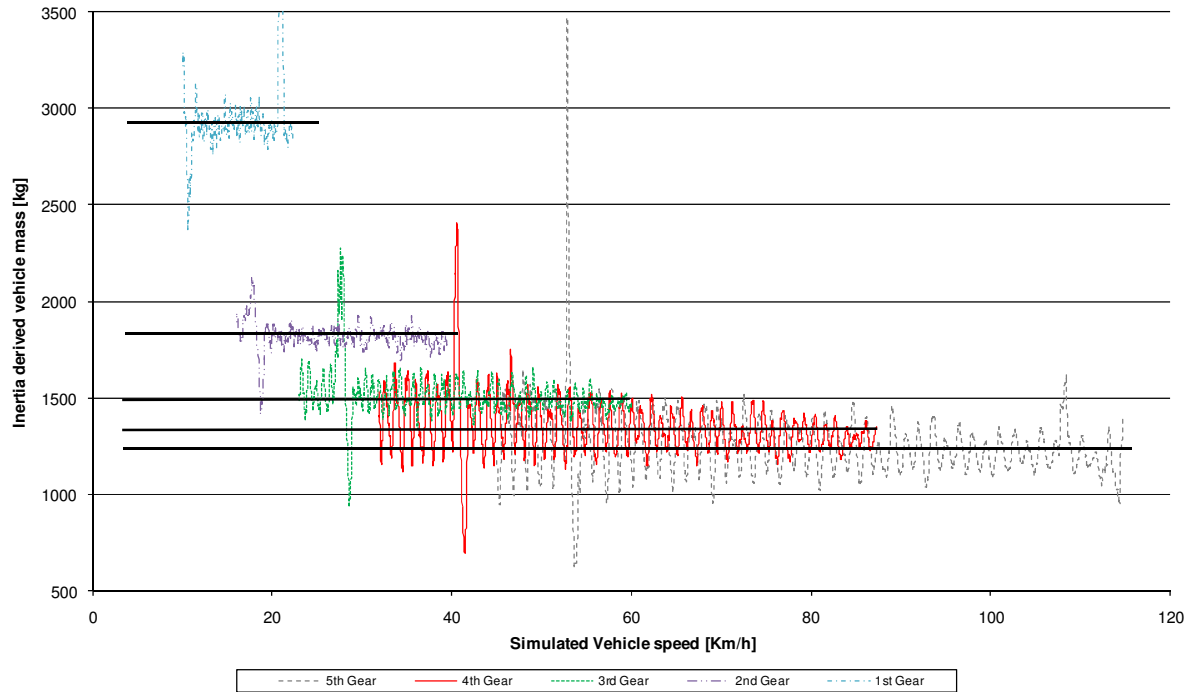


Figure 5. 8: Inertia derived vehicle mass versus simulated vehicle speed for gears 1 through 5.

Initial thoughts were that this variation in equivalent inertia was the result of having measured the engine torque at the engine and not at the wheels as prescribed by the method (torque could only be measured at the engine). However this torque was calculated back to a force at the wheels using the fixed drivetrain gear ratios and thus this could not have been the reason for the spread in effective inertia values.

The evident problem with the simulated effective vehicle inertia was verified using a different method, (European Communities 1999: Appendix 6) using the recorded ramp-down data. This prompted an in-depth review of the derivation of the mathematical equations 3-9 through equation 3-12 that were used in the determination of the effective vehicle inertia using simulation program 3.

A detailed review of Conradie's(2001) derivation of equations 3-9 through 3-12 required the further studying of two of Conradie's(2001) source texts, Hong(1996) and Gillespie(1992). Renouf(1979) was also studied for additional information. This review exposed the cause for the incorrect effective vehicle inertia simulation.

Conradie(2001) defines the equivalent rotational inertia of a vehicle as follows:

$$J_v = J_{vl} + J_{dt} \quad 5-5$$

Conradie(2001) defined the vehicle effective rotational inertia applied at the engine as follows:

$$J_{vl} = \frac{f_m M R^2}{G_{ft}^2} \quad 5-6$$

and the drivetrain rotational inertia applied at the engine as:

$$J_{dt} = J_c + \frac{1}{G_t^2} \left\{ J_t + J_{dr} + \frac{1}{G_f^2} (J_f + J_w) \right\} \quad 5-7$$

Conradie(2001) derives equation 3-10 with the contribution of Gillespie's(1992) by defining a mass factor. Conradie(2001) then references Equation 3-12 for the drivetrain torque which was derived by Hong(1996).

However, Gillespie(1992) derives the available tractive force at the surface of a vehicles wheels based on an engine torque output as:

$$F_x = \frac{T_e N_{tf} \eta_{tf}}{r} - \{ (I_e + I_t) N_{tf}^2 + I_d N_f^2 + I_w \} \frac{a_x}{r^2} \quad 5-8$$

This equation was then manipulated to yield the required engine torque for an applied force at the wheels so that the derived rotational inertia could be compared with that given in equation 3-12. This manipulation yielded:

$$T_e = \frac{F_x r}{N_{tf} \eta_{tf}} - \alpha_e \left\{ \frac{I_w}{N_{tf}^2} + \frac{I_d}{N_t^2} + I_t + I_e \right\} \quad 5-9$$

Gillespie(1992; 26) defined the effective vehicle mass ($M + M_r$) using Newton's second law and equation 5-8 as follows:

$$(M + M_r) a_x = \frac{T_e N_{tf} \eta_{tf}}{r} - F_R - F_A \quad 5-10$$

The mass factor was defined as:

$$\text{Mass factor} = \frac{M + M_r}{M} \quad 5-11$$

and provides a representative mass factor number as:

$$\text{Mass factor} = 1 + 0.04 + 0.0025 N_{tf}^2 \quad 5-12$$

Thus it can seen that M_r represents the equivalent mass of the rotating components (the drivetrain). The second term on the right-hand side represents the loss of tractive force due to the inertia of the engine and drivetrain components. This indicates that:

$$M_r = \{(I_e + I_t)N_{tf}^2 + I_d N_f^2 + I_w\} \frac{1}{r^2} \quad 5-13$$

Thus, it is evident that the inclusion of the mass factor (which is partly comprised of the equivalent mass M_r) in equation 3-10 as done by Conradie(2001) resulted in the compensation of the J_{dt} term within the J_{vl} term. This can be further motivated by comparing Hong's equation 3-12 to the bracketed portion of the right hand side of equation 5-13.

$$J_c + \frac{1}{G_t^2} \left\{ J_t + J_d + \frac{1}{G_f^2} (J_f + J_w) \right\} \cong \left\{ \frac{I_w}{N_{tf}^2} + \frac{I_d}{N_t^2} + I_t + I_e \right\} \quad 5-14$$

Equation 5-14 gives the derived drivetrain inertia when applied at the engine with the left side terms of the equation having been derived by Hong(1996) and the right hand side terms as manipulated from its derivation as given in equation 5-9. The approximately equal to symbol was used as the notation and the position of some of the applied masses varied during their derivations. However both authors provide a concurrent derivation based on their respective diagrammatic powertrain analogues.

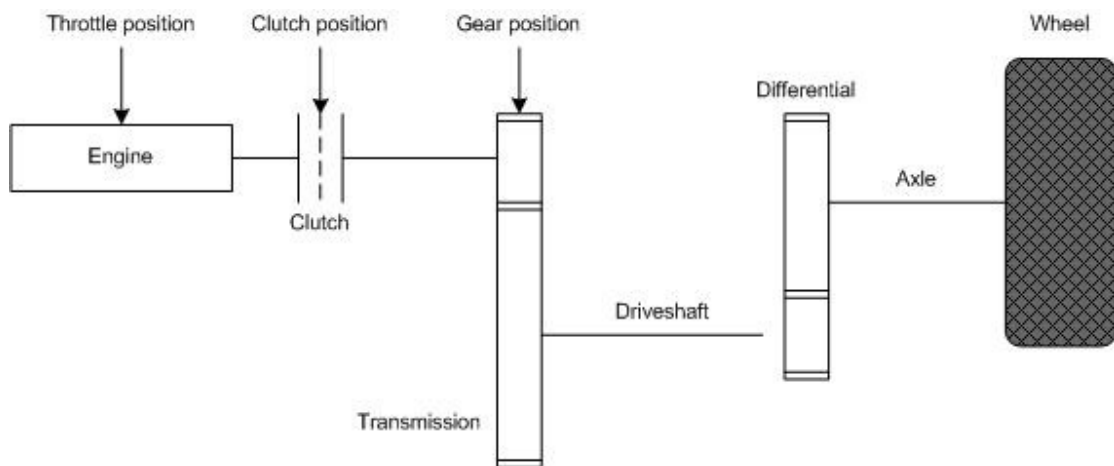


Figure 5. 9: Representative Powertrain system as used by Conradie (2001), Gillespie(1992) and Hong(1996)

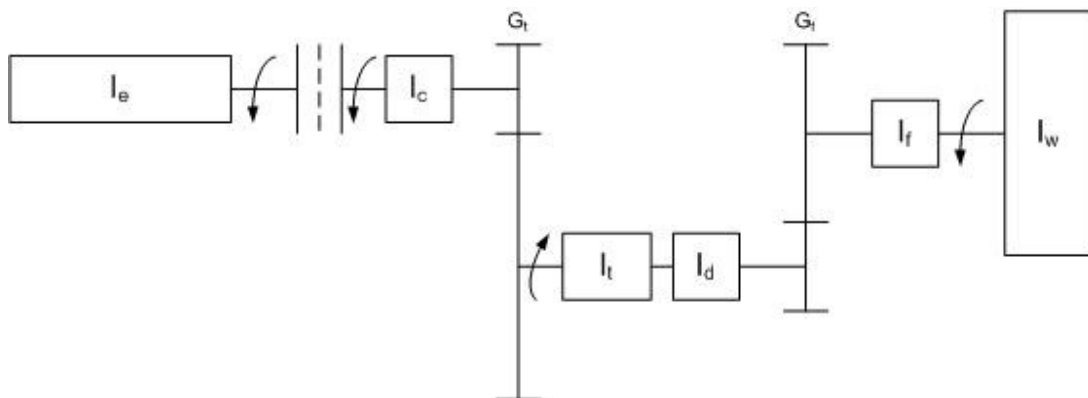


Figure 5. 10: Powertrain system analogue as plotted by Hong (1996) and referenced by Conradie(2001)

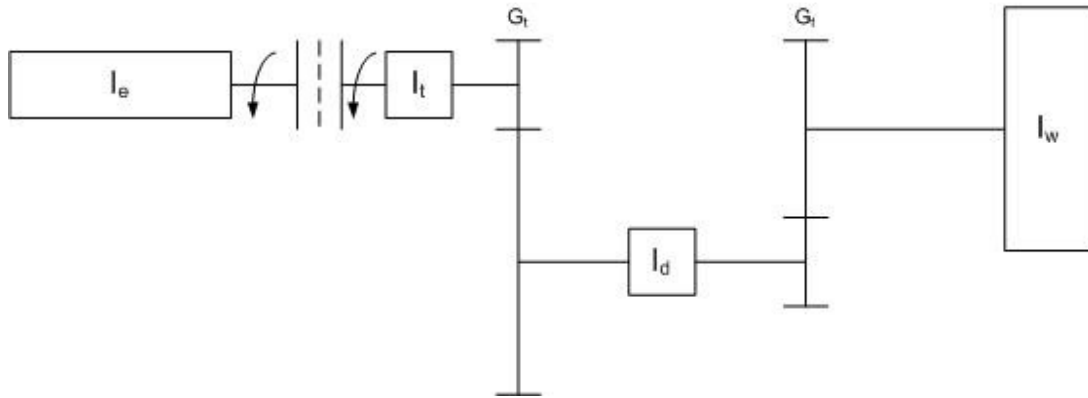


Figure 5. 11: Equivalent Powertrain system analogue as was plotted by Gillespie(1992)

Figure 5. 10 and Figure 5. 11 plot the point of application of the transmission inertia that differed between Hong and Gillespie with Hong applying the transmission at the output shaft of the transmission and Gillespie applying it at the input shaft. It should also be noted that Hong applies final drive inertia as well as wheel inertia were Gillespie considers only applied wheel inertia.

Based on the standing of equation 5-14 and by Gillespie's definition of the mass factor, it can be shown that Conradie's derived total vehicle inertia resulted in the equation to follow and not as referenced equation 3-9 claims:

$$J_v = J_{vl} + 2J_{dt} \quad 5-15$$

It was the effect of the over compensation of the simulated powertrain inertia that was believed to result in the incorrect equivalent inertia values as displayed in Figure 5. 8. If this over-compensation was removed by disregarding the effects of equation 3-12 (this would be the simplest method) it would be expected that simulated equivalent vehicle inertia would have be corrected and would have fallen within the 5% deviation from the theoretical equivalent inertia as required by the European Communities (1999).

Due to CAE's commercial commitments for the test stand, by the time the simulated effective vehicle inertia review had been concluded, the test engine had already been removed from the test stand and no further testing was possible. However, during the effective vehicle inertia review, runs fourteen through eighteen were conducted and these provided some partial support for the simulated vehicle inertia having been the cause of the incorrect fuel consumption. Runs fourteen and eighteen were conducted at 66% of the actual vehicle test weight with ECE prescribed aerodynamic and rolling resistance drag. These two runs yielded reduced average fuel consumption over the combined cycle of 7.39L/100km. This reduction on a percentage basis reduced the total cycle error to 5% from an average of 11% obtained over the first four runs. Run sixteen and seventeen were conducted at the actual vehicle mass with the actual and ECE standard prescribed aerodynamic and rolling resistance. These two runs once again yielded combined cycle fuel consumptions in excess of 10% of factory claimed figures.

The reduction in fuel consumption during runs fourteen and eighteen clearly indicate the vehicle mass as having a dramatic effect on the fuel consumption over the urban as well as the extra-urban cycles. Run fifteen, having been run at half the vehicle's mass would have aided in the determination of the reduction in the fuel consumption with respect to simulated effective vehicle inertia, however, this run was not be completed.

After having completed the verification testing, it was found that equation 5-12 was also incorrectly defined in Gillespie (1992). The equation should have read as follows Gillespie(1995):

$$\text{Mass factor} = 1 + 0.04N_{if} + 0.0025N_{if}^2 \quad 5-16$$

It was found that this equation had been incorrectly referenced in multiple texts dating from the original derivation by Tamborek in 1952 all the way through to 2011. This corrected equation if applied would have increased the vehicles simulated effective inertia on a gear ratio dependant basis, however, the anticipated change in the simulated effective vehicle inertia would have been minimal.

Figure 5. 12 and Figure 5. 14 display the engine speed and torque of the fourth urban cycle and the start of an extra-urban cycle while conducting a complete ECE cycle. The ECE cycle recorded simulated vehicle speed from where this extract was removed is shown in Figure 5. 16. The selected portion of the cycle was enlarged so that the engine response during simulated pull-away, gear change up and gear change down can be clearly plotted.

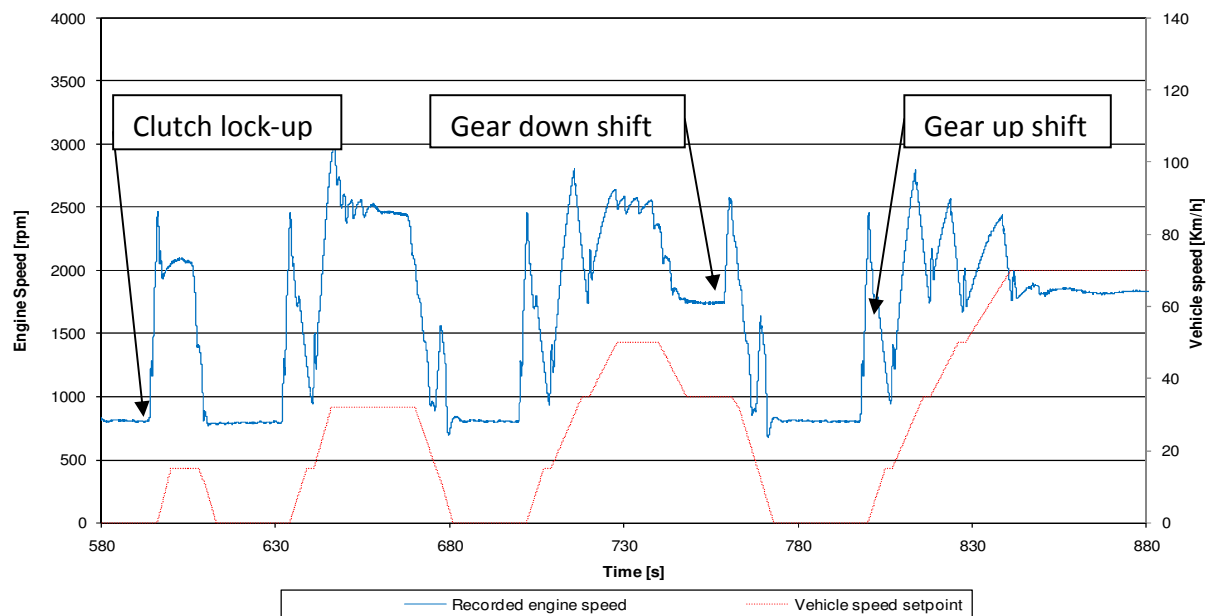


Figure 5. 12: Engine speed versus time for simulation program 3 while simulating an ECE cycle

During gear change simulations it can be seen that the clutch transfer torque was reduced to zero as would occur under ideal circumstances in a real vehicle. The engine throttle demand was also reduced to zero thereby resulting in a negative engine torque output and a loss in engine speed. This was evident during the period of a gear change although the loss in vehicle speed was small. This was as a result of the clutch torque having been reduced to zero. Completing the gear change was an increase in the engine speed as the throttle demand value was increased and the clutch transfer torque was increased until the clutch lock-up occurs.

Determining the accuracy of a vehicle pull-away or gear change simulation had many complications. Simulation program 3 was intended to simulate human pull-away and gear change behavior and not idle behavior. The difficulty in comparing the simulation and actual human pull-away and gear change behavior was a result of the lack of available information discussing human/vehicle interaction.

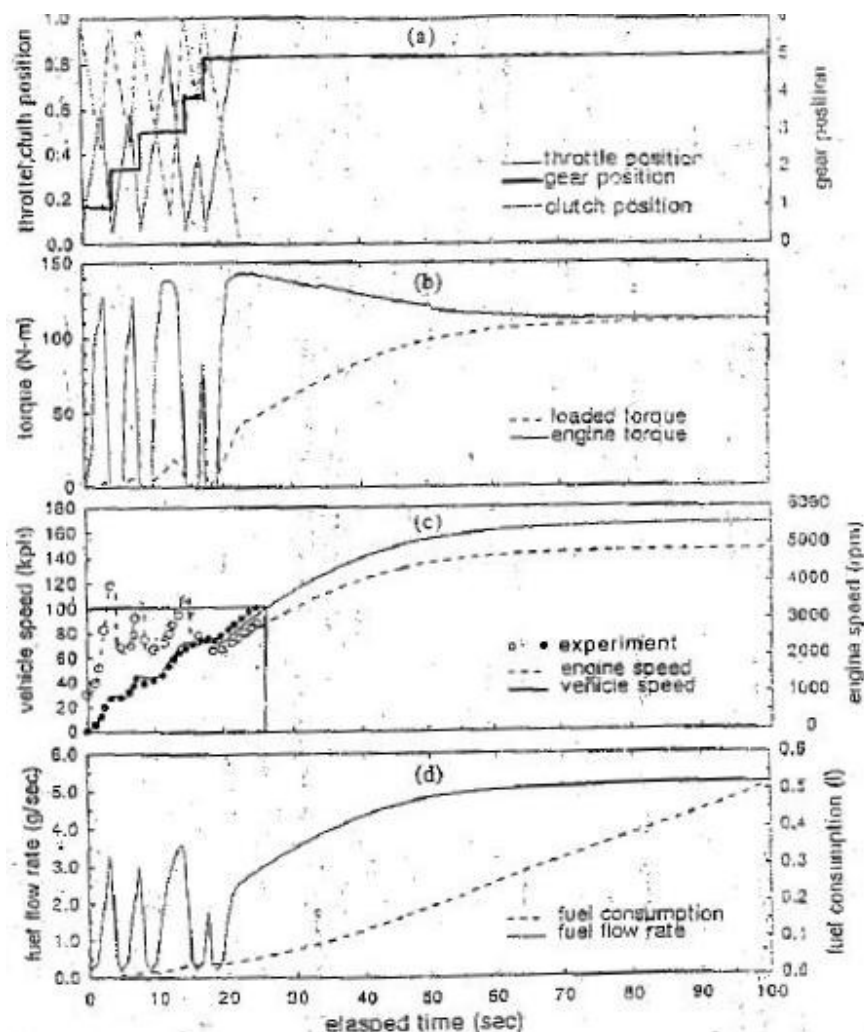


Figure 5. 13: Simulated transient operating conditions including gear change simulation. Hong (1995)

The results plotted in Figure 5. 12 were compared to the gear change simulation information produced by Hong (1995) while simulating a vehicle of similar engine capacity, vehicle mass and transmission ratios. Hong's results are show as Figure 5. 13. Simulation program 3's and Hong's results were believed to concur respect to obtained engine loading, engine speed and resulting vehicle speed. It was however evident that the engine torque produced by simulation program 3 during pull-away simulation was excessive and found to be caused by excessive engine throttle demand during the pull-away simulation.

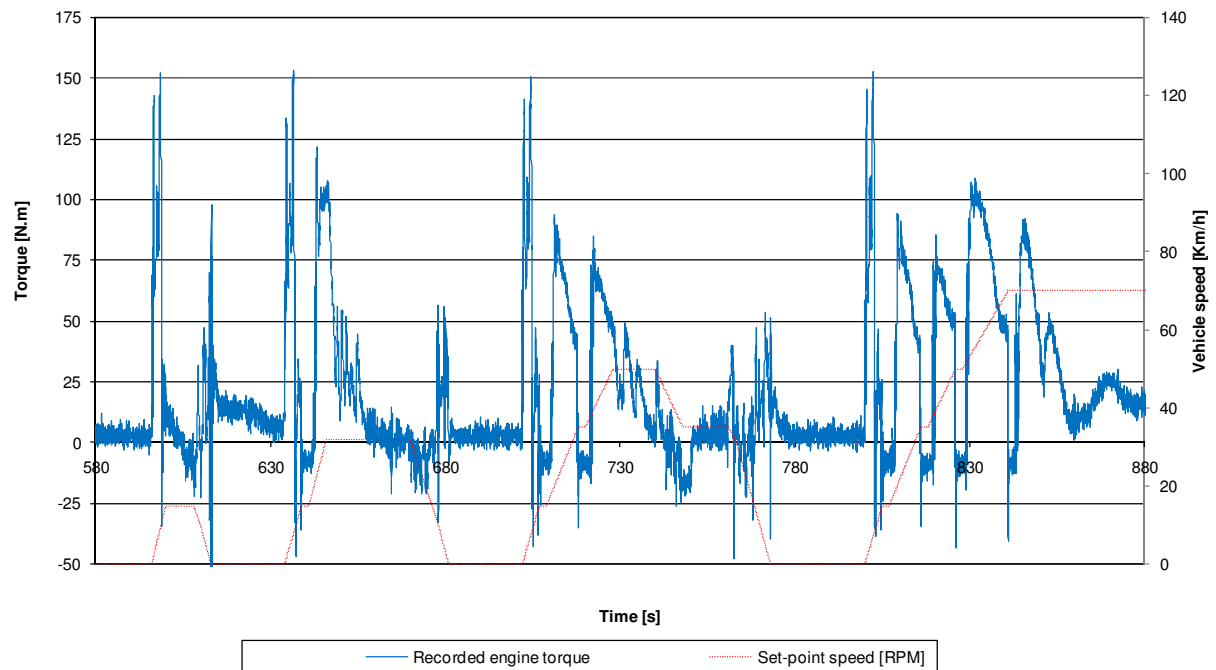


Figure 5. 14: Torque versus time for simulation program 3 while simulating an ECE cycle

Figure 5. 14 and Figure 5. 15 plot the produced engine torque and engine throttle demand percentage respectively. These graphs show recorded data during the same run and time period as in Figure 5. 13. Figure 5. 14 shows that during gear change simulation engine torque was reduced as an effect of the throttle closing, as can be seen in Figure 5. 15. These figures also show the excessive engine torque produced during simulated pull-away as a result of the large engine throttle demand. This large engine throttle demand during simulated pull-away was not understood and could not be explained until the problems with the simulated vehicle inertia became apparent.

The engine applied load as a result of the equivalent vehicle rotational inertia was proportional to the square of the drivetrain's overall gear ratio. Therefore, the applied simulated vehicle inertia was largest in the first gear where the overall drivetrain ratio was the largest. At the same time any error that occurred during the calculation of the equivalent vehicle rotation inertia would have been propagated by a factor proportional to that of the square of the overall drivetrain gear ratio. The previously discussed error in the calculation of the effective vehicle rotational inertia resulted in the simulated vehicle mass at pull-away equating to $\pm 2900\text{kg}$. This

mass was double the vehicles actual mass. The effects of a vehicles mass on the required engine throttle demand during pull-away had not been researched, however it was not hard to hypothesize that if a vehicle mass was doubled, the effect on all aspects relating to a vehicles pull-away would have been dramatic.

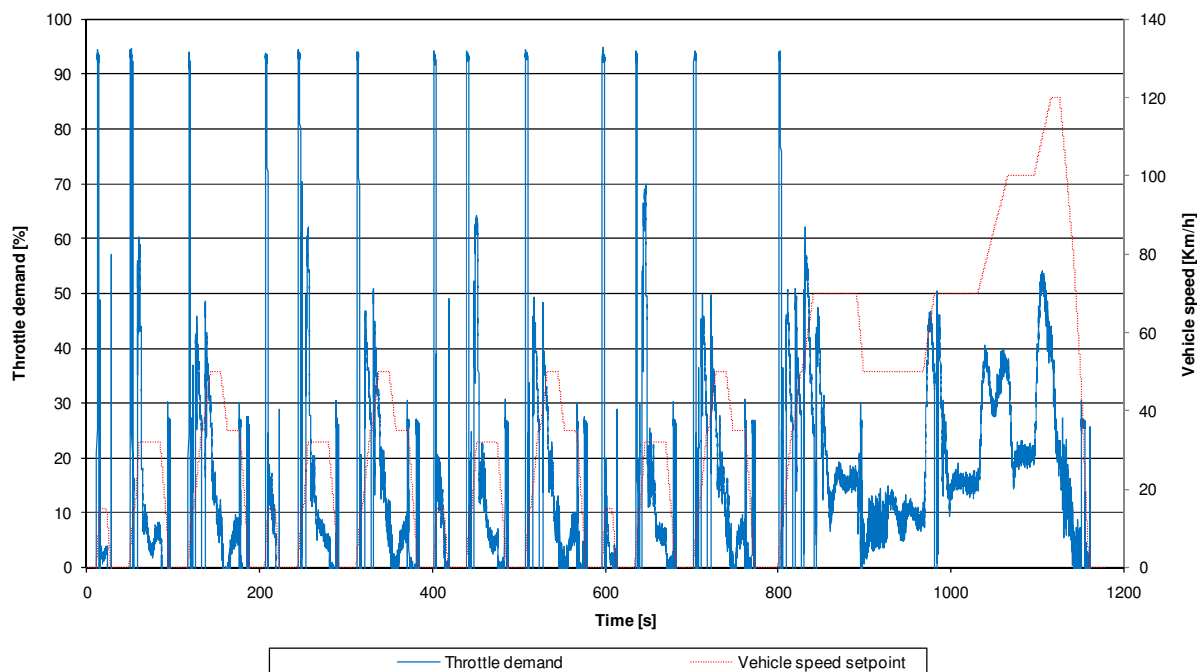


Figure 5. 15: Throttle demand versus time for simulation program 3 while simulation an ECE cycle

5.3.2 Ability to follow a provided cycle

The ability of a human driver controlling a vehicle along a provided cycle on a rolling road, or similarly the ability of a simulation conducted on an engine test stand to follow a cycle, is critical. So much so that the South African National Standard (2009) states that the actual vehicle speed must remain within a tolerance of ± 2 km/h from the setpoint speed for the provided cycle when conducting a light duty vehicle emissions test. It was elected that the national specified standard tolerance set at ± 2 km/h, would be the evaluation criteria used to evaluate simulation program 3 ability to follow a provided cycle.

Figure 5. 16 displays the simulated vehicle speed plotted for test 16 while following an ECE cycle using simulation program 3. Also plotted is the ± 2 km/h vehicle speed tolerance trends wherein the vehicle speed needed to remain based on SANS regulations. It can be seen in Figure 5. 16, that the vehicle speed was maintained within the imposed tolerance with exception of ± 2 seconds following a halt in vehicle acceleration. This overshoot could be reduced by further optimization of the throttle demand PID controller which was responsible for controlling vehicle speed. This optimization would be engine and test stand specific and due to the reduced evaluation time available caused by the addition of simulated vehicle inertia investigation, this optimization was not possible. Other points which exceeded the confines of

the vehicle speed tolerance were at simulated pull-away and gear changes, however these points were within the two seconds provided in the SANS for gear changes and hence this situation was found to be acceptable.

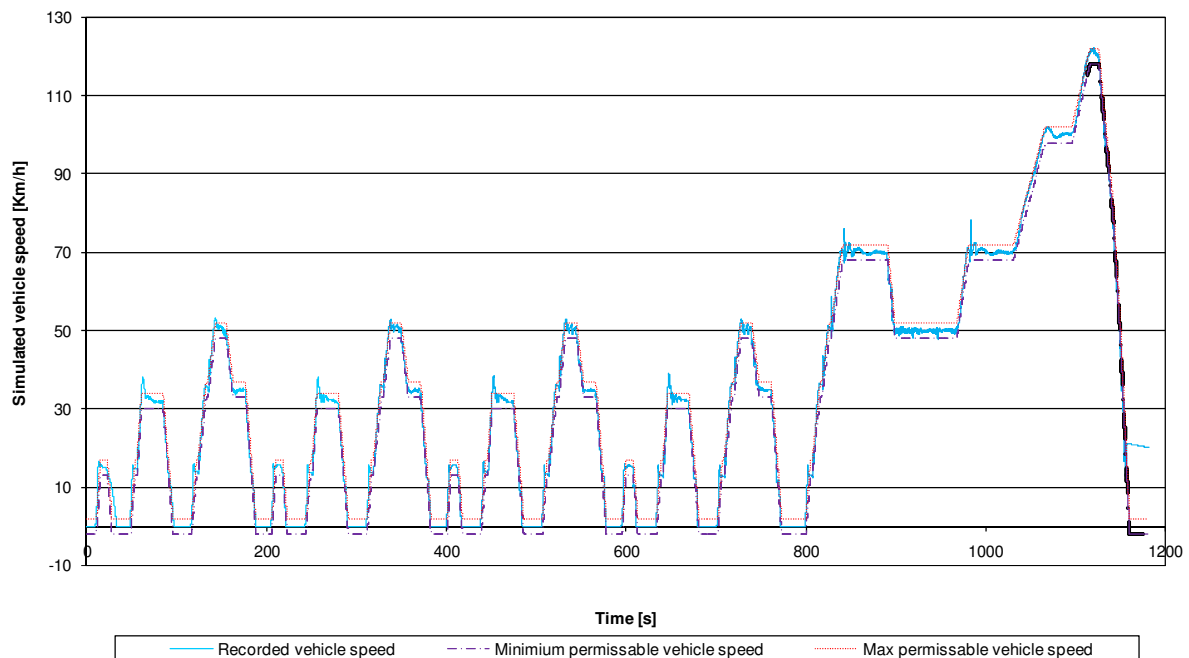


Figure 5. 16: Simulated vehicle speed versus time for simulation program 3 while simulating an ECE cycle

5.3.3 Repeatability and reproducibility of results

The repeatability and reproducibility of a system such as the one developed is critical to its success in industry. If test results cannot be repeated on a test stand to a defined level of accuracy, the accuracy of the test should be questioned. If a test cannot reproduce equivalent results with equivalent test engines on similar test stands, this can make the produced results at any one test facility questionable. The same testing principle should be applied to the evaluation and testing of any of the test equipment required to run test. This poses a problem for the evaluation of simulation program 3 as only a single test stand and test engine were available for the evaluation.

It was determined that a suitable compromise for the evaluation of simulation program 3 would be the running of the same engine and test stand where the vehicle parameters would bear minor changes that would effectively emulate or simulate the changes that would be present if differing test stands were used. The simulated vehicle speed from multiple runs would then be evaluated to confirm that the system could repeat and to some extent reproduce the same simulated vehicle speed regardless of the small changes to the vehicles properties. The recorded engine output torque would then be evaluated to ensure that changes to the simulated vehicle properties were effective in changing the engine loading patterns and thereby simulating a change in test stands.

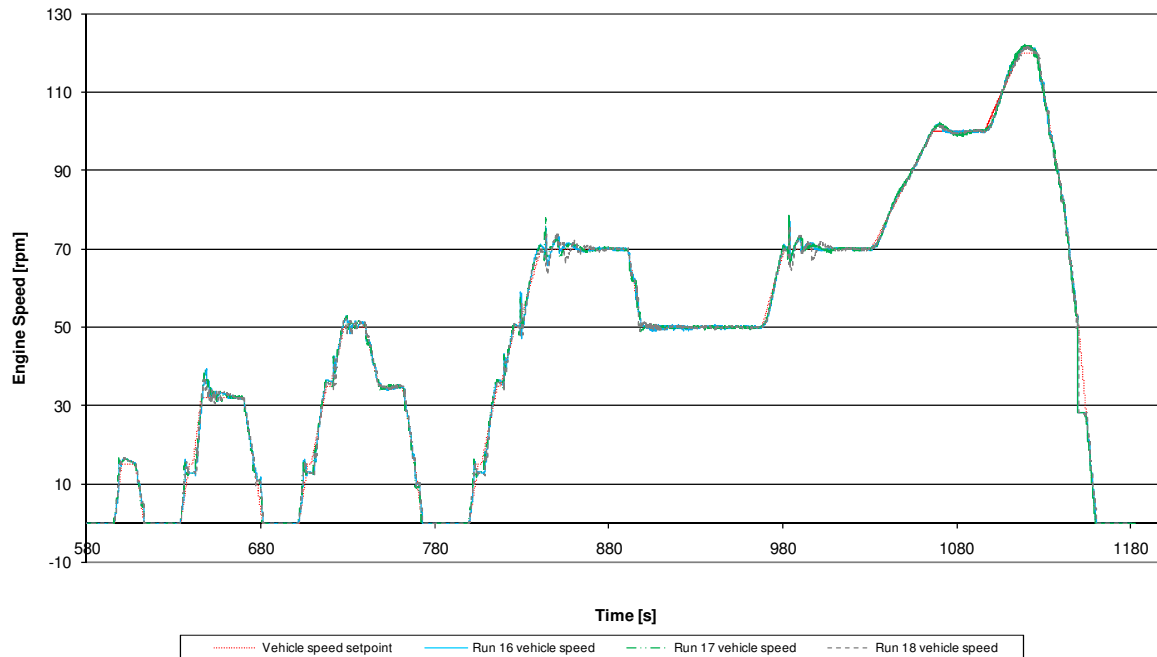


Figure 5. 17: Engine speed versus time for runs 16, 17 and 18

Figure 5. 17 plots the recorded simulated vehicle speed against time. As can be seen from the figure, when the three runs were plotted on the same graph their response to the setpoint profile was the same. This clearly indicates a high level of repeatability with respect to simulated vehicle speed. Recorded engine speed although not depicted, was reviewed and had the same overlaying pattern as is present in Figure 5. 17. This was to be expected as the recorded engine and simulated vehicle speed were related on a basis proportional to the drivetrains overall gear ratio.

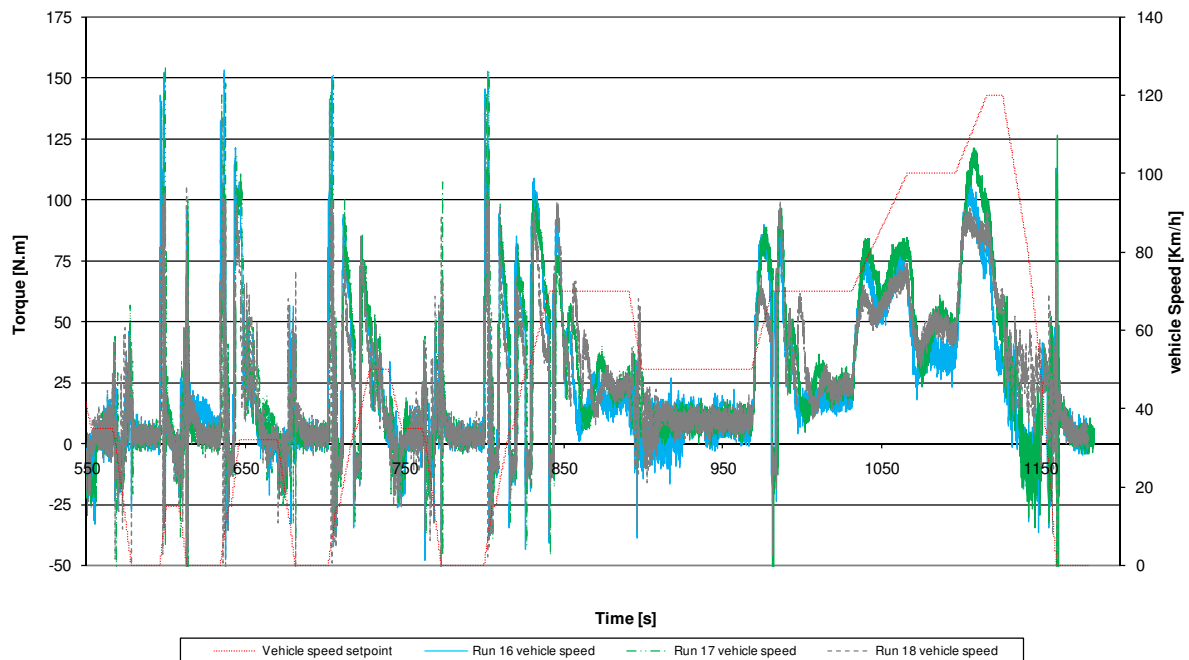


Figure 5. 18: Engine torque versus time for runs 16, 17 and 18

Figure 5. 18 shows the recorded engine torque of runs 16, 17 and 18 against time. Small variations in engine torque in response to the minor changes to the vehicle parameters were recorded as was expected. Run 16 possessed the actual vehicle properties and was used to provide a bench mark of intended system performance against the performance of the system when simulated test cell altering properties were changed. For run 17 aerodynamic drag and rolling resistance applied were increased so as to simulate variations in calibration or differential in engine power output with respect to throttle position, between test stands. For run 18 aerodynamic and rolling resistance loads applied were increased but had a reduced vehicle mass. This resulted in run 17 and 18 having similar steady state engine torque output but varying transient engine torques out. This variation in transient engine torque was used to simulate a varying rotational mass of the test stand components.

From the recorded simulated vehicle speed plotted in Figure 5. 17 it can be seen that simulation system 3 successfully managed to repeat and reproduce the simulated vehicle speed results with respect to the changes made to simulate the possible variations in loading that may occur among different test cells.

6 CONCLUSION

In the search to develop competitive vehicles, automotive manufacturers turned to advanced technologies with the intention of applying enticing technologies into their vehicles that exceeded that of their competitors. At the same time public awareness of green house gases and their effects resulted in more stringent legislation worldwide with regard to the permissible emissions of automobiles of both light and heavy duty designation. To overcome the ever more stringent emissions standard automotive manufacturers once again turned to advanced technologies to aid them. As the emissions standards reduced the permissible quantities of specified emissions, more advanced technologies were being applied resulting in more advanced tools being developed. The use of steady state engine testing technology has been given way to more advanced transient engine testing technology. This report documents the development of a vehicle and road load simulation program as well as its application on an existing dynamic engine test stand.

The overall objectives of this dissertation were to develop a vehicle and road load simulation for an engine dynamometer intended for emissions testing and powertrain development. Three simulation programs were developed. The first simulation program preprocessed velocity profiles making use of an engine characterization curve. This data was then provided to the test stand and the engine performance recorded. The accuracy of this simulation program was found to be highly dependent on the engine characterization data and ultimately yielded poor results. It was thought that better results would have been obtained by using real-time engine data in place of the engine characterization. The programmatic structure as well as the pre and post run processing concept of the simulation made the real-time evaluation of a test exceptionally difficult. The importance of this was not realized until multiple runs had to be processed only to find they were not valid. This simulation model was abandoned due to its dependence on prior measured engine characterization data and its inability to allow for the evaluation of a test while a test was being conducted.

The second simulation program was developed as an offline development environment for the real-time hardware in the loop simulation program. It made use of engine characterization data to simulate an engine so that developed code could be tested. This program was necessary as it allowed for safe development of the system and allowed an initial phase of testing of the simulation at no risk to the engine or test stand and its respective support equipment. This program was continuously developed and evaluated in a round-robin format until the software was developed significantly to allow for safe running of the system with the engine on the test stand. As this was purely a development program, no test results were documented.

Simulation program 3 involved real-time hardware in the loop system that ran on a real-time operating system with a National Instruments DAQ card. This card acquired data from an existing dynamic engine test stand consisting of an eddy current brake and an AC drive motor. The engine characterization data used during the development of simulation program 2 was replaced and the required data was obtained in real-time from the engine test stand. The ECE cycles velocity profile was used for the evaluation of the program. In total 18 complete ECE runs

were attempted during the evaluation of simulation program 3. As a vehicle with an engine similar to that on the test stand was not available, the simulation accuracy was evaluated on the measured fuel consumption over a complete ECE cycle and compared to those published values of the vehicle manufacturer.

Initial runs made during the evaluation yielded poor fuel consumption results. Fuel consumption was excessive and the proportion of the fuel consumed between the urban and extra-urban cycle differed to that which was published.

It was found that the load applied to the engine as a result of the simulated vehicle aerodynamic and rolling resistance using available equations, was lower than that which would have been applied had the equations specified by SANS (2009) been used. The difference in the applicable forces was a result of the SANS equation deriving these drag forces from values given in the standard, based on the vehicles mass category. The SANS equation for the drag force were thus believed to represent the worst case scenario for each vehicle in a set weight category. The equations yielded vehicle drag forces based on the simulated vehicles actual properties. When the simulated vehicles aerodynamic and rolling resistance determined using available equations was changed using made-up parameters so that the SANS prescribed loading could be applied, urban cycle fuel consumption increased slightly and a larger increase in the extra-urban fuel consumption was experienced. This concurred with the fact the low speed loads were similar however the high speed load of the SANS method was higher. This change in the loading lead to an increase in the complete cycle fuel consumption making the overall error larger but it improved the proportional difference between the urban and extra-urban fuel consumption when compared to the proportions claimed.

While evaluating simulation program 3 and the excessive fuel consumption, an inconsistency with the applied simulated effective vehicle rotational inertia was found. The applied simulated vehicle rotational inertia was verified using the method prescribed by SANS (2009). This method calculated the simulated effective vehicle rotational inertia and represented it as an effective vehicle mass. This was done using data collected during simulated vehicle ramp-downs. The vehicle effective mass varied for each gear when it should have remained constant at the simulated vehicle mass. It was discovered that Conradie's (2001) derivation of the effective vehicles inertia as was used in simulation program 3 over-compensated by the amount equivalent to that of the rotational inertia of the drivetrain.

It was also found that the effective mass of the vehicle which was used to calculate the effective vehicle rotational inertia at any instant was incorrectly calculated due the author's reference of an equation from Conradie. This equation was in turn referenced from a miss-printed equation from Gillespie (1992), which was subsequently corrected in Errata and Clarification Gillespie (1995). Many texts dating from the original publication through to text release at the beginning of 2011 continue to reference the miss-printed equation, thus the use of the incorrect equation in Conradie's work and the subsequent use in this work before the author's discovery of the miss-printed are unfortunate. It is recognized that the incorrect calculation of the effective mass further affected the derived effective vehicle rotational inertia.

Unfortunately the engine test stand was no longer available to confirm the total impact on the fuel consumption however when the effective simulated vehicle rotational inertia thought to be suspect, run 18 was conducted. This was conducted at a reduced vehicle mass so as to provide an insight into the effects of the vehicle inertia. Run 18 yielded a fuel consumption rate over an ECE cycle that was comparable to those claimed by the manufacturer and were in the correct proportions with respect to urban and to extra-urban cycle fuel consumption.

It can be concluded that with the use of Simulation system 3, $\pm 7\%$ more fuel is consumed than is claimed by the vehicle manufactures over the duration of a complete ECE cycle. If the data provided by run 18 is considered, it can be estimated that this error would be reduced to $\pm 3\%$ over the duration of a complete ECE cycle if the effective rotational inertia is corrected.

7 RECOMMENDATIONS

1. It would be recommended that an effort be put into the synchronization of the dynamometer and drive motors speed control. This would allow the speed differential that was required to prevent the motor from driving the dynamometer on the used test stand to be reduced.
2. Very little information surrounding human control or actuation of vehicle controls during vehicle pull-away could be found during the literature review. It would be recommended that a study be conducted into this human vehicle interaction and compared to the results obtained and an accurate simulation developed that could be used by a vehicle simulation program.
3. It would be recommended that a flexible drivetrain simulation model be developed. This would however require an engine test stand capable of a high frequency response to speed setpoint changes.
4. The development of an additional application that would determine the optimal circuit racing line and provide the simulation program with the corresponding velocity profile that would allow a simulated lap to be run on the engine test stand.
5. The development of the offline simulation mode. Even if this tool was slightly inaccurate, it could assist in comparative evaluation of the effects on vehicles fuel consumption or emissions caused by changes to the drivetrain or aerodynamics so long as the results are repeatable.

8 REFERENCES

- Aird, F. (1997) Aerodynamics for racing and performance cars, Berkley Publishing Group, New York, USA, pp.11-18.
- Akinobu, M. A. (1991) Robotic Driver on Roller Dynamometer with Vehicle Performance Self Learning Algorithm, Nissan Motor Co., Ltd., SAE 910036.
- Atmel.C. (2002) FPGA technology in detail. INTERNET. http://bertram-family.com/felix/soc_course_files/week-2.pdf Cited 14 October 2010.
- AVL. (2010) Engine emissions Testing. INTERNET. <http://www.avl.com> Cited 7 October 2010.
- Bosch GmbH. (2007) Automotive Handbook, Seventh Edition, Robert Bosch GmbH, Germany.
- Clive Maxfield. (2004) The Design Warriors Guide to FPGA's, Burlington, USA.
- Conradie, P.A. (2001) The development of a dynamic engine-testing facility, University of Stellenbosch, RSA.
- Delphi. (2010) Worldside emissions standards, Passenger cars and light duty trucks, European Regional Headquarters and Customer Technical Center, Luxembourg.
- Delphi. (2010), Worldside emissions standards, Heavy Duty & Off-Road Vehicles, European Regional Headquarters and Customer Technical Center, Luxembourg.
- Ecopoint Incorporated. (2008) Standards. INTERNET.<http://www.dieselnet.com> Cited 15 December 2009.
- European Communities. (1999) Directive 1999/96/EC of the European Parliament and of the Council of 13 December 1999 on the approximation of the law of the member states relating to the measurement to be taken against the emissions of gaseous and particulate pollutants from compression ignition engines for the use in vehicles, and the emission of gaseous pollutants from positive ignition engines fueled with natural gas or liquefied petroleum gas for use in vehicles amending council directive 88/77/EEC, European Parliament and the Council of the European Union, European Union.
- Froude Engineering. (1978) Eddy-Current Dynamometers, EC Range, Froude Engineering Limited, Gregory's Bank, Worcester, WR3 8AD, England.
- Gillespie T.D. (1992) Fundamentals of Vehicle Dynamics, Second Edition, Society of Automotive Engineering Inc. pp 1-35.
- Hailperin, M.(2007) Operating systems and middleware: supporting Controlled interaction, Thomson Course Technology, Massachusetts, United States of America.
- Heywood, J.B.(1988) Internal combustion engine fundamentals, McGraw-Hill Companies, Inc., Singapore, pp.49-160.
- HBM. (2007) Mounting instruction – Torque flange – T10F, HBM, Darmstadt, Germany.
- Hong, C.W. (1995) An automotive dynamic performance simulator for vehicular powertrain system design, International Journal of Vehicle Design, Vol 16, No's 2/3. pp 263-281.
- Hong, C.W. (1996) Dynamic simulation of road vehicle performance under transient accelerating conditions, Part D: Journal of Automobile Engineering, Proceedings of the Institution of Mechanical Engineers, Vol 210. pp 11-21.
- Horiba Automotive Test Systems. (2010) CVS-7000. INTERNET.<http://www.horiba.com> Cited 6 October 2010.

Lussier, R.N. (2006) Management fundamentals, third edition, Thomson Learning, Ohio, United States of America, pp.112-114.

Renouf, M.A. (1979) Prediction of the fuel consumption of heavy goods vehicles by computer simulation, TRRL Supplementary Report 453, Transport and Road Research Laboratory, Crowthorne, Berkshire.

Merrion, D.F. (2003) Heavy duty diesel emissions regulations –past, present, and future, SAE International, United States of America.

Northcote, N.M. (2006) The modeling and control of an automotive drivetrain, University of Stellenbosch, RSA.

National Instruments, (1997) Fuzzy Logic for G Toolkit Reference Manual, National Instruments, Austin, Texas, United States of America.

National Instruments, (2009) Introduction to FPGA Technology: Top Five Benefits. INTERNET. <http://zone.ni.com/devzone/cda/tut/p/id/6984> Cited 14 October 2010.

National Instruments, (2010) FPGA – Under the Hood. INTERNET. <http://zone.ni.com/devzone/cda/tut/p/id/6983> Cited 14 October 2010

Plint, M and Martyr, A. (1995) Engine testing theory and practice, Butterworth-Heinemann, Oxford, Great Britain, pp.202

Schenck Pegasus GmbH. (2001) Hydraulic Dynamometer Typ D, Schenck Pegasus GmbH, Darmstadt, Germany.

Serway, R.A. (2000) Physics for scientists and engineers with modern physics, fifth edition, Harcourt College Publishers, Inc., Orlando, USA.

Shames, I.H. (2003) Mechanics of fluids, fourth edition, McGraw-Hill Companies Inc., New York, USA, pp.666-675.

Shigley, J.E and Mischke, C.R. (2003) Mechanical Engineering design, Sixth metric edition, McGraw-Hill Companies, Inc., New York, USA.

Sommerville, I. (2004) Software Engineering, Pearson Education Limited, Essex, England.

South African National Standard. (2009) Uniform provisions concerning the approval of vehicles with regard to the emission of pollutants according to engine fuel requirements, South African Bureau of Standards, South Africa.

Taborek, J.J. (1957) Mechanics of vehicles, Mechanics of Vehicles, Cleveland, Penton, USA, pp.31-34.

Yuting, R. (1997) Road load simulation using effective road profile, Society of Automotive Engineers Inc., pp.19-28.

Winkler, D and Guhmann, C. (2006) Synchronising a Modelica® real-time simulation model with a highly dynamic engine test-bench system, Department of electronic measurement and diagnostic technology, Berlin, Germany, pp.275-281.

Appendix A

NI PCI-6221 (37-PIN)

General

Form Factor:	PCI
Operating system:	Windows, Real-time, Linux, Mac OS
Measurement type:	Digital, Frequency, Quadrature encoder, Voltage
DAQ product family:	M Series
LabVIEW RT support:	Yes
RoHS Compliant:	Yes

Analog input

Number of channels:	16 SE/8 DI
Sample rate:	250 kS/s
Resolution:	16 Bits
Simultaneous sampling:	No
Maximum voltage range:	-10...10 V
Range accuracy:	3100 μ V
Range sensitivity:	97.6 μ V
Minimum voltage range:	-200...200 mV
Range accuracy:	112 μ V
Range sensitivity:	5.2 μ V
Number of ranges:	4
On-board memory:	4095 samples

Analog output

Number of channels:	2
Update rate:	833 kS/s
Resolution:	16 Bits
Maximum voltage range:	-10...10 V
Range accuracy:	3230 μ V
Minimum voltage range:	-10...10 V
Range accuracy:	3230 μ V
Current drive:	5 mA

Digital IO

Number of channels:	10 DIO
Timing:	Hardware, Software
Maximum clock rate:	1 MHz
Logic level:	TTL
Maximum input range:	0...5 V
Maximum output range:	0...5 V
Input current flow:	Sinking, sourcing

Programmable input filters:	Yes
Output current flow:	sinking, sourcing
Current drive (channel/total):	24 mA/176 mA
Watchdog timer:	No
Supports programmable power-up states:	Yes
Supports handshaking I/O:	No
Supports pattern I/O:	Yes

Timer

Number of counter/triggers:	2
Resolution:	32 Bits
Maximum source frequency:	80 MHz
Minimum input pulse width:	12.5 ns
Logic levels:	TTL
Maximum range:	0...5 V
Time base stability:	50 ppm
GPS synchronization:	No
Pulse generation:	Yes
Buffered operations:	Yes
Debouncing/glitch removal:	Yes
Number of DMA channels:	2

Timing/Triggers/Synchronization

Synchronization bus (RTSI):	Yes
Triggering:	Digital

REAL TIME PC SPECIFICATION

General

PC Manufacturer:	Mecer®
Model number:	-
Processor Manufacturer and series:	Intel® Pentium®
Frequency:	
RAM:	1.00GB
Operating System:	Pharo Lab ETS
Version:	LabVIEW real time module
Hardrive capacity:	32GB
Hardrive format:	fat32
Network card:	Intel®

HOST PC SPECIFICATION

General

PC Manufacturer:	Hewlett Packard
Model number:	Compaq nx8220

Processor Manufacturer and series:	Intel® Pentium® M
Frequency:	1.6GHz
RAM:	2.00GB
Operating System:	Microsoft® Windows® XP Professional
Version:	2002, Service pack 3
Hardrive capacity:	75GB
Hardrive format:	NTFS

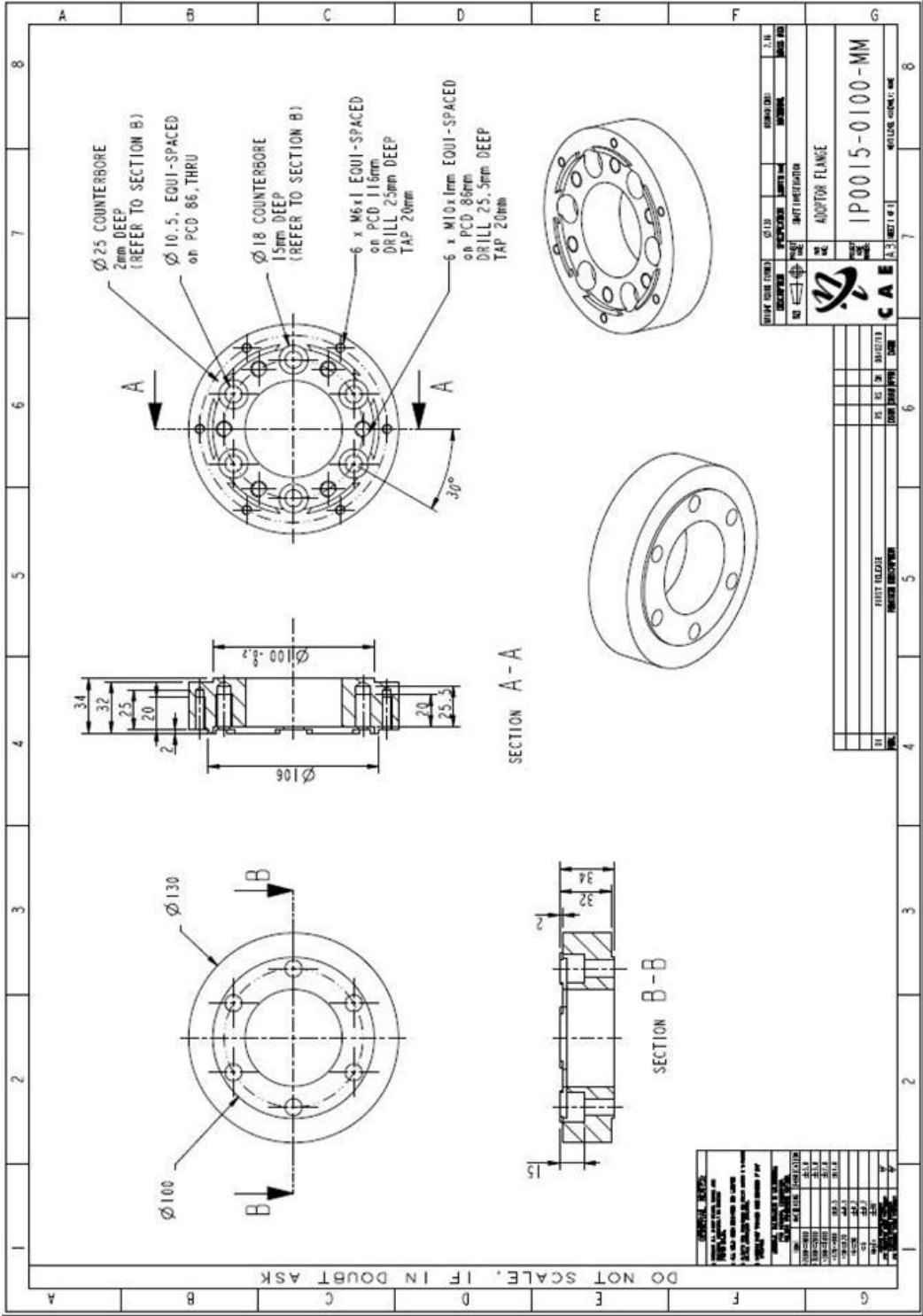


Figure A. 1: C.V. Adapter Flange

Appendix C

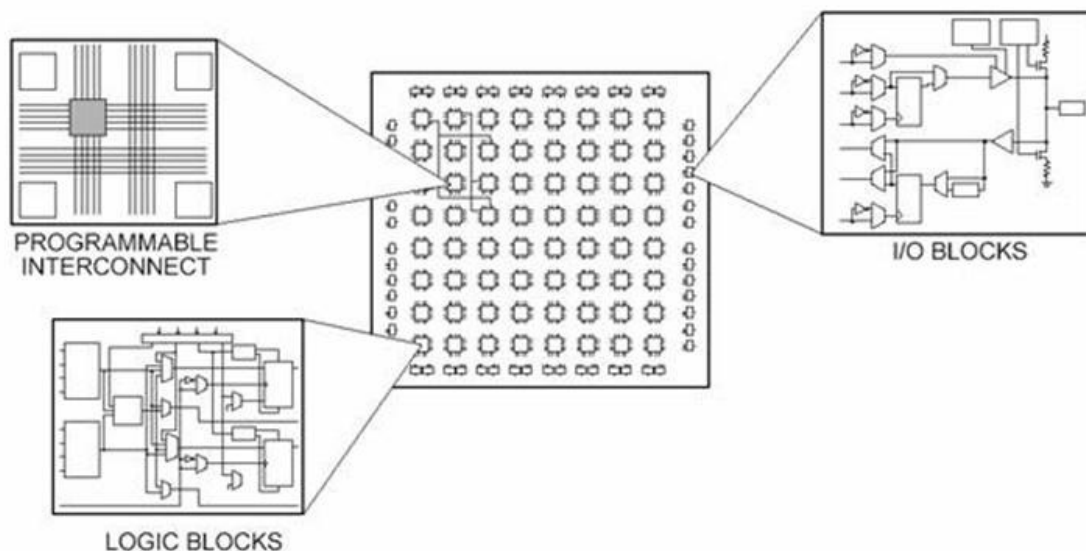
FIELD PROGRAMMABLE GATE ARRAYS

According to National Instruments, Field Point Gate Arrays are the most high level, reprogrammable silicon chips. Digital computing tasks in software are developed and then compile to a configuration file or bit-streams that contain information on how the components should be wired together.

Maxwell (2004) describes the 'Field programmable' portion of the FPGA's name as referring to the fact that its programming takes place 'in the field'. This may mean that FPGA's are configured in the laboratory, or it may refer to modifying the function of a device resident in an electronic system that has already been deployed in the outside world.

National Instruments (2009) proposes five advantages to using FPGA chips over ASIC type chips:

1. Performance
2. Time to market
3. Cost
4. Reliability
5. Long-term maintenance



Appendix E. 1: Abstract view of an FPGA (National Instruments, 2010)

"FPGA's occupy the middle ground between PLD's and ASIC's because their functionality can be customized in the field like PLD's, but they can contain millions of logic gates and be used to implement extremely large and complex functions that previously could only be realized only using ASIC's" (Maxwell, 2004).

National Instruments (2010) indicates that the most critical components of an FPGA are as follows:

1. Configurable logic blocks
2. Fixed function logic blocks, such as multipliers
3. Memory resources like block RAM

At the lowest level, configurable blocks of logic, such as at slices or logic cells, are made up of two basic things: flip-flops and look-up tables. Flip-flops are binary shift registers used to synchronize logic and save logic statements between cycles. Look-up tables are used to implement all combinatorial logic as truth tables which are a predefined list of outputs for every combination of inputs. Fixed function logic blocks are used to save on LUT and flip-flops usage during mathematical and signal processing application. The use of these predefined blocks is justified by the example of over 2000 operations being required to complete the multiplication of two 32 bit numbers. If predefined blocks were not used, this “simple” operation would require a large percentage of the available resources.

“User-defined RAM, embedded throughout the FPGA chip, is useful for storing datasets or passing values between parallel loops” (National Instruments, 2010). More than 30 percent of the flip-flops available on an example FPGA chip could be used to store 100 values in an array as opposed to less than 1 percent of an embedded RAM block on the same example FPGA. As such RAM could therefore be used as an effective means of storing data from one cycle to the next or between two parallel loops.

A fundamental advantage of FPGA’s is the inherent parallel execution of FPGA’s allowing for inherent pieces of hardware logic to be driven by different clocks.

Appendix D

DETAILED LABVIEW OPERATING PRINCIPLES

The host PC ran the Windows XP operating system produced by Microsoft, with the LabVIEW development environment installed onto it. The host's on-board network adaptor was used to connect to the target PC via an Ethernet cable which was connected to the PC100 Ethernet card installed in the target PC. The on-board network adapter in the target PC could not be used as it was constructed using a processor chipset that the Pharo Lab ETS operating system did not have a drive for. The connection between the PC's was used to deploy compiled code from the development environment on the host PC, to the real-time OS on the target PC. The connection was also used by the developed software for passing data between the display on the host PC and the real-time environment on the target when the developed program was in a runnable state.

The target PC was integrated into the test stand and thus had to be capable of data acquisition as well as signal generation. The target and host PC's would have best been viewed as the target PC operating independently as a machine or device with the host PC being the display and operating panel of the target PC, opposed to being viewed as two PC's in a network. The following hardware was procured to create the host and target PC's:

Table D. 1: Procured hardware

Target	Host
<ol style="list-style-type: none">1. Desktop Personal Computer (see Appendix A.2).2. Intel PC100, PCI Ethernet card.3. National Instruments PCI 6221 (37 PIN) data acquisition card (see Appendix A.1). This PCI card was installed into the RT target PC and was used to acquired data and generate signals.	<ol style="list-style-type: none">1. HP nx8220 laptop computer.

Operating systems make use of middleware, commonly termed a device driver, to allow software to interact with hardware. Device driver are dependent on the type of hardware as well as the operating system and as such each piece of hardware/OS combination requires its own device driver.

PharoLab ETS (the target PC's real-time OS) had a limited set of Ethernet and processor chipsets to which their operating system has device drivers. Due to the limited device driver set available for PharoLab ETS, all the target PC's hardware components had to be meticulously selected base on their chipset so as to ensure a device driver was available.

Obtaining the required devices fitted with the necessary chipsets was not a mundane task. Local vendors were unaware of the chipset on the hardware they distributed and many could not determine the chipset. This resulted in lengthy period being spent contacting various vendors, distributors and importers so as to obtain the correct components for the target PC. It was also discovered that many of the available hardware drivers provided for ETS were for

discontinued (no longer manufactured or not available in RSA) component or top-end components that were not cost effective solutions for this project.

The developed software comprised of two components, the user interface running on the host PC and the real-time component running on the target PC. Data was relayed between the two PC's via the Ethernet cable which enabled interaction amongst the two PC's. This communication was not deterministic. On the target PC, the tasks required to run "simultaneously" were placed in separate loops. These loops could to some extent be considered as threads as they had many properties in common with threads. Thread start times could be staggered using an offset delay. The target PC was a single core machine, thus staggering of thread execution start times was part of a strategy that was implemented to avoid more than one thread being in a runnable state at any moment. The target PC's root VI (Virtual Instrument, the equivalent of an object in C++ code) could contain up to 256 loops/threads which could each contain further VI's. Thread frequency and CPU designation were further properties of these threads and thus allowed for multi-rate processing of tasks (many tasks being processed at different frequencies).

Ensuring there was sufficient time and resources available to run each of the created threads in its allocated time slice was the responsibility of the programmer. Gantt charts were created to help ensure program changes were feasible as far as thread timing was concerned.

During the development, methods used to handle acquired and generated data in the real-time loop/thread had to be carefully considered. Simple tasks such as shifting all the elements in an array by one space (as is done during the implementation of some circular arrays) became a resource intensive process and required special attention to ensure that thread execution deadlines were not over-run. Variable type selection had to be played off between data size (increased variable size requires an increase in processing time) and value accuracy (integer: 16bit; double 32bit) .e.g. an integer value could be used for engine speed opposed to a double value as speed would at best (lowest) be measured to one revolution per minute.

A requirement that developed during programming was the passing of data between threads of different execution frequency (e.g. a high speed acquisition loop to a slower data saving loop). This required a specialized method (use of real-time global variables) to be used that ensured data integrity. A similar method was used to send data to the host PC from the target but any data sent from a high priority or high frequency loop was first sent to a low priority low frequency loop before transmitting to the host PC. This prevented the possibility of any delays to the high speed, high priority loop that could have been caused by transmission delays between the two PC's.

Many modern compilers provided an object orientated software design approach. LabVIEW was no exception to this approach however LabVIEW was a graphical programming compiler opposed to a text base programming language. Thus, each part of the developed program was broken down into VI's which were loosely spoken, equivalent to Objects. Each VI had its own fundamental task to complete. VI's contents were determined by dividing the physical

components of an automobile into object however there were certain circumstances where one object had to take control of or interact with multiple other objects to complete the simulation. An advantage to the VI or object orientated development was that one object could be easily swapped out with another newer version. Thus if one aerodynamic model was to be replaced with another, this could easily be done.

Appendix E

CHANGES MADE TO THE OFFLINE SIMULATION MODELS CODE TO ENABLE ITS REUSE IN THE REAL-TIME ONLINE MODEL

1. The simulated engine was removed and was replaced by analog outputs for the engine speed and the throttle position demand signals. The simulated engine response to the demands was replaced by analog inputs for measured torque and engine speed measurements. These signals were filtered using a 5th order Butterworth filters.
2. The offline model set the idle speed to a user defined minimum engine speed. With the online model, real data measured from the engine was used and thus the correct engine idle was achieved.
3. Once the simulation program was running, it was discovered that it would be convenient not only to be able to change gears at set engine speeds as was done for the second program, but to be able to change gears at time based setpoints in the test cycle. This meant that once the simulated vehicle reached a specified point in the test cycle, a gear change up or down depending on what was specified, would occur regardless of the engine speed. Time base gear selection was achieved by the user providing the required gear for each simulated vehicle speed setpoint in the velocity profile input file. For each iteration, the required gear would be read from the input file and if a gear change was required, the gear ratio would be changed and a gear change would be simulated using the method described in 4.6.3.1.

Appendix F

TEST FAILURE / INCIDENT REPORT



CUSTOMER	TEST DESCRIPTION	CAE PROJECT NUMBER
CAE/VWSA/SASOL	Internal development	IP0015
DATE INCIDENT OCCURRED	TEST STATUS AT TIME	REPORT NUMBER
2010/01/14	Preliminary engine performance measurement and characterisation	IP0015-TF01

1. FAILURE / INCIDENT DETAIL

At 10:09 on Thursday 14/01/2010 the intermediate shaft, transmission bell-housing and engine to dynamometer shaft, located in test cell ATL 07 failed. Failure of the engine to dynamometer coupling components occurred while testing an EA113 1.6l Volkswagen engine (engine number: BHW 086 082) coupled to a Froude EC-38 dynamometer which was further coupled to a 40Kw Siemens servo motor (model number: 1PH7167-2HG00-0LJ3) such as to allow for transient engine loading. Failure occurred at 28:28:00 engine hours, the total run time of the engine since arrival at CAE.

The engine was installed in test cell ATL 07 on 10/12/2009 having previously run 15:59:00 engine hours as a KRDL dummy engine at CAE. All engine history prior to this is unknown to CAE as all previous running occurred at Volkswagen of South Africa. From the time of installation in test cell ATL 07, the engine had completed eight performance curves starting at 100% throttle demand (INCA label pv_av) and reducing by 10% on each subsequent run. On the 19/12/2009 an engine oil leak was observed by the test engineer after completing a performance curve at 20% throttle demand. The engine did no further running until inspected by the mechanics on 11/01/2010 at which stage a leaking grub screw located in the front of the head under the CAM belt cover was repaired.

There after a further performance curve was run at 20% throttle demand. Upon completion oil was found under the engine and a winding noise was heard from the shaft area while the engine was idling. The engine was inspected by the engine mechanic and the test engineer. During the inspection it was unclear whether the origin of the oil was residual from the previously repaired leak or whether the oil was originating from what appeared to be a hair line crack in the engine block located at the left rear corner of the engine under the exhaust port of cylinder 4. The engine to dynamometer shaft was replaced during the inspection due to a failed spherical plane bearing.

The engine was then run warm (engine oil 105 °C) under low load conditions with continuous inspections for further leaking oil. No oil appeared to be leaking from the engine and the shaft noise was now gone, so it was decided to continue testing the engine with routine inspections so as to determine if the engine would leak under load.

During the run up of the engine to start a 10% throttle demand performance curve the engine was running at 4500 rpm and 10% throttle demand. The engine speed was then increased to 5000 rpm and 10% throttle demand. The engine ran for 13 seconds at 5000 rpm before the speed was increased again to 5500 rpm. Failure occurred during this ramp at 5120 rpm and 2 seconds into the ramp.

During the incident the test engineer was in the control room and pushed the emergency stop button 2 seconds after the initial failure. The engine stopped and the dynamometer and Siemens servo motor coasted to a stop under their own inertia. Once the test cell was safe to enter, all damage was photographed before anything was moved.

COMPILED BY:-	D Kunniger	DATE:-	2010-01-20
FILE : CAE20100119_IP0015-TF01_Incident Report			Page 1 of 15

TEST FAILURE / INCIDENT REPORT



2. ROOT CAUSE OF FAILURE / INCIDENT

From the information provided in investigation / data section, this incident was caused by failure of the engine to dynamometer coupling components. The cause of failure within this assembly is unknown although there is some evidence indicating that the engine to dynamometer shaft was the initial point of failure.

The data shows that the engine was operating normally and there is no evidence of the engine being the source of a sudden increase or decrease in load or engine speed that would result in an excessive loading condition.

Figure 8 shows the intermediate shaft having a bend in it and Figure 9 shows the twisting of the steel on half the cross section of the shaft at the point of failure. The bend indicates the presence of a force perpendicular to the shaft while the twisted steel at the failed point of the shaft indicates a failure due to excessive torsion loading. The existence of an external perpendicular force causing the shaft to bend, seize at one end and then partly fail due to excessive tension caused by the bending of the shaft and then finally failing due to torsion loading, would require the failure of the engine to dynamometer shaft, dynamometer or test engine. From the information provided in the following section, the engine does not appear to have failed and from post incident inspection, the dynamometer appears to be in good working order.

Figure 13 and Figure 14 show the failed engine to dynamometer shaft. It could be hypothesised that if the shaft reaches a harmonic of its natural frequency, this would have caused the rubber dampers to oscillate back and forth with an increasing magnitude. This could cause excessive loading of the shaft dampers causing a twisting action within the damper. This twisting action compounded with the already existing load could cause the damper to tear out its mountings (mounting are intended to support torsion load not axial) by rotating perpendicular to its axis of rotation. This rotation would cause failure of the spherical plane bearing support section of the engine to dynamometer shaft as can be seen in Figure 8. Once rotated out of position, it would be expected that the damper would not have enough momentum to break out of the shaft guard. This would cause the dampers to continue rotating in an uncontrolled fashion within the guard. While rotating out of position it may have applied a force perpendicular to the shaft axis causing the bending of the intermediate shaft as well as the damage to the continuous velocity joint (Figure 19). Once the intermediate shaft had bent to a critical point, it began to fail on the tension half of the bending moment. This initial failure caused the shaft bend angle to increase enough to allow the intermediate shaft to engine/dynamometer couple to run against the inside of the shaft guard. This coupling then caught on a nut welded to the inside of the shaft guard (Figure 18) causing the partly failed intermediate shaft to fail completely due to torsion loading. The coupling would have enough momentum to break through the shaft guard and complete the failure as is visible in the section Photographs.

3. INVESTIGATION / DATA

During the incident no data was intentionally recorded by the test engineer as the intended test had not begun yet. However, "black box" data was recorded for 75 seconds prior to and 75 seconds after the incident.

In the graphs provided below, the break in the plotted data indicates the moment the emergency stop button was pressed. The "black box" data did not record 1 second before and after the emergency stop was pressed, hence the reason for the break in the plotted data.

COMPILED BY:-	D Kunniger	DATE:-	2010-01-20
FILE : CAE20100119_IP0015-TF01_Incident Report			Page 2 of 15

TEST FAILURE /INCIDENT REPORT



Project : ETA Modules - Road load simulation
Engine No: BWH 086 082
VW EA113 1.6L with Shurlok 7.6 ECU
on 2010/01/14, using 95RON Fuel

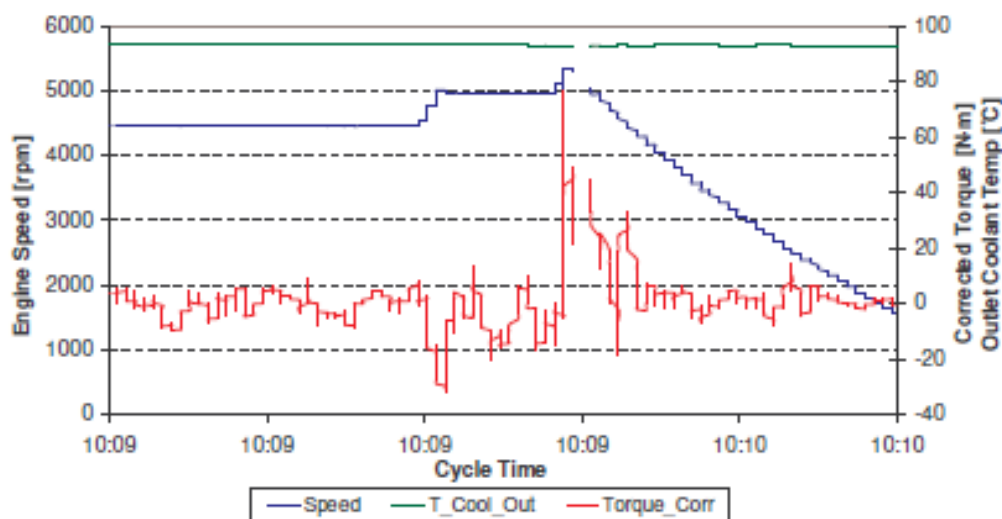


Figure 1: Dynamometer speed and corrected engine torque as recorded by the torque flange

Figure 1 (enlarged image of the moment of the incident is shown in Figure 2) shows a sharp increase in torque at the point of failure. This is due to a sudden high ramp rate slowing of the dynamometer. Torque values remain elevated for a further 5 seconds due to the slowing of the dynamometer.

COMPILED BY:-

D Kunniger

DATE:-

2010-01-20

FILE : CAE20100119_IP0015-TF01_Incident Report

Page 3 of 15

TEST FAILURE /INCIDENT REPORT



Project : ETA Modules - Road load simulation
Engine No: BWH 086 082
VW EA113 1.6L with Shurlok 7.6 ECU
on 2010/01/14, using 95RON Fuel

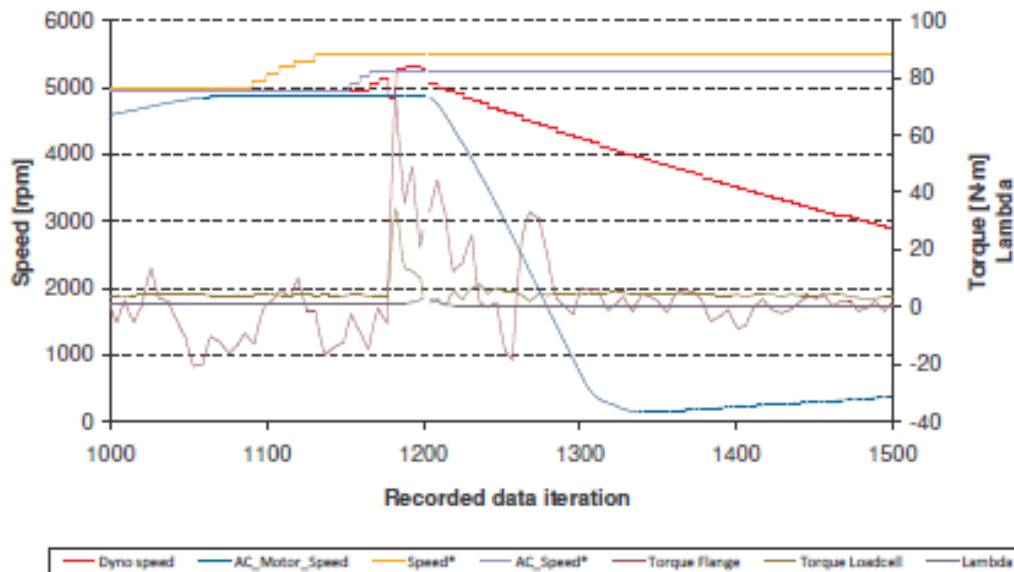


Figure 2: Recorded Dynamometer speed and torque at the moment of the incident

COMPILED BY:-

D Kunniger

DATE:-

2010-01-20

FILE : CAE20100119_IP0015-TF01_Incident Report

Page 4 of 15

TEST FAILURE /INCIDENT REPORT



Project : ETA Modules - Road load simulation
Engine No: BWH 086 082
VW EA113 1.6L with Shurlok 7.6 ECU
on 2010/01/14, using 95RON Fuel

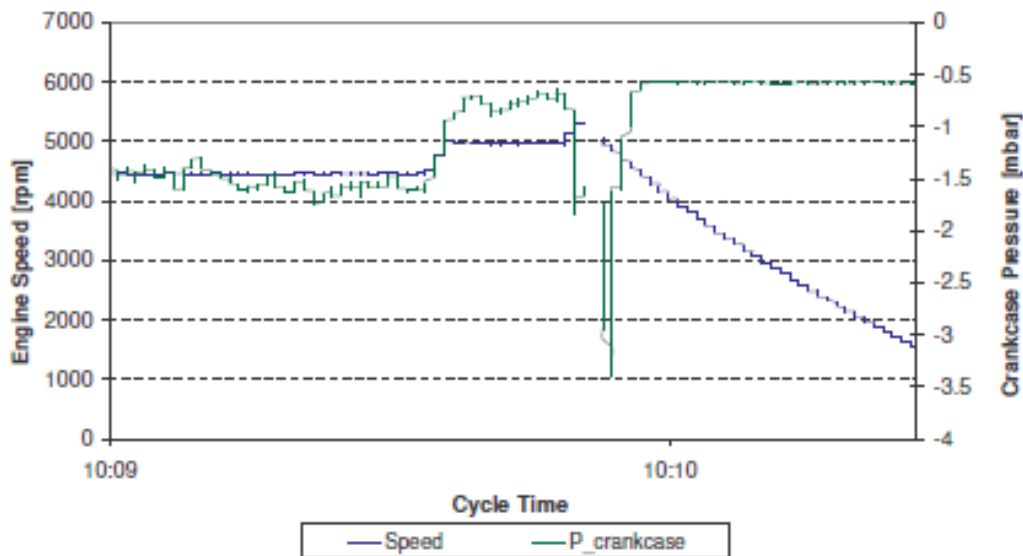


Figure 3: Engine Crankcase pressure and speed

From the negative crankcase pressures shown in Figure 3, it is evident that piston or ring failure did not occur and from Figure 4 it is evident that sufficient oil and fuel pressure were present for safe operation of the engine and thereby ruling out seizure of the engine.

COMPILED BY:-

D Kunniger

DATE:-

2010-01-20

FILE : CAE20100119_IP0015-TF01_Incident Report

Page 6 of 15

TEST FAILURE /INCIDENT REPORT



Project : ETA Modules - Road load simulation
Engine No: BWH 086 082
VW EA113 1.6L with Shurlok 7.6 ECU
on 2010/01/14, using 95RON Fuel

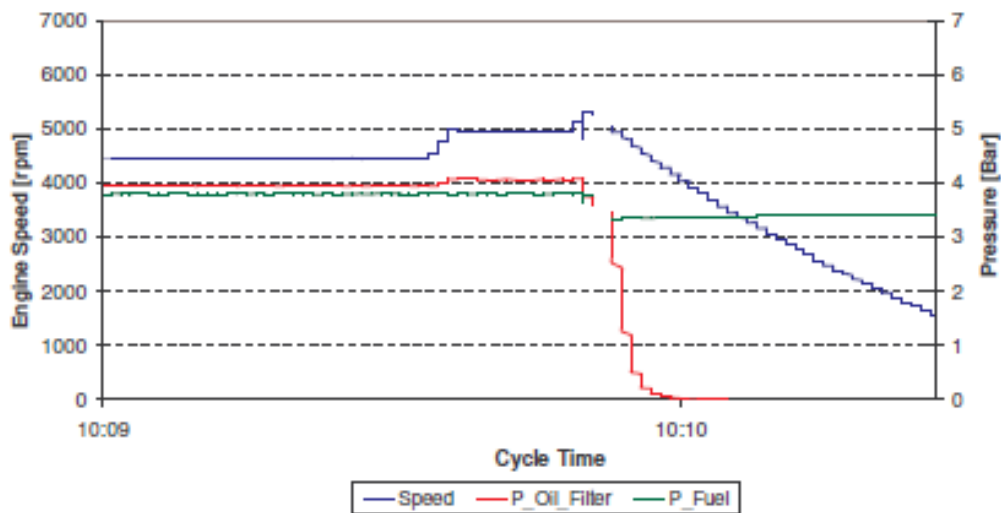


Figure 4: Oil filter pressure, fuel pressure and engine speed

COMPILED BY:-

D Kunniger

DATE:-

2010-01-20

FILE : CAE20100119_IP0015-TF01_Incident Report

Page 6 of 15

TEST FAILURE /INCIDENT REPORT



Project : ETA Modules - Road load simulation
Engine No: BWH 086 082
VW EA113 1.6L with Shurlok 7.6 ECU
on 2010/01/14, using 95RON Fuel

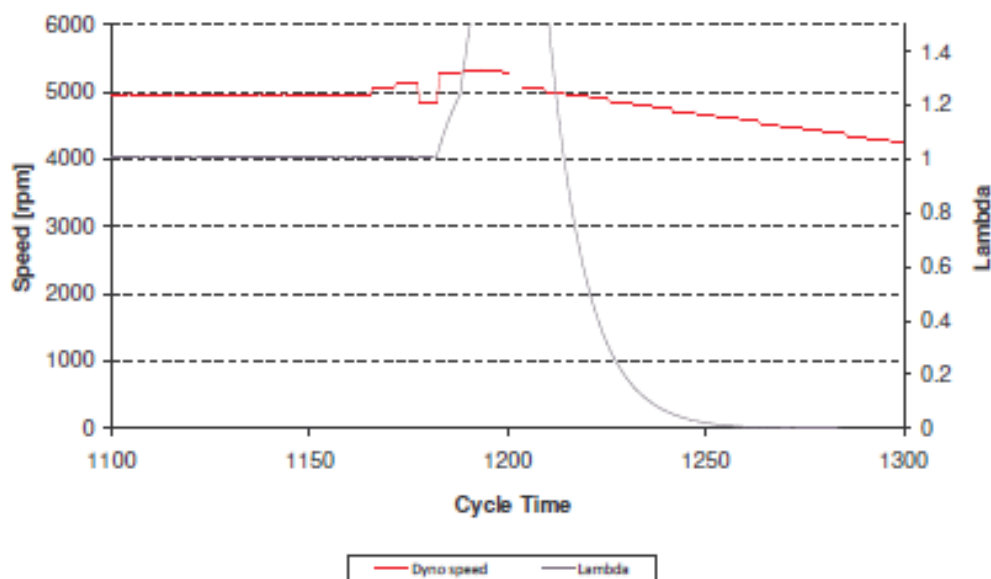


Figure 5: Lambda and engine speed

Figure 5 shows that the engine ECU went into fuel cut off/overrun mode at the point of the failure. The fuel cut off was as a result of the failure and not a contributing factor causing the failure. This can be stated as the fuel cut off; based on lambda value, only occurred after the sudden decrease in rpm or the moment of failure.

COMPILED BY:-

D Kunniger

DATE:-

2010-01-20

FILE : CAE20100119_IP0015-TF01_Incident Report

Page 7 of 15

TEST FAILURE /INCIDENT REPORT



Project : ETA Modules - Road load simulation
Engine No: BWH 086 082
VW EA113 1.6L with Shurlok 7.6 ECU
on 2010/01/14, using 95RON Fuel

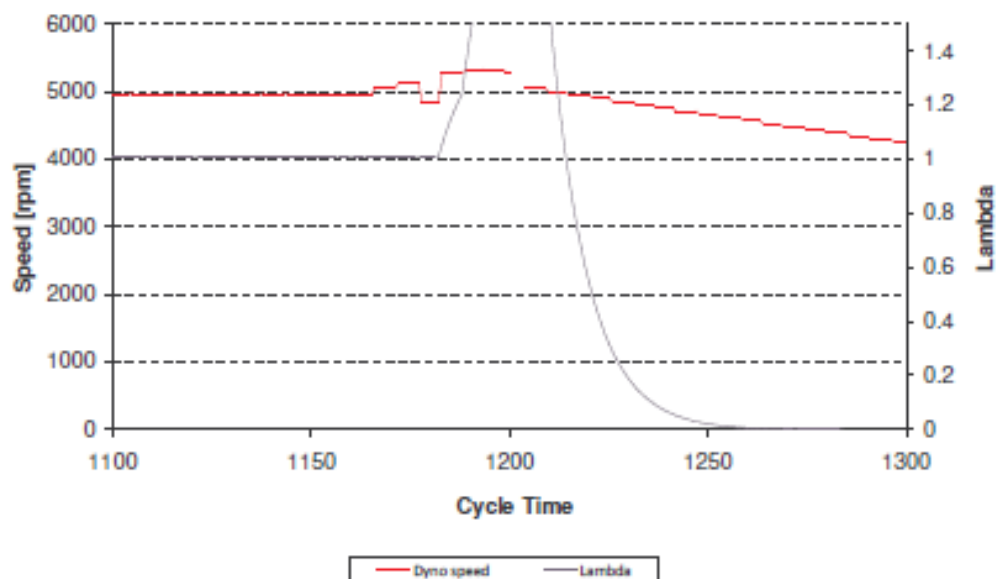


Figure 5: Lambda and engine speed

Figure 5 shows that the engine ECU went into fuel cut off/overrun mode at the point of the failure. The fuel cut off was as a result of the failure and not a contributing factor causing the failure. This can be stated as the fuel cut off; based on lambda value, only occurred after the sudden decrease in rpm or the moment of failure.

COMPILED BY:-

D Kunniger

DATE:-

2010-01-20

FILE : CAE20100119_IP0015-TF01_Incident Report

Page 7 of 15

TEST FAILURE /INCIDENT REPORT



Project : ETA Modules - Road load simulation
Engine No: BWH 086 082
VW EA113 1.6L with Shurlok 7.6 ECU
on 2010/01/14, using 95RON Fuel

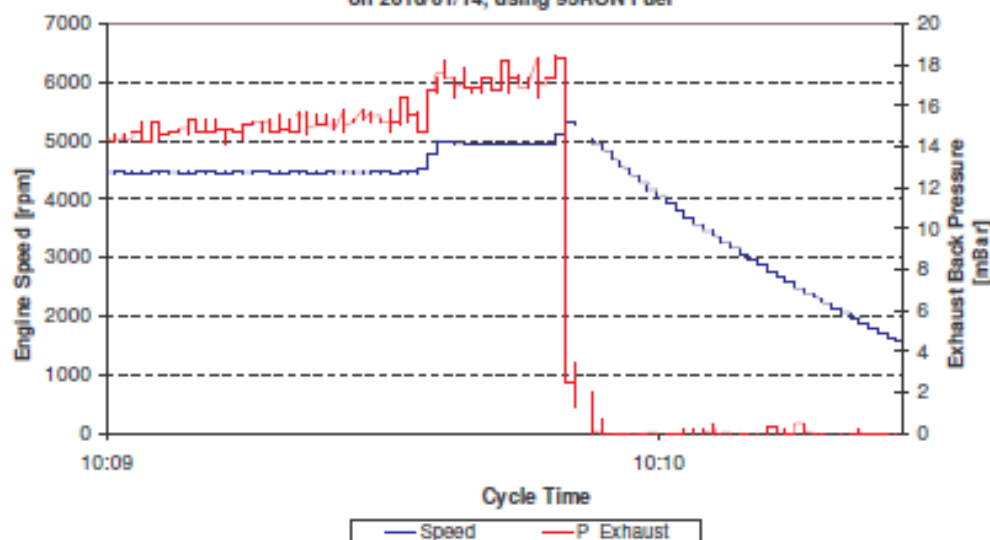


Figure 6: Exhaust pressure and engine speed

Figure 6 shows the exhaust back pressure. The sudden drop in back pressure at the point of failure was as a result of the fuel cut off displayed in Figure 5.

Figure 7 shows the intake manifold pressure. Consistent manifold pressure indicates consistent operation of the engine (e.g. throttle body butterfly stationary).

COMPILED BY:-

D Kunniger

DATE:-

2010-01-20

FILE : CAE20100119_IP0015-TF01_Incident Report

Page 8 of 15

TEST FAILURE / INCIDENT REPORT



Project : ETA Modules - Road load simulation
Engine No: BWH 086 082
VW EA113 1.6L with Shurlok 7.6 ECU
on 2010/01/14, using 95RON Fuel

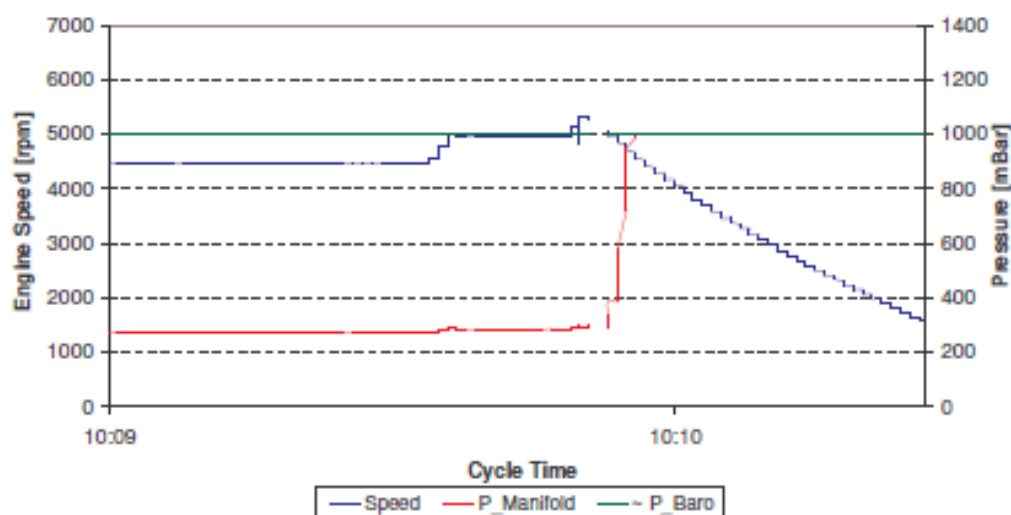


Figure 7: Barometric pressure, Manifold pressure and engine speed

4. RECOMMENDATIONS / CORRECTIVE ACTIONS

It is recommended that a study be conducted into the natural and resonating frequencies of the engine to dynamometer shaft. This study should include steady state and dynamic loading of the shaft at steady state and dynamic speed set points to determine its natural response to such loading. As there is no evidence to support the cause of the failure beyond to suggest the engine dynamometer shaft to be the initial point of failure, such a study would provide great insight into the natural response of a shaft under engine test conditions and may provide reason for this failure and will allow for the correct shaft design and selection for future use.

Further it is recommended that the shaft design and installation guide be reviewed upon completion of the fore mentioned study to ensure that they comply with the findings of the study.

All welded tabs used to secure the two halves of the shaft guard together need to be reinforced to prevent the two from coming apart in the event of a future shaft failure. The inner surface of the shaft guard needs to be smooth with no objects protruding through the inner surface of the cover and there by creating an object for a failed shaft to catch onto. A second shaft retaining plate (visible in Figure 18) needs to be inserted into the shaft guard so that one retaining plate is present at each end of the shaft. This will ensure that a shaft only rotated about its intended rotational axis in the event of a failure.

5. PHOTOGRAPHS

COMPILED BY:-

D Kunniger

DATE:-

2010-01-20

FILE : CAE20100119_IP0015-TF01_Incident Report

Page 9 of 15

TEST FAILURE /INCIDENT REPORT



Figure 8: Failed intermediate shaft (left) and engine to dynamometer shaft (right)



Figure 9: Twisted steel at the failure point of the intermediate shaft (Left)

COMPILED BY:-

D Kunniger

DATE:-

2010-01-20

FILE : CAE20100119_IP0015-TF01_Incident Report

Page 10 of 15

TEST FAILURE /INCIDENT REPORT

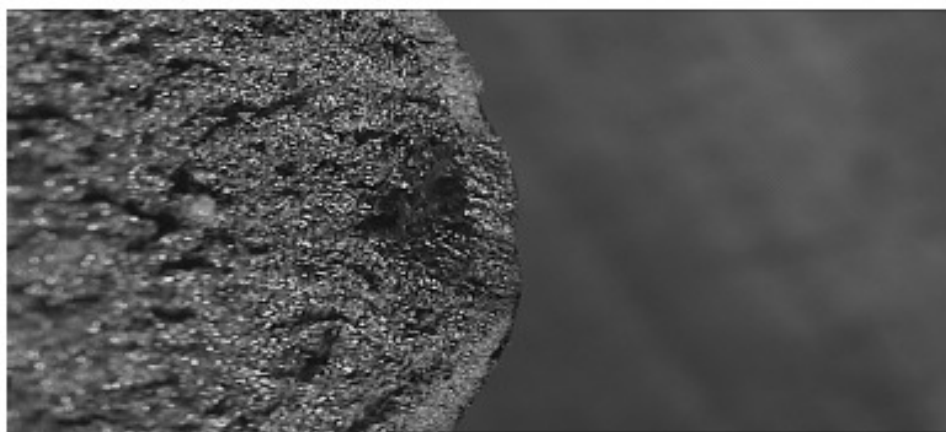


Figure 10: Main shaft, spherical plane bearing support end of failure.

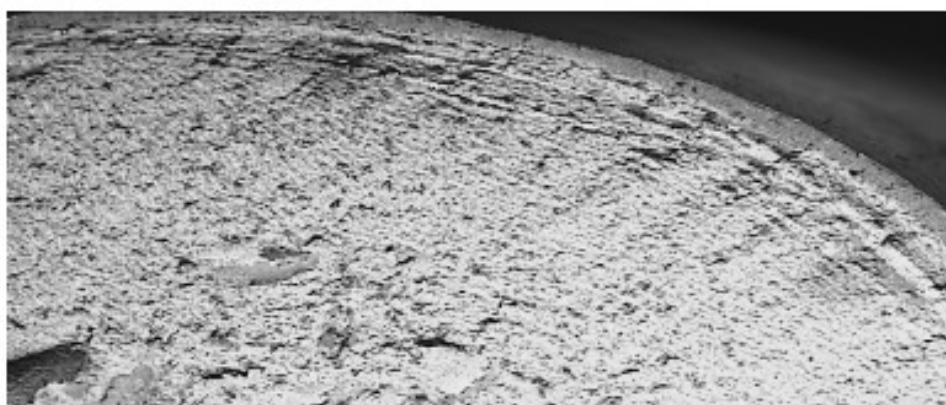


Figure 11: Intermediate shaft, engine to dynamometer end of failure.

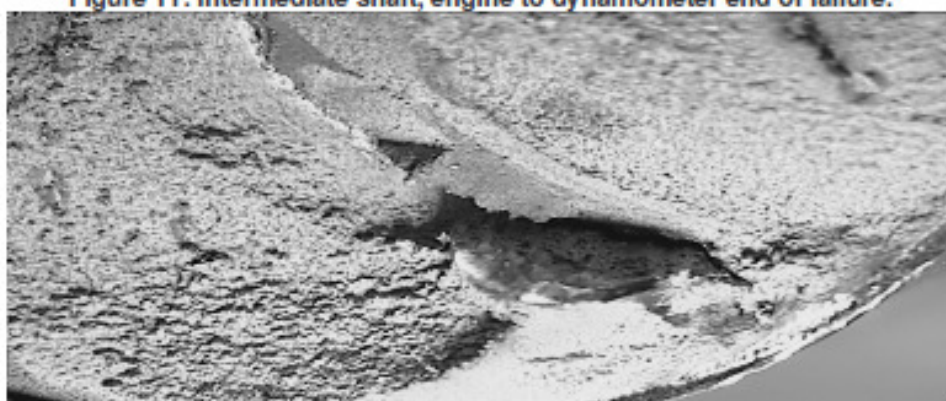


Figure 12: Intermediate shaft, engine to dynamometer end of failure.

COMPILED BY:-

D Kunniger

DATE:-

2010-01-20

FILE : CAE20100119_IP0015-TF01_Incident Report

Page 11 of 15

TEST FAILURE /INCIDENT REPORT



Figure 13: Failed intermediate shaft (left component) and engine to dynamometer shaft (centre and right)



Figure 14: Failed engine to dynamometer shaft.

COMPILED BY:-

D Kunniger

DATE:-

2010-01-20

FILE : CAE20100119_IP0015-TF01_Incident Report

Page 12 of 15

TEST FAILURE /INCIDENT REPORT

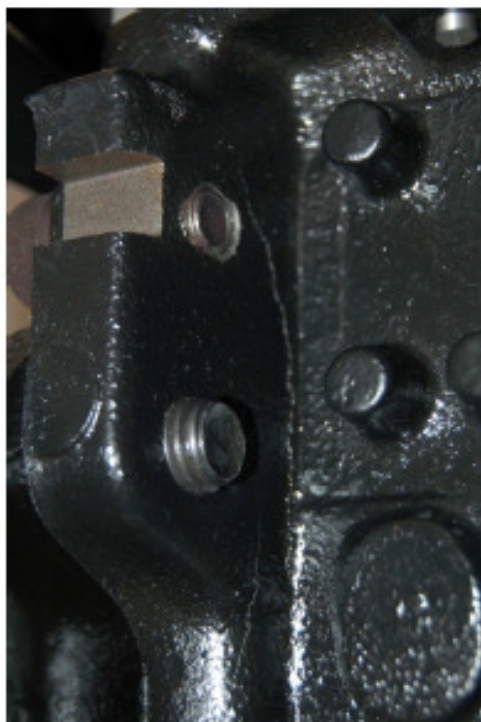


Figure 15: Crack located at the top left rear corner in the engine block.



Figure 16: Crack in the transmission bell housing.

COMPILED BY:-

D Kunniger

DATE:-

2010-01-20

FILE : CAE20100119_IP0015-TF01_Incident Report

Page 13 of 15

TEST FAILURE /INCIDENT REPORT



Figure 17: Shaft cover and intermediate shaft to engine/dynamometer shaft coupling as located after the incident.

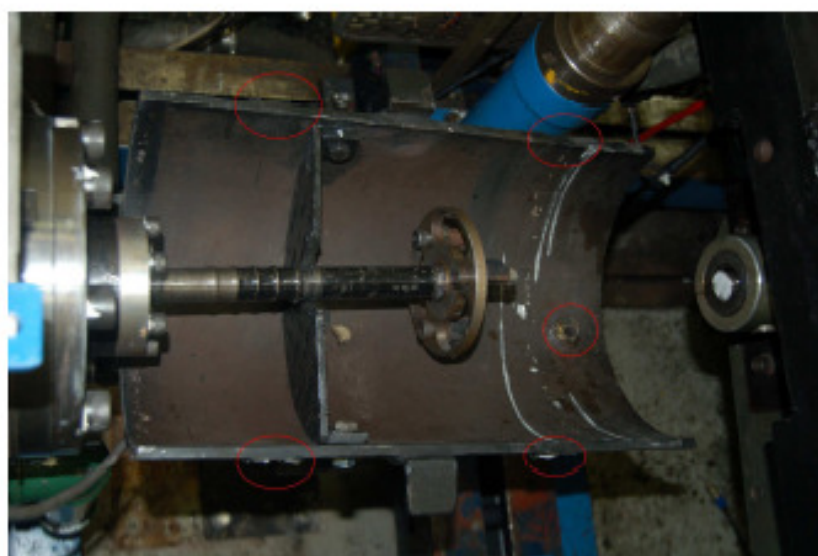


Figure 18: Engine to dynamometer shaft as found after the incident. Note the nut welded to the inside of the shaft guard and the broken off securing eyes for the top half of the guard.

COMPILED BY:-	D Kunniger	DATE:-	2010-01-20
FILE : CAE20100119_IP0015-TF01_Incident Report			Page 14 of 15

TEST FAILURE /INCIDENT REPORT



Figure 19: Damaged constant velocity joint that forms part of the engine to dynamometer shaft.



Figure 20: Damaged shaft dampers that form part of the engine to dynamometer shaft.

COMPILED BY:-

D Kunniger

DATE:-

2010-01-20

FILE : CAE20100119_IP0015-TF01_Incident Report

Page 15 of 15